Control Strategies and Reduced Models for the Smart Power Cell

Vom Fachbereich für Physik und Elektrotechnik

der Universität Bremen

zur Erlangung des akademischen Grades

Doktor-Ingenieur (Dr.-Ing.)

vorgelegte Dissertation

von

Holm Hinners, M. Sc.

aus Bremen, Deutschland

Referentin:	**Prof. Dr.-Ing. Johanna Myrzik**
Korreferent:	**Prof. Dr.-Ing. habil. Christian Rehtanz**
Eingereicht am:	5. Juni, 2023
Tag des Promotionskolloquiums:	11. Dezember, 2023

If there be cure or charm
To respite, or deceive, or slack the pain
Of this ill mansion: intermit no watch
Against a wakeful foe, while I abroad
Through all the coasts of dark destruction seek
Deliverance for us all
— John Milton, *Paradise Lost*

Kurzfassung

Diese Dissertation repräsentiert eine Weiterentwicklung des Konzepts der Smart Power Cell (SPC). Ziel ist die flächendeckende Integration von dezentralen, erneuerbaren Stromerzeugern mittels geregelter Unterbereiche. SPCs sind grundsätzlich in der Lage, interne Stabilität zu gewährleisten, während Leistungsflusssollwerte verfolgt werden für die Verbindungen mit dem Rest des Stromnetzes und anderen Energienetzen wie dem Gasnetz und dem Fernwärmenetz. Die Arbeit baut teilweise auf existierender Forschung zur SPC auf, erweitert aber deutlich den Umfang und die Gültigkeit mit neuen Modellelementen und Reglern.
Im Speziellen wird die Modellbildung der Knoten in der SPC erweitert mit einer neuen Reglerstruktur in diesen Knoten, welche die Komplexität und Flexibilität diverser Erzeugungsanlagen bündelt und als einzelne Erzeugungsanlage mit einfachem dynamischen Verhalten der SPC gegenüber präsentiert. Hierfür genutzt werden Überlegungen zum Übertragungsverhalten der Anlagen sowie der energetischen Flexibilität und deren Aggregation. Es entsteht dann für den Regler am Knoten ein Optimierungsproblem mit Nebenbedingungen. Die existierenden Regler zur SPC als Ganze werden erheblich verbessert und sind nun in der Lage, Sollwerten für mehr als eine Verbindung aus der SPC heraus zu folgen. Die Spannungsregelung der SPC wird ebenso verbessert, um diverse Probleme zu vermeiden, die aus der vorherigen Struktur erwachsen konnten. Ebenso wird der Integrator der bestehenden Struktur um eine fraktionale Ableitung erweitert, um Oszillationen zwischen Reglern zu unterdrücken. Für die SPC wird dann eine Modellreduktion auf Basis metaheuristischer Optimierungsmethoden entwickelt, um eine Simulation mehrerer SPCs im Verbund zu ermöglichen. Für das Übertragungsnetz wird ein weiterer Regler entwickelt, welcher die Spannung im Übertragungsnetz regelt, indem den SPCs Sollwerte für die Verbindung zum Übertragungsnetz gesandt werden. Jede Reglerebene einzeln sowie deren Interaktion wird im Zeitbereich simuliert, um die Effektivität des Konzeptes zu zeigen.

Abstract

This dissertation represents a further development of the concept of the Smart Power Cell (SPC) which aims to solve the issues associated with widespread integration of distributed and renewable generators using controlled subdivisions. SPCs are broadly designed to maintain internally stable behavior while tracking power flow reference signals at their interconnections to other parts of the power grid and other energy grids like gas and district heating. Building partly on existing models for the SPC, this dissertation substantially expands the scope and validity of the models using additional control layers while also developing more flexible and advanced controllers for existing layers.
Specifically, the modeling of buses inside the SPC is expanded with a new control structure which bundles the complexity and flexibility of distributed generators connected to that bus and which presents this aggregation as a single, simplified generator to the SPC. Transfer function considerations and the aggregation of energetic flexibility are used for this purpose. A constrained optimization problem arises at the bus, which the bus controller solves. Existing controllers for the SPC as a whole were substantially improved and are now capable of tracking reference values for more than one interconnection between the SPC and other parts of the grid or other energy grids. Voltage control inside the SPC was also improved to avoid a variety of problems that may appear as a result of the previous structure. The integrator used in the previous controller was expanded with a fractional derivative to dampen oscillations between controllers. A model-order reduction based on metaheuristic optimization was developed for the SPC to allow more computationally efficient simulation of an interconnection of SPCs. Additional controllers were developed for the transmission grid which control the high-voltage side voltages by generating reference signals for the SPC interconnections. Each control layer was simulated in the time domain both individually as well as their interaction to demonstrate the effectiveness of the concept.

Danksagung

Ich möchte meinen Dank zum Ausdruck bringen gegenüber meiner Doktormutter, Prof. Johanna Myrzik, welche diese Arbeit immer mit wertvollen Ansichten unterstützt hat. Ich möchte auch Prof. Christian Rehtanz danken für seine Bereitschaft, die Rolle des Zweitgutachters auszufüllen. Ich empfinde tiefe Dankbarkeit gegenüber Dr.-Ing. Daniel Mayorga Gonzalez. Seine Arbeit bildet die Grundmauern dieser Dissertation und seine Modelle waren der Anfang meiner. Meine erste Veröffentlichung basierte erheblich auf der selbstlosen Ideenspende Daniels und erlaubte es mir, früh in meiner Karriere eine renommierte Konferenz zu besuchen.
Ich bin dankbar gegenüber meinen Kollegen in der Arbeitsgruppe für die vielen Diskussionen, welche wir bezüglich unserer Arbeit hatten. Im Speziellen möchte ich Dr.-Eng. Sergio Contreras Paredes und Dr.-Ing. Desmond Ampofo danken für ihre Bereitschaft, mir als Regelungstechniker die damals noch unbekannten Minuzien des Energiesystems zu erklären.
Ein Großteil dieser Dissertation basiert auf der Arbeit, die im Rahmen des Prioritätsprogramms 1984 für die Deutsche Forschungsgemeinschaft durchgeführt wurde und ich danke der DFG für die finanzielle Förderung. Die Diskussionen, die wir in unserer Forschungsgruppe EMoCoSy hatten, waren äußerst nützlich in der Erweiterung meines Verständnisses zum Problem des zellularen Netzes.
Schlussendlich, und mehr als allen anderen, möchte ich meinen Eltern und meinem Bruder danken. Ohne sie würde ich in der gegenwärtigen Form nicht existieren, geschweige denn diese Dissertation.

Contents

List of Symbols and Abbreviations

The used symbols, subscripts, superscripts and abbreviations are listed and described in the table below, separated by the chapter they are first used in.

Symbols

Symbol	Explanation	Unit SI
General Notation		
$\vec{\ }$	Vector	
$\mathbf{A}$	Matrix	
$x(t)$	Time Dependence	
$\bar{u}$	Complex Value	
$\vec{S}$	Apparent Power Vector	VA
Chapter 3		
$\vec{r}$	Apparent Power Reference Signal (Vector)	VA
$\vec{r}_{S\to B}$	Apparent Power Reference Signal Transmitted from SPC to Bus Controller	VA
r_P	Active Power Reference Signal	W
r_Q	Reactive Power Reference Signal	var
B	Flexibility Region of a Distributed Generator	
F	Bus Flexibility Region	
T	Transfer Function Denominator Time Constant	
${}^0T$	Transfer Function Numerator Time Constant	
K	Transfer Function Gain	
T_Σ	Approximated Transfer Function Time Constant	
i_d	Index for n_d Connected Devices	
Chapter 4		
$\vec{r}_{S\to B,P}$	Active Power Reference Signal Transmitted from SPC to Bus Controllers	W
$\vec{r}_{S\to B,Q}$	Reactive Power Reference Signal Transmitted from SPC to Bus Controllers	var

Symbol	Explanation	Unit SI
$r_{T\to S,P}$	Active Power Reference Signal Transmitted from TSO to SPC	W
$r_{T\to S,Q}$	Reactive Power Reference Signal Transmitted from TSO to SPC	var
$\vec{y}_P$	Active Power Measurement Signal from Interconnections	W
$\vec{y}_Q$	Reactive Power Measurement Signal from Interconnections	var
$y_{i,U}$	Measured Voltage at Controllable SPC Bus i	pu
i_b	Index for n_b Controllable Buses in SPC	
k	Index for m Tracked Interconnections in SPC	
$\vec{D}_{i_b}$	Row Vector with Distance Scaling Coefficients for Interconnections	
$K_{i_b}(s)$	Control Functions	
$\vec{e}_P$	Active Power Control Errors at Interconnections	W
$\vec{e}_Q$	Reactive Power Control Errors at Interconnections	var
K_U	Fuzzy Voltage Controller	
Γ	Scaling Function	
Chapter 5		
ε	Optimality Function for Optimization	
$\vec{O}$	Parameter Vector of Grey-Box Model	various
$r_{T\to S,P}$	Active Power Reference Signal Transmitted from TSO to SPC	W
$r_{T\to S,Q}$	Reactive Power Reference Signal Transmitted from TSO to SPC	var
$\vec{y}_P$	Active Power Measurement Signal from Interconnections	W
$\vec{y}_Q$	Reactive Power Measurement Signal from Interconnections	var
$\vec{y}_{P,\text{full}}$	Active Power Measurement Signal from Interconnections (Full Model)	W
$\vec{y}_{P,\text{red}}$	Active Power Measurement Signal from Interconnections (Reduced Model)	VA
$\vec{y}_{Q,\text{full}}$	Reactive Power Measurement Signal from Interconnections (Full Model)	W
$\vec{y}_{Q,\text{red}}$	Reactive Power Measurement Signal from Interconnections (Reduced Model)	VA
$\vec{v}_{p,\text{new}}$	Particle Velocity (Particle Swarm Optimization)	As $\vec{O}$
$\{r_p, r_g\}$	Random Variables on $[0, 1]$	
$\{\omega, \gamma_p, \gamma_g\}$	Weights	
$\vec{O}_{\text{best,ptcl}}$	Best Position in Particle's History	As $\vec{O}$
$\vec{O}_{\text{best,global}}$	Best Position in Global History	As $\vec{O}$
r_r	Lévy Flight Variable	
Chapter 6		

Symbol	Explanation	Unit SI
$\vec{r}_{T\to S,P}$	Active Power Reference Signal Transmitted from TSO to SPC Controllers	W
$\vec{r}_{T\to S,Q}$	Reactive Power Reference Signal Transmitted from TSO to SPC Controllers	var
i_s	Index for n_s Controllable SPCs	
j	Index for m_{i_s} Controllable Buses in SPC i_s	
$F_{i_s j}$	Flexibility Region of Bus j in SPC i_s	VA
u_{dead}	Voltage Deadband	pu
C	Voltage Sensitivity Scalar	

Abbreviations

Abbreviation	Definition
AC	Alternating Current
DC	Direct Current
ADN	Active Distribution Network
SPC	Smart Power Cell
TSO	Transmission System Operator
DSO	Distribution System Operator
OLTC	On-Load, Tap-Changing (Transformer)
LV	Low Voltage
MV	Medium Voltage
HV	High Voltage

List of Figures

List of Tables

Introduction

The emission of carbon dioxide and other greenhouse gases is producing a warming effect in Earth's atmosphere and has raised average global temperatures by more than 1 °C since the beginning of the industrial revolution at the time of this writing. Eliminating the greenhouse gas emissions of the power grid is an indispensable element of climate change mitigation. However, a power grid based on renewable generators differs in fundamental ways from the traditional power grid based on synchronous generators. It is the purpose of this introductory chapter to provide an overview of this transition and to contrast the past and the future. The challenges of this transition provide the basic motivation for the rest of this thesis.

1.1. Traditional Power Grid Control

The classical power grid was based on synchronous generators largely connected to the high-voltage grid and loads being connected to medium- and low-voltage grids. Power flowed uniformly from the generators in the transmission grid downwards to medium- and low-voltage grids. For the most part, industrial loads were connected to both medium- and low-voltage distribution grids whereas residential loads were, and are, connected to the low-voltage grids. The traditional grid is shown in figure 1.1.

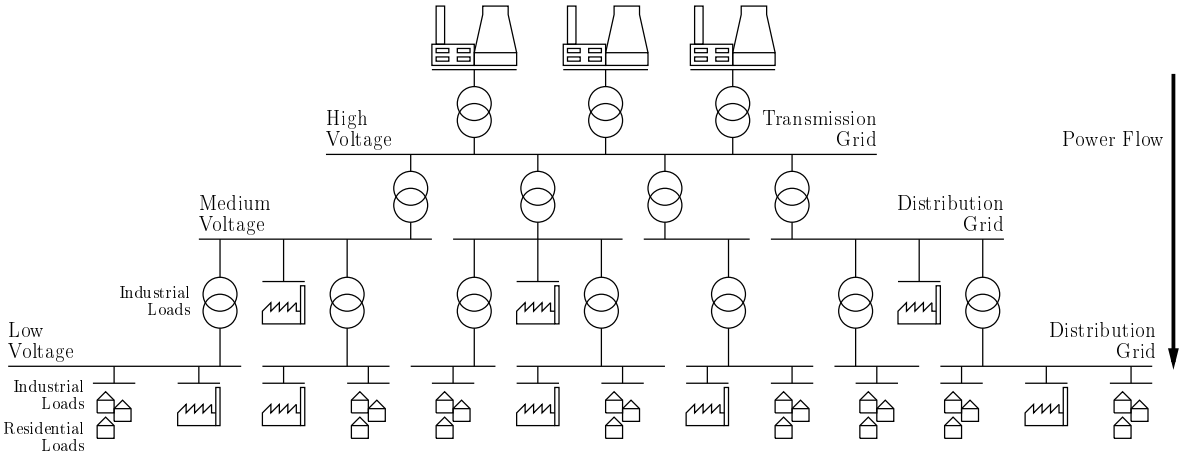

Figure 1.1: Traditional Power Grid

The load in the power grid is subject to constant change. To maintain acceptable system

behavior, grid operators use a variety of control mechanisms. An extensive overview is given in [Kundur 1994] and [Schwab 2012]. The fundamental requirements are:

1. Acceptable voltages. The voltages everywhere in the grid must be within the regulation band, such as $230\,\mathrm{V} \pm 10\%$ at the lowest voltage level. The relevant norm within Germany is DIN EN 50160.

2. Stable frequency. In alternating current grids, the frequency must be kept within the regulation band. In Europe, as defined by the ENTSO-E Network Code, control action begins at $50\,\mathrm{Hz} \pm 0.02\,\mathrm{Hz}$. Within the 0.02 Hz deadband, the balance of generation and consumption is maintained using the inertia of synchronous generators.

3. Respecting technical limits. Lines, cables, substations and other physical grid elements must obey current, power, and thermal limits.

Voltage control in AC grids is accomplished using reactive power and the variable turn ratios of on-load tap-changing (OLTC) transformers. Reactive power for the purpose of voltage control can come from a variety of sources, such as generators or phase shifters [Schwab 2012].
Frequency control in traditional AC grids is tied to active power balance due to the rotating energy of large synchronous generators. An imbalance in the active power balance results in an imbalance of the mechanical and electrical torque at the generator and either slows down or speeds up the generators, directly changing the frequency. This results in a global, coupled control problem of active power balance and frequency control and the easily measured frequency control error can be used as a proxy for active power balance. Active power generation is then used to reduce the frequency control error [Schwab 2012].
In traditional power grids, since little-to-no generation is located in lower voltage levels and distribution grids can be appropriately sized to prevent voltage violations, downstream grids are generally represented in models as simplified, large loads varying over time and power flows to these loads from the generators through the transmission grid. Operating points are periodically calculated for the dispatchable generation units in the high-voltage grid and continuous controllers shift the operating point of the generators to maintain local voltage and frequency. Traditional power grid control therefore only takes place in the transmission grid. There are different control mechanisms and each control mechanism acts on different time scales:

1. Primary and secondary control target frequency and active power balance using large, synchronous generators spread out through the transmission grid. It is a global control problem in the sense that the same frequency control error is observed by all controllers. As defined in the ENTSO-E Load-Frequency Control Code:

   (a) Primary control acts on millisecond-to-second timescales using proportional control by all generators that observe the control error.

   (b) Secondary control acts more slowly using integral control on second-to-minute timescales by the control area responsible.

2. Voltage control targets local voltages using reactive power generation or consumption and acts on millisecond-to-second timescales. It is a local control problem in the sense that the power plant controls the voltage at its bus in the transmission grid and by extension in some limited geographical area around it.

3. At longer timescales, these continuous controllers are supplanted by optimization-based, discontinuous methods that include economic and long-term grid resilience constraints in addition to voltage control and power balancing. These methods output new operating points to the synchronous generators on minute-to-day timescales. This control mechanism overlaps with tertiary control to make sufficient generation capacity available for control action and with time control to maintain the usability of the power grid frequency for time keeping.

1.2. Transition to Renewable Generation

In a power grid based on renewable energy generators such as wind and solar power, much of the generation migrates to the medium- and low-voltage grids. Renewable generators also exist in much greater number because of their smaller capacity individually compared to traditional generators. In such a grid, power no longer flows uniformly from the transmission grid down to the lower-voltage grids but instead might flow back up into the transmission grid towards areas of the grid elsewhere if there is more local generation than consumption. Renewable generators are also subject to constant and sometimes rapid changes in generation capacity as weather conditions change. This represents a constant fluctuation in the *control authority* of the generators, that being the limits of their capacity to affect the system and the desirability of the dynamic properties of the control action[1].
The power grid after transition to wind and solar power is shown in figure 1.2. These differences have been noted for some time [Schwab 2012, p. 556][Jenkins et al. 2010] and a number of difficulties are associated with this transition:

1. Increased computational complexity. The traditional grid had positive side effects for the simplified modeling of the grid: since downstream grids contained no generation, they could be approximated as large loads [Karlsson et al. 1994]. Such simplifications are not possible in a grid where most of the generation capacity and control authority is located in downstream grids.

2. Increased dynamic and control complexity. The control variables of the grid are primarily its generators, and the classical generators were limited in number, had large

[1] This terminology is widespread in control systems engineering, but particularly so in aircraft flight control where aerodynamic nonlinearity can mean that control surfaces lose their ability to meaningfully affect the behavior of the aircraft, for example at excessively low air speed or high angle of attack. Cf. [Stevens et al. 2015].

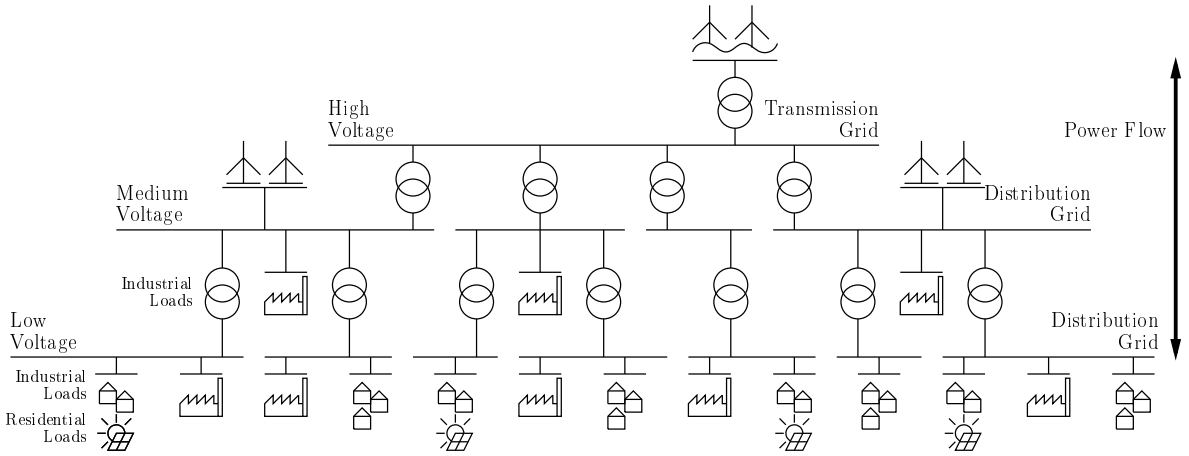

Figure 1.2: Future Power Grid

control authority over the grid, and comparatively benign and well-understood dynamic behavior. This is replaced with a larger number of smaller, dispersed generators, flexible loads, and storages whose capacity and control authority change dramatically and sometimes rapidly over time and whose dynamic behavior varies substantially. The much higher density of distributed generator controllers inside the grid also leads to stronger inter-area oscillations between controllers [Singh et al. 2014; Weber et al. 2016; You et al. 2017].

Due to these challenges, it is not expected that the power grid can accept the replacement of a large share of total power generation with distributed generators without changes to its operation and control [Jenkins et al. 2010; Stoustrup 2019]. One approach to tackle these challenges is based on the concept of a cellular power grid [*Zellulares Energiesystem* 2019]. In this concept, the grid is subdivided into cellular subsystems which are each under some manner of control that seeks to contribute to local stability. The interaction of these controlled subdivisions is then further controlled in some other way and as a network of cells, this is expected to contribute to overall grid stability because of the decentralization of the burden of complexity. The concept of the cellular power grid encompasses a fairly wide array of approaches of different capabilities. The concept explored in this work is the Smart Power Cell (SPC).

1.3. The Smart Power Cell Concept

The principle underpinning the Smart Power Cell (SPC) is one of controlled bundling and aggregate modeling [Mayorga Gonzalez 2021]. Since many difficulties associated with the transition to distributed and renewable energy resources are related to computational complexity, it makes sense to decentralize the problem as much as possible.
SPCs are intended to

1. be a bundling of geographically close grid elements (as opposed to virtual power plants, which are not necessarily close),

2. control the power generation and consumption inside,
3. provide an ability to support upstream networks or other power cells,
4. be in some way reducible to a lower-complexity model for simulation studies,
5. utilize innovative hybrid and multi-modal interfaces.[2]

Historically, model-order reductions and controller design were seen as not intrinsically related subjects since, by and large, model-order reductions were made in the context of control theory specifically to allow controller design in a more desirable form, such as lower controller order or more efficient validation on the system. This approach is apparent in books such as [Dittmar 2017; Grüne et al. 2017]. Similarly, in the power grid, controllers are designed at some point based on their own specifications, and then at some later point, a simplified model is designed for this or another part of the grid that represents the local behavior at lower computational cost. Alternatively, the system itself might be reduced in complexity to allow more manageable design of the controller. Rather than seeing the proliferation of generators and their controllers as merely a challenge, it can be seen as an opportunity. The power grid based on renewable energy requires a vast array of controllers to maintain beneficial interactions between all its controllable installations, such as generators, storages, flexible loads, etc. These controllers can be designed from the ground up with a view towards eventually simplified modeling. After all, it is the closed-loop behavior which is relevant for the reduced model of a controlled system, and the closed-loop behavior is subject to controller design by engineers.
In figure 1.3 is a conceptual illustration of two medium-voltage SPCs, interconnected through the medium-voltage grid, the high-voltage grid, and an alternative energy carrier grid (like the gas or district heating grids). To the buses are connected a variety of flexible loads (FL), storages (ST), distributed generators (DG), as well as traditional loads (filled triangles). The various controllers in the SPC maintain as much as possible the internal stability of the SPC and, through the medium- and high-voltage interconnections, support the operation of other SPCs.
Since the SPC is intended to aggregate some part of the medium- and low-voltage grids and to make itself controllable as an element in the high-voltage grid, distribution system operators (DSO) would be primarily responsible for the establishment and management of the SPC and their role in the operation of the grid would increase. The interaction between SPCs would occur primarily through the transmission grid, just as with the interaction between large conventional power plants, and would be the prerogative of transmission system operators (TSO) who would continue to be integral in balancing the interests of different SPCs.

[2] A hybrid network in this case is one which uses both AC and DC and multi-modal interfaces are connections to other energy grids such as district heating and gas.

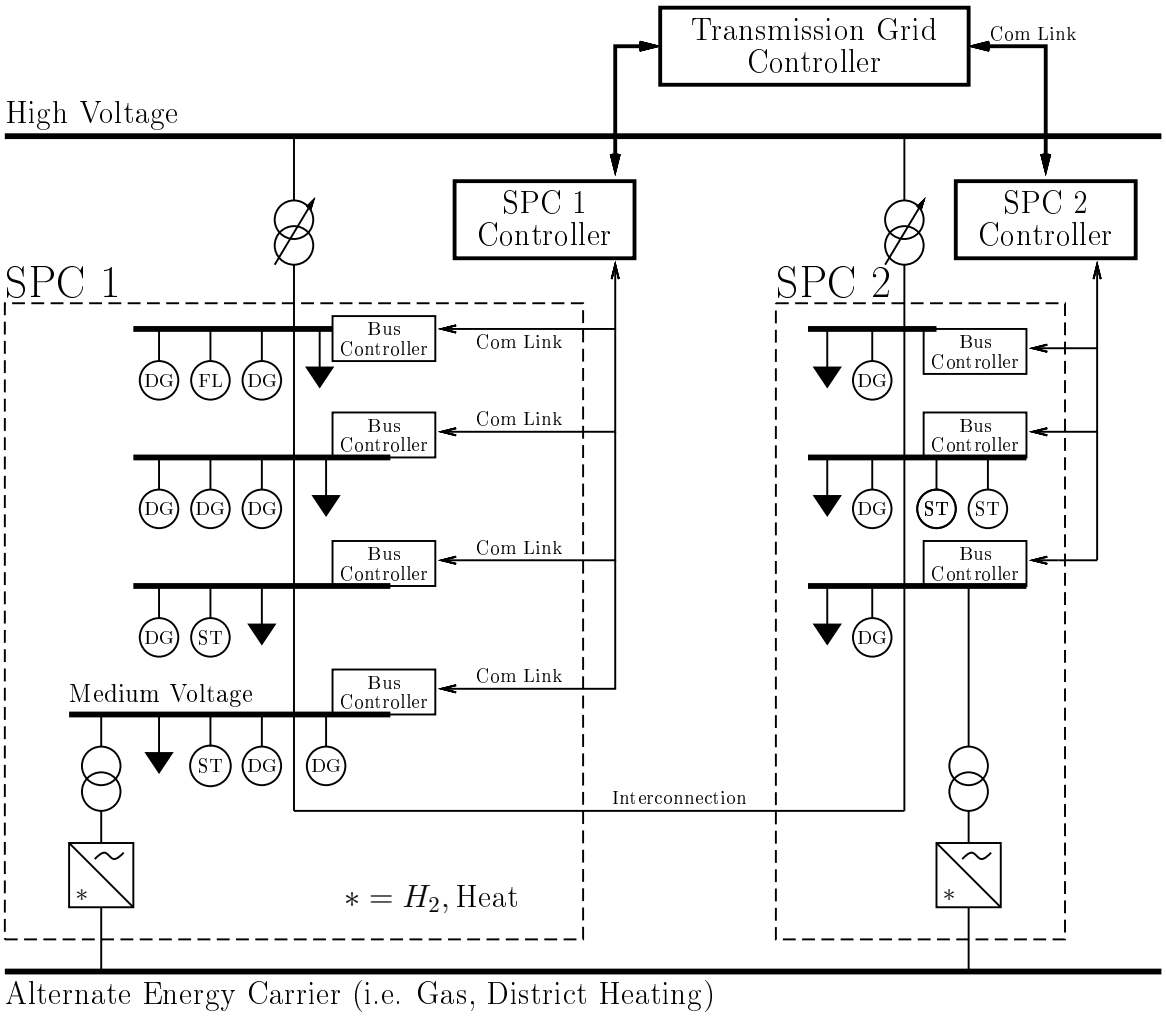

Figure 1.3: Illustration of two SPCs, with Distributed Generators (DG), Flexible Loads (FL), and Storages (ST)

1.4. State of the Art

Since the Smart Power Cell concept covers a wide array of topics from different fields, such as power system modelling, model-order reduction, and control theory, only a general overview of the state of the art will be given here and the focus will be on comparable developments and trends. Separate sections covering the state of the art as it is relevant to the chapter in question will be given in later chapters. Existing work that contributed specifically to the Smart Power Cell will be covered in the research questions as part of section 1.5 to offer a more detailed comparison to this work.
One of the largest and most relevant research publications was the ELECTRA project [Cabiati et al. 2018], which proposed a structure quite similar to an SPC interconnection in the sense that it included local, controlled cells which were dispatched to interact with each other in some way beneficial to grid security. While this project proposed far-reaching concepts and capabilities, it did not produce concrete technical solutions to many of its open questions. For example, in [MacDougall et al. 2016], one of the

project's research papers, a control algorithm was defined using black-box optimization to maintain power balance in a subsection of the grid, but it had no real capability to influence interconnections with other parts of the grid in a controlled fashion and it was not a continuous algorithm to begin with and mainly covered market optimization.
Another cellular approach with very similar design features compared to the Smart Power Cell concept was presented in [Kroposki et al. 2020]. It highlighted many of the same challenges that the SPC faces, namely real-time control, asynchronous measurement and control, robustness, and issues with scalability and computational complexity. A hierarchy similar to the one presented in this work was shown which aggregated sections of the grid into cells and supercells and controlled the active and reactive power flow at the interconnections of the cells. Shortcomings of the program include the rigid formalism of the concept and its very high computational cost at runtime: simplifications were made to allow Optimal Power Flow-like algorithms to run rapidly, but no consideration was given to the possibilities offered by continuous control. The concept therefore requires large computational resources to administer the cells and their controllers only react on a timescale of a minute or so, which is still too slow to control the cell adequately at faster timescales. In some ways, the concept can be considered a special case of Smart Power Cell.
Recent review and concept publications addressing cellular power grids such as [Waffenschmidt 2022; Waffenschmidt et al. 2020] have also stopped short of covering any specific research developments related to cellular grids due to a general dearth of solid results. While there is substantial agreement on the potential of cellular grids, research and development is characterized by a relative abundance of concept publications compared to developmental ones and there is poor agreement on the exact structure, requirement, and features of cellular power grids. This can be illustrated using existing research concerning Active Distribution Networks (ADNs). ADNs are a broad category of distribution network hosting some degree of control and autonomous operation. Since cellular grids will largely be constructed out of what are now the distribution grids, cellular grids are by definition a type of ADN. This broader field of research has produced a bewildering array of publications in recent years which range from very limited control such as the electric vehicle charging station voltage control in [Zaferanlouei et al. 2022] to more capable controllers such as the grid-connected frequency control and islanded load balancing in [Karagiannopoulos et al. 2020] and the day-ahead optimization of [Usman et al. 2023]. As a very brief summary, there are certain broad categories of power grid controller development for distributed generation that have a solid development basis:

1. Optimization-based methods for ADNs such as [Blasi et al. 2021; Karthikeyan et al. 2019; Karagiannopoulos et al. 2020; Usman et al. 2023]. These generally provide voltage control in the ADN and some of them also provide ancillary services to the transmission grid. Due to the iterative nature of the optimization and the setpoint-style, not continuous output, these algorithms generally run on minutes-to-days timescales and are suitable for all grid sizes provided they each run on an appropriately sized subsection or cell (in a national grid, such algorithms would dispatch entire ADNs and not individual generators). These methods can be

viewed as extensions and adaptations of the optimization-based algorithms used in traditional power grid control and various improvements have been made to allow running them at somewhat shorter timescales.

2. Droop control for Distributed Generators (DG) such as [Meng et al. 2019; X. Li et al. 2019] imitates the relationship between frequency and active power found in traditional generators. This improves the interaction of traditional generators with renewable generators, but does not solve many other issues. Such control algorithms act on millisecond-to-second timescale and can broadly be included in the subject of primary and secondary control since they do not provide local voltage control, only wide-area frequency control, on short timescales.

3. Voltage control for distributed generation such as [C. Zhang et al. 2023; Nguyen et al. 2021; Othman et al. 2020]. These are true controllers and provide voltage control for some collection of distributed generators, but they lack the other capabilities that the SPC requires of its generation, namely the support for upstream networks or other power cells, nor are they easily reducible for modeling and control.

4. Traditional controllers for synchronous generators in the transmission grid, inasmuch as synchronous generators are still present. These behave largely the same as they have in the past, but due to their smaller number and reduced control authority as a whole, their ability to provide voltage control in the transmission grid alone is questionable.

Some of the control schemes described above approach the capabilities required for the controllers of the Smart Power Cell, but the lack of a coherent concept across voltage levels and timescales into which these developments fit makes them largely unusable for the SPC. Nevertheless, where appropriate, these and similar developments will be covered in the various later chapters describing elements of the SPC. As mentioned previously, a more expansive view of the state of the art is provided individually in chapters 3 to 6.
Much of this work builds on the foundation in [Mayorga Gonzalez 2021] where the Smart Power Cell concept was introduced and algorithms developed for a basic level of functionality including SPC controllers, the determination of SPC flexibility regions, and a cross-voltage-level transmission grid model to study their interaction. Due to the direct relationship between these two works, differences and further developments will be highlighted in more detail in the next section.

1.5. Research Questions

From the gaps in the state of the art as described in the previous section arise the following research questions:

1. How should the generators, loads, storages, multimodal interfaces, etc in the SPC be modeled and controlled to follow desired generation profiles and to reduce their complexity?

2. How should the SPC be controlled to maintain local stability and to be able to contribute to the stability of other SPCs?

3. What are some of the consequences and possible remedies of a drastic increase in controller density?

4. How should the SPC model be reduced in complexity to make an interconnection computationally feasible?

5. How should an interconnection of SPCs be controlled to generate appropriate reference functions for SPCs to follow?

Specifically, "local stability" in the SPC will mean acceptable voltages at all buses. The contribution of the SPC to the operation of other SPCs and the transmission grid will be the ability of the SPC to track reference signals for the active and reactive power flows at the interconnection with the transmission grid and/or interconnections through the medium-voltage grid.
In [Mayorga Gonzalez 2021] the existing material especially regarding the SPC controller is significant, but several opportunities for further development exist:

1. Distributed generators (possibly aggregated DGs) in the medium-voltage Smart Power Cell are assumed to have first-order transfer behavior without proof. It should be shown why this is reasonable, if it is indeed, and to provide proof or algorithms that make it possible.

2. SPCs contribute to the stability of each other by tracking power flow reference signals at their interconnections. Before this thesis, they were not able to track reference signals for more than a single interconnection *in total* with the transmission grid and other Smart Power Cells. Existing controllers should be replaced with controllers capable of tracking reference signals for more than one interconnection out of the SPC.

3. Voltage control for the SPC is performed by freezing the controllers of all generators in the Smart Power Cell if a voltage violation is detected at any bus and awaiting a response by the OLTC (on-load, tap-changing) step transformer to move the voltage profile away from the violation. This carries substantial risks:

   (a) The voltage violation might be far away from the transformer and voltage gradients in the Smart Power Cell could be steep enough to freeze controllers but not provoke a response by the OLTC step transformer since the OLTC merely observes the voltage at the medium-voltage side and does not communicate with the SPC controller. This would freeze the Smart Power Cell until random changes in the loads or a loss of generation capacity changes the voltage profile.

(b) Voltage violations might even be exacerbated if the controllers are frozen and a variation in the loads or a stochastic variation of generation capacity causes a development in the direction of the violation (such as a reduction in load during overvoltages).

(c) Eventually this would be cleared by the OLTC, but at what point the OLTC is able to detect these violations at the medium-voltage side depends on the voltage profile at the time and the voltage violation may or may not reach critical levels.

This voltage controller should therefore be replaced with a continuous voltage controller which does not freeze.

4. An interconnection model of Smart Power Cells was investigated without the interconnection reference signals being based on specific control or dispatch algorithms, but merely chosen by the operator without any technical significance to demonstrate the fundamental interoperability of the SPC. Controllers should be developed for the transmission grid-level interaction of the SPCs. Furthermore, the model of the interconnection should not use synchronous generators, which are slowly being decommissioned.

5. The simulation of interconnected Smart Power Cells was excessively slow due to the size of the model. Sufficiently sophisticated internal control of the Smart Power Cell should make development of a reduced-order model possible to offer large computational savings.

These opportunities for further development provide the basis for much of the work in this document.

1.6. Contributions

The work presented here intends to fill these gaps and combine it with existing work to have a complete control framework for the SPC across different voltage levels, including the transmission grid. This thesis will also strive to make complexity reduction and model simplifications a central part of the development. Specifically, the modeling and control framework includes:

1. Controllers and aggregated modeling for individual generators, flexible loads, storages, etc. This is accomplished using transfer function considerations for the various controllable installations connected to the medium-voltage grid, the aggregation of energetic flexibility, and the solution of a constrained optimization problem to generate appropriate setpoints. This presents the various controllable installations connected to a medium-voltage bus inside the SPC as a single, aggregated installation to the SPC controller. Time domain simulations demonstrate the effectiveness of the approach.

2. Controllers and reduced modeling for the Smart Power Cell. The new controllers for the SPC are able to respond to multiple interconnections and provide continuous, dynamic voltage control inside the SPC. They also feature advanced methods to suppress controller oscillations, which is demonstrated in time domain simulations. A reduced SPC model is generated using metaheuristic optimization of a grey-box model structure and is validated using time domain simulations.

3. Controllers for an interconnection of Smart Power Cells. The developed controllers generate reference signals for the interconnections between the different SPCs and the transmission grid to maintain acceptable voltages at all buses in the transmission grid in response to a severe disturbance of generation capacity. The reduced models of the SPC allow simulation in the time domain of such an interconnection in reasonable time and the controllers swiftly return the system to the voltage deadband without undue oscillations.

More generally, the control and modeling framework developed in this work is consciously designed to be modular and adaptable and to not rely on specific algorithms in each layer of the control architecture. It should be possible to replace parts of the architecture without inherently making other elements of it non-functional. Various alternatives to the controllers and reduced models used in this thesis will be discussed in later chapters and some of the mathematical explorations are not directly necessary for the specific controllers described in this thesis, but are conceivably necessary for other controllers. This will be noted as such.

1.7. Structure of this Thesis

Due to the very different topics covered by this thesis, the state of the art is split between the introduction and the various chapters to allow a granular coverage of existing developments. Each of the main chapters will contain their own, separate state of the art. The author's publications correspond broadly to the main chapters in this thesis and both text elements and figures have been adapted from those sources.

1. Chapter 1 contains this introduction.

2. Chapter 2 contains another introductory chapter which describes the proposed controller structure in its entirety in broad strokes so that the relationship between the controllers in the different chapters is more transparent.

3. Chapter 3 covers the controllers and the simplified modeling of distributed generators, flexible loads, storages, etc, connected to a single bus inside the SPC and is based on the transfer function considerations and constrained optimization developed in [Hinners, S. F. Contreras, et al. 2022].

4. Chapter 4 covers the internal control of Smart Power Cells based on a combination of multi-variable control, linear-parameter varying control and fractional

control for interconnection power flow and internal voltage profile and is based on [Hinners, Mayorga Gonzalez, Myrzik, and Rehtanz 2019], with some more recent improvements to the control function.

5. Chapter 5 covers the model order reduction based on metaheuristic optimization of a grey-box model structure and validation based on a reference signal sweep of Smart Power Cells for wide-area simulation and is based on [Hinners, Mayorga Gonzalez, and Myrzik 2019a] and [Hinners and Myrzik 2021].

6. Chapter 6 covers the controllers for the interconnection of Smart Power Cells based on deadband integral voltage control and their response to severe disturbances of generation capacity and is based on [Hinners, S. F. Contreras, et al. 2023].

7. Chapter 7 contains the conclusions and an outlook.

8. Appendix chapters A through C contain explorations and explanations of various concepts related to control and mathematical modeling which were omitted in the interest of brevity in the main body of the thesis.

Controller Structure

This chapter will give an overview of the control structure covered in more detail in the main chapters of this thesis. No specific algorithms for parameter synthesis will be explored, but some general mathematical relationships will be established to help the reader understand the interaction between controllers later in this thesis and the signals they exchange. In particular, this chapter will establish the hierarchical nature of the control architecture and its similarities and differences to cascade control.
The output of a controller can generate reference signals for other controllers. If the output of one controller is transmitted as a reference signal to exactly one controller, this is called cascade control. For example, this is widely employed for the control of electrical drives. There, the motor speed controller generates a current control reference signal and the current controller controls the motor. In a servo drive, a position controller outputs the reference motor speed, and the motor speed controller outputs the reference motor current, and so on. These controllers are generally SISO (single-input, single-output) and the rule of thumb is that lower-level controllers should react faster than higher-level ones to prevent oscillations. Notably, different controllers in a cascade control loop target measurements of different units — in the previous example of a servo drive, the position controller, the motor speed controller, and the current controller all target evidently different units of measurement.

2.1. Hierarchical Control

If one controller generates several reference signals for different lower-level controllers, this is called hierarchical control. An illustration is given in figure 2.1. Such a hierarchical structure arises somewhat naturally from any attempt to bundle the power grid's complexity using controllers — different locations or regions are controlled in different ways and their interaction must in turn be controlled by some other set of controllers, which then are controlled in some other way until a sufficiently high level of control and abstraction is reached that doesn't require an additional layer of control.
Hierarchical control is in many ways more general and complex than cascade control. Since higher-level controllers output reference signals for more than one controller, they might be MIMO (multiple-input, multiple-output). Due to potentially different dynamic properties of lower-level controllers, it can be difficult to guarantee that a lower level controller reacts faster than a higher-level one. In any case, different controllers might oscillate against each other if they target the same output variable or their output

variables are coupled, so oscillations are a recurring challenge in hierarchical control. These interactions are not ordinarily present in a cascade control loop.

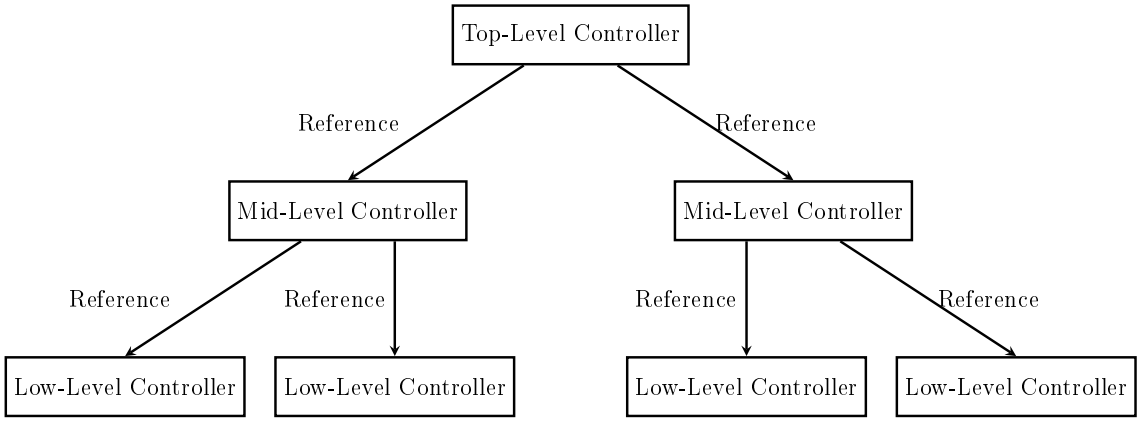

Figure 2.1: Hierarchical Control

2.2. Control Structure for the SPC

As explained in chapter 1, many challenges associated with the Smart Power Cell (SPC) are related to computational complexity and decentralizing the problem is attractive. The SPC concept also inherently tends towards a hierarchical control structure of some sort since the Smart Power Cell contains controllers by definition and so do any distributed generators connected to it. The Smart Power Cell would also not replace transmission grid operators (TSOs), so they would also still maintain some fashion of control. A hierarchical control structure naturally arises from this scenario and it is the intent of this work to provide a systematic framework as well as research into all constituent parts. Four different controller types will be included in the hierarchy:

1. A TSO-level controller. The output of this controller are reference signals to the SPCs for their active and reactive power flows at the interconnections to stabilize the high-voltage side voltages.

2. An SPC-level controller. It tracks the reference signals of the TSO-level controller and outputs reference signals to the buses inside the SPC. It also maintains the SPC's voltage levels using these output signals.

3. A bus-level controller. It follows the reference signals of the SPC-level controller and outputs reference signals to the device-level controllers.

4. A device-level controller. Devices are any grid installation controllable for active or reactive power flow generation or consumption, such as generators, storages, flexible loads, multimodal interfaces, etc.

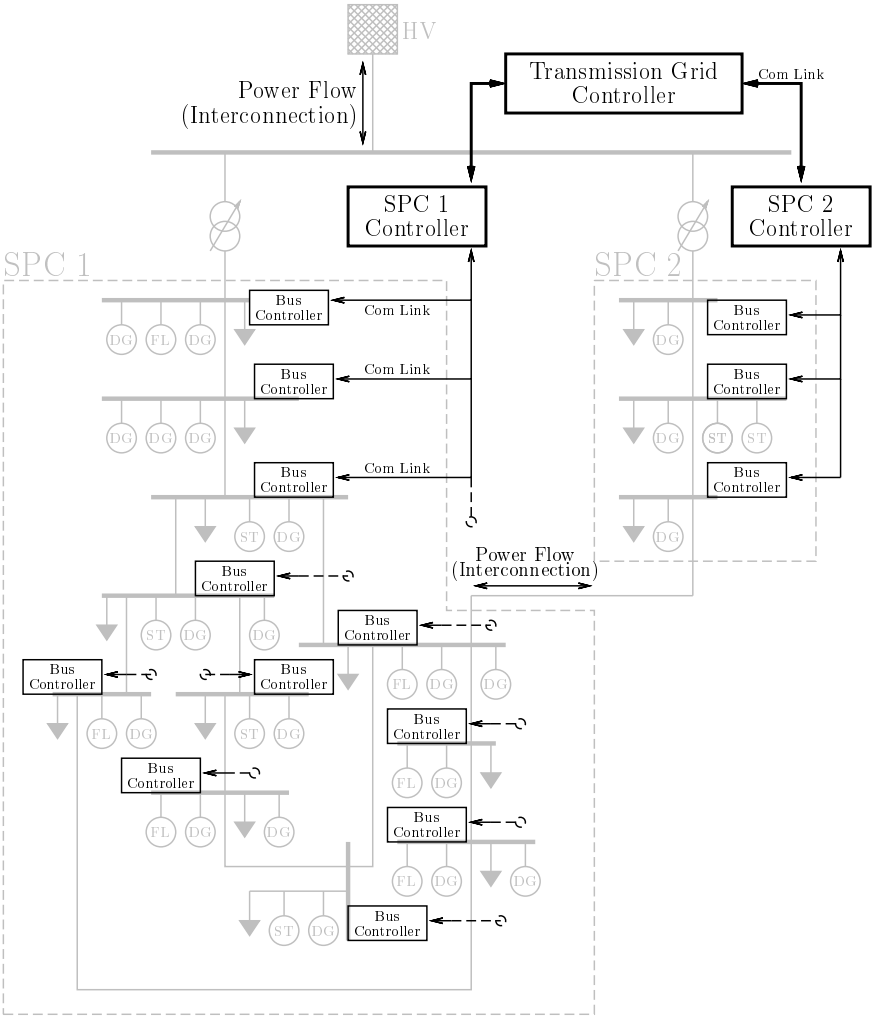

Figure 2.2: Location of Controller Architecture in an Example Grid with Distributed Generators (DG), Flexible Loads (FL), and Storages (ST), Structure Based on [Strunz et al. 2014]

An illustration of the location of the three highest levels of controllers inside the grid is given in bold in figure 2.2. The device controllers would be located at the various devices connected to the buses, but are omitted in the interest of compactness.
The interaction of a controller with its superior controller is mutual. It receives a reference signal which it is expected to track from the upper-level controller, but it also sends a status report signal back up towards it. What exactly this status report consists of depends on the requirements of the upper-level controller. The different chapters in this work will go into more detail what signals a controller requires from its subordinate controllers, but examples of what the subordinate controller might send upwards are:

1. The flexibility region of whatever the controller governs.
2. Dynamic parameters representing the behavior of whatever the controller governs.
3. The voltage at the local bus.

This signal flow between the controllers is shown in figure 2.3 as a block diagram without the feedback loop. The "other data" sent to the controllers could be local measurement data or data reported upwards by lower-level controllers.

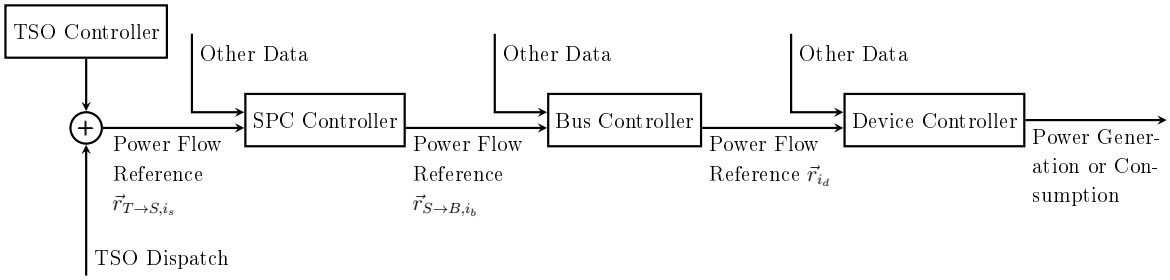

Figure 2.3: Controller Hierarchy Overview

Another schematic of the controller architecture is given in figure 2.4 using the abstract and simplified signal flow. Each controller outputs a reference signals to the controllers directly below it in the hierarchy (just as in figure 2.1) and receives from all of them a collection of status signals.

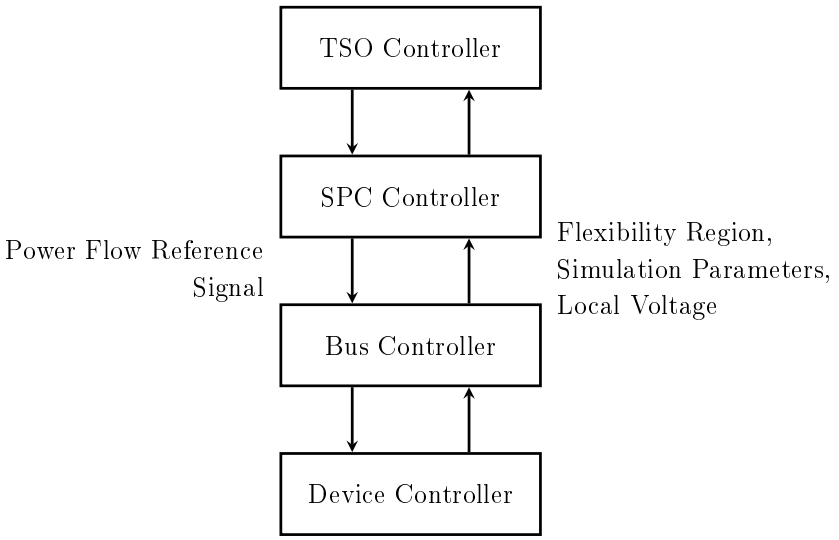

Figure 2.4: Signal Flow

The structure of this thesis is such that topics will be covered increasing in scale and complexity. Device modelling and control will be discussed together with the bus controller first in chapter 3 and their simplified dynamics described. With this known, their simplified dynamics are integrated into the SPC controller in chapter 4, and its dynamics discussed. A simplified model for the SPC is then derived in chapter 5 that can be used to investigate the TSO controller in chapter 6.
This work will refer to a signal as a "reference signal" if it is the input for *any* controller, not necessarily just the one being discussed in that chapter. This is done to avoid confusion between chapters when a signal that is a control output in one chapter is

a reference signal in a different chapter for a different controller. A controller will be described to receive a reference signal in the classical sense, but also to generate, output or send a reference signal, which would otherwise be called a control output as long as this output is a reference signal for a different controller. An overview of these reference signals is given below, but also in Symbols and Abbreviations.

$\vec{\bar{r}}_{T\to S}$	Apparent Power Reference Signal from TSO to SPC Controllers
$\vec{\bar{r}}_{S\to B}$	Apparent Power Reference Signal from SPC to Bus Controllers
$\vec{r}$	Apparent Power Reference Signal from Bus to Device Controller

These signals can be split into their active power and reactive power parts, and according to the lower-level controller to which they are transmitted. Since the i-th row is transmitted to lower-level controllers, the signal becomes a row vector. For the TSO-to-SPC signal this means that

$$\vec{\bar{r}}_{T\to S} = \vec{r}_{T\to S,P} + j\cdot\vec{r}_{T\to S,Q} = \begin{bmatrix} r_{T\to S,P,1} + j\cdot r_{T\to S,Q,1} \\ r_{T\to S,P,2} + j\cdot r_{T\to S,Q,2} \\ \vdots \\ r_{T\to S,P,n_s} + j\cdot r_{T\to S,Q,n_s} \end{bmatrix} \begin{matrix} \vdots \\ \} \Rightarrow \text{To SPC 2} \\ \vdots \\ \vdots \end{matrix} \tag{2.1}$$

$$\Rightarrow \vec{r}_{T\to S,i_s} = r_{T\to S,P,i_s} + j\cdot r_{T\to S,Q,i_s}, \tag{2.2}$$

where i_s is the i_s-th SPC controlled by the TSO for n_s controlled SPCs by the TSO. For the SPC-to-bus signal this means that

$$\vec{\bar{r}}_{S\to B} = \vec{r}_{S\to B,P} + j\cdot\vec{r}_{S\to B,Q} = \begin{bmatrix} r_{S\to B,P,1} + j\cdot r_{S\to B,Q,1} \\ r_{S\to B,P,2} + j\cdot r_{S\to B,Q,2} \\ \vdots \\ r_{S\to B,P,n_b} + j\cdot r_{S\to B,Q,n_b} \end{bmatrix} \tag{2.3}$$

$$\Rightarrow \vec{r}_{S\to B,i_b} = r_{S\to B,P,i_b} + j\cdot r_{S\to B,Q,i_b}, \tag{2.4}$$

where i_b is the i_b-th bus controlled by the SPC (a generic, single SPC being discussed at the time) for n_b controlled buses by the SPC. The bus-to-device controller is expressed somewhat differently since the algorithm calculates the rows independently (for n_d controlled devices):

$$\begin{aligned} \vec{r}_1 &= r_{1,P} + j\cdot r_{1,Q} \\ \vec{r}_2 &= r_{2,P} + j\cdot r_{2,Q} \\ &\vdots \\ \vec{r}_{n_d} &= r_{n_d,P} + j\cdot r_{n_d,Q} \end{aligned} \tag{2.5}$$

This chapter gave a broad overview of the control hierarchy introduced in this thesis and introduced the signal flow between controllers, albeit without details regarding the algorithms used by the controllers or the algorithms used to generate them. The mathematical formulation for the reference signals used by the controllers was given and is consistent with later descriptions.
In the following chapters, these controllers and their related model-order reductions are described. The next chapter will explore the bus controller first.

Bus Controller

The previous chapter described the controller structure in general terms. In this chapter and the following chapters, the elements of the controller structure will be described increasing in scale. The simplest controllable element of the future power grid (for the purposes of this thesis) is a single distributed generator, storage, flexible load, multi-modal interface, or some other kind of controllable installation capable of generating or absorbing electric power. Together all of these possible installations will be referred to as distributed devices. Their modeling and control has important repercussions for the rest of the grid since it is their dynamic behavior that forms the basis of the control response observed in the wide-area grid. In the renewable, decentralized power grid of the future, various combinations of these devices would be connected to the buses in the low- and medium-voltage grids, and if these devices are not standardized in terms of their controlled behavior, the collective dynamic behavior arising from them at the bus would be quite rich and difficult to generalize or simplify at higher levels of abstraction. It is therefore desirable to control the variety of devices connected to a bus in such a way as to generate behavior simple enough to make it possible to represent buses in some simplified way, for example as single, large installations of various flexibility regions with somewhat different dynamic properties. A bus controller with these design goals is the subject of this chapter.
The location of the bus controller inside the controller hierarchy with the current chapter in bold is given in figure 3.1. The various distributed devices connected to the medium-voltage bus are shown together with their bus controller and the signals sent and received by the bus controller. An example schematic of the bus controller inside the grid and with the rest of its proposed control architecture is given in figure 3.2.

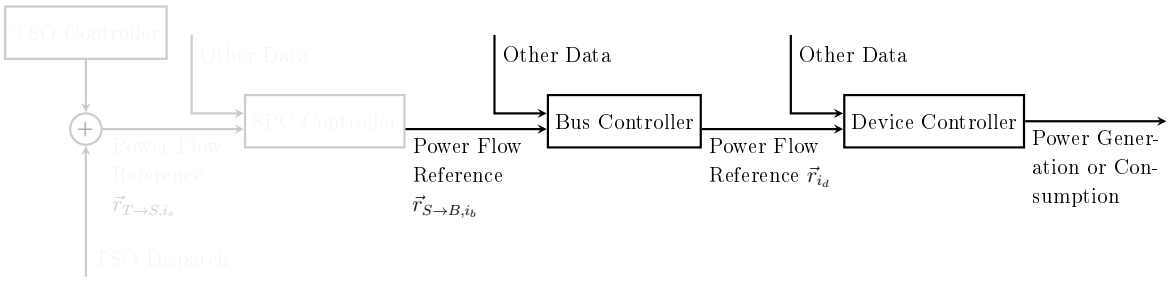

Figure 3.1: Controller Hierarchy Overview (Current Chapter in Bold)

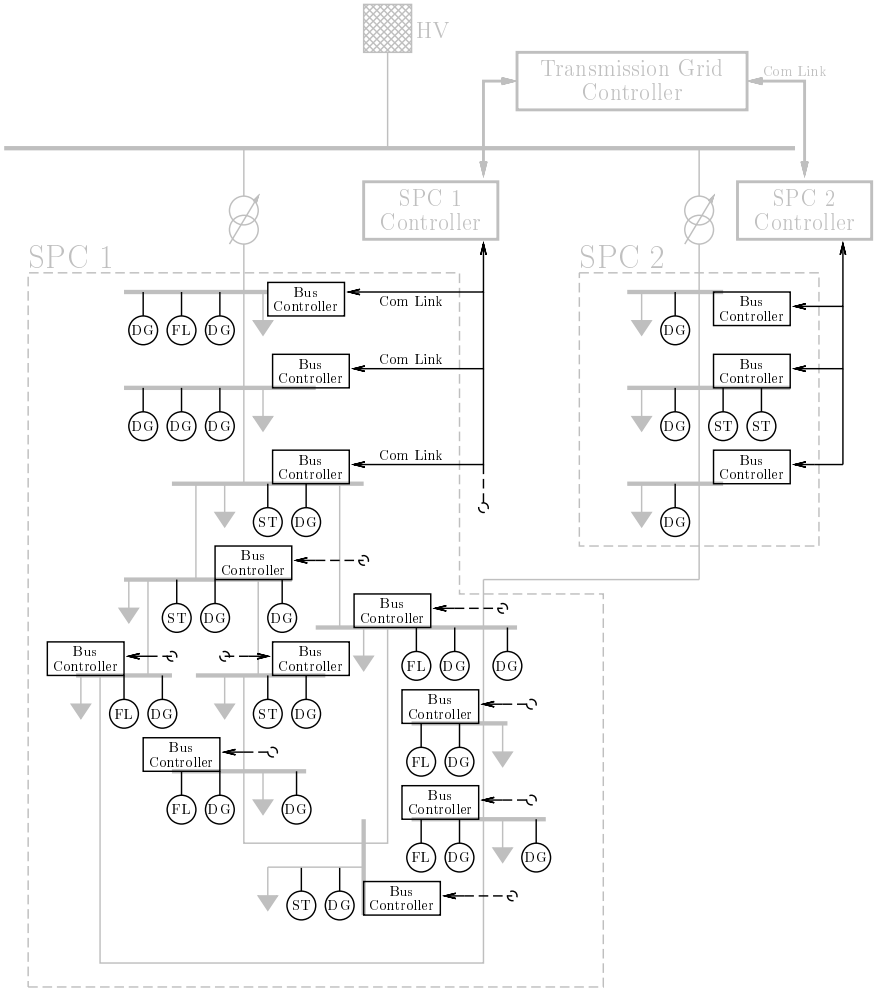

Figure 3.2: Location of Bus Controllers in an Example Grid with Distributed Generators (DG), Flexible Loads (FL), and Storages (ST), Structure Based on [Strunz et al. 2014]

3.1. Design Goals of Bus Controller

The design goal of this level of the controller architecture — the bus controller — is the following:

1. Aggregating all controllable generators, storages, multi-modal interfaces and loads connected to a single low- or medium-voltage bus and making them controllable as a single, virtual device.

2. Aggregating the flexibility regions of these devices.

3. Designing a controller for the aggregated, virtual device which results in simple dynamic behavior. This simplifies modeling and control at higher levels of abstraction in the control architecture of the SPC and the wide-area grid.

The concept of the aggregation is illustrated in figure 3.3.

The terminology here of "a single bus" is obviously somewhat open to interpretation. Conceptually, the intent is that the aggregated devices are so closely located that differences in voltage between the devices even at different operating points are insignificant. Voltage limits can then be ignored for the controller design in this chapter. Instead, voltage control for the single bus to which the aggregated device is connected is handled by the next higher-level controller in the distribution grid as part of the Smart Power Cell control problem in chapter 4 using the specific reference signals sent by the SPC controller to the bus controller.

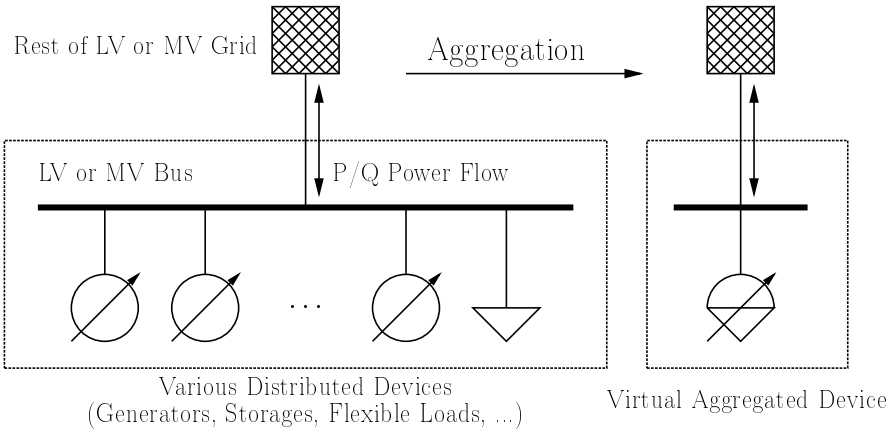

Figure 3.3: Aggregation of Distributed Devices

3.2. State of the Art

Designing a bus controller with the stated intention of reducing the dynamic complexity of connected devices is an unusual and novel approach. For example, publications such as [Ghosh et al. 2016] and [Y. Li et al. 2019] are concerned with using wind farms for the provision of ancillary services, but they do not include complexity reduction as one of the goals of the controller design. This leads to a complex dynamic control response which can make the grid difficult to operate at high levels of renewable energy generation.
Three specific computational challenges exist for the bus controller that result from the design goals above:

1. the aggregation of the flexibility regions (it is assumed the individual flexibility regions are known at all times to the connected devices and communicated to the bus controller),

2. the calculation of appropriate and feasible reference signals for each device connected to the bus which yield desired sum power generation or consumption and the desired dynamic behavior from the aggregated virtual device,

3. and aggregation of the dynamic behavior of the devices for simulation by controllers further up in the hierarchy which may rely on a dynamic mathematical model of the bus behavior.

The aggregation of the flexibility regions of different devices is reasonably well-explored: the aggregation of energetic flexibility in the broadest sense is a Minkowski sum of vector spaces. This description can be found, for example, in [Müller et al. 2015]. This allows assigning the bus feasible reference values for the active and reactive power generation or consumption without having to represent the flexibility regions of individual devices at higher levels of the power grid control structure.
The calculation of such appropriate reference signals transmitted to each device that yield requested sum power flows is a control problem of distributed devices which seeks to calculate desired power generation or consumption levels for each controllable device in such a way that control goals for the grid are fulfilled. Recent years have given rise to a very large and colorful variety of such controllers. The closest mathematical relatives are the various classes of microgrid control such as linear-quadratic Gaussian control in [Ouammi et al. 2015], or in [Y. Zhang et al. 2013] using decomposition and subgradient methods for optimization of the device allocation. However, these controller only optimized for traditional economic goals. Distributed model-predictive control was used by [Yi et al. 2021] using a neurodynamic communication framework for frequency control and similar distributed optimization was used in [Cady et al. 2015] and also in [Chen et al. 2015] including both technical constraints and economic objectives. Similar allocation problems can also be found in research concerning virtual power plants, starting with classic research papers such as [Strbac 2007; Giuntoli et al. 2013] and later improvements such as [Kardakos et al. 2016]. However, these works introduced virtual power plants as a static aggregation which sought to optimize the economic performance in the energy market and did not cover their dynamic behavior. Even dynamic virtual power plant controllers that did react to grid conditions such as [Muuß et al. 2015] did so on long (i.e. non-dynamic, on the order of minutes or hours) timescales. In short, while there is a large variety of different approaches related to control and optimization with a view on economic objectives, the complex dynamic effects this has on the grid are not studied nor are these effects a part of the controller design. A controller that fulfills these objectives while also reducing dynamic complexity has not been developed. Classical load model aggregation is unsuitable for the device aggregation described here because of the bidirectionality of their power flows and the much greater complexity in behavior that results from this. In contrast, some efforts have been made to aggregate variable-frequency drives (VFDs) using generic models in [Mitra et al. 2020] and of active distribution networks using machine learning in [Kontis et al. 2019]. However, both approaches are severely limited because they either only cover a class of VFDs or investigate the steady-state response after a voltage drop.
All these approaches regard aggregation and control as essentially decoupled tasks: first a controller is designed and then, completely independently and generally in a different publication by different authors, an attempt is made to provide a reduced-complexity model. This approach misses an opportunity that will be explored here: the controlled behavior of a controllable device or an aggregation of devices is a result of the controller design and not random. By designing a controller specific to the requirements of aggregation as well as operation, it is possible to generate closed-loop behavior that inherently results in a desired aggregation. This is the approach chosen in this chapter.

3.3. Aggregated Flexibility Region

The flexibility region B of a distributed device connected to the power grid is a vector space in the complex plane, the active power generation or consumption being along the real axis and the reactive power generation or consumption being along the imaginary one. The possible shapes of such a vector space generally fall into one of a few categories; for example, the flexibility of a generator is roughly a filled semicircle bounded by a maximum apparent power S and limited to $\Re(B) \geq 0$. A storage device has either a full circle or a line along the real axis, depending on the device's power electronics and their ability to provide reactive power. These vector spaces change over time as a storage device is charged and discharged or environmental conditions change and generators can provide more or less power. For example, a storage device at full charge resembles a generator in that it cannot absorb any active power and its flexibility region is reduced to a semicircle. The exact shape of the flexibility region of a device depends on the device and the degree of faithful modeling, but examples can be found, for example, in [Riaz et al. 2019] and [D. A. Contreras et al. 2019].
The aggregation of flexibility regions represented by vector spaces B_1 and B_2 is the Minkowski sum $B_1 \oplus B_2$ [Müller et al. 2015]. For computational reasons, vector spaces with smooth hulls such as those bounded by a constant apparent power S are usually represented as polytopes, just like those with non-smooth hulls. This approximation is easily computed using sampling. The Minkowsi sum is commutative and therefore the sequence of addition is irrelevant. This implies that the aggregated flexibility region F of a bus with n_d connected devices, each with flexibility region B_{i_d}, is simply the sequence of Minkowski sums:

$$F = \overset{\oplus}{\sum_{i_d=1}^{n_d}} B_{i_d}. \tag{3.1}$$

Note that B_{i_d} does not have to be convex, though this somewhat simplifies computation. Minkowski sums of polygons such as the flexibility regions in this chapter are not difficult or expensive to compute. Convex Minkowski sums run in worst-case linear time $O(m + n)$ for polygons with $\{n, m\}$ vertices and non-convex Minkowski sums run in worst-case polynomial time $O(n^2 m^2)$. This extends to any number of polygons because the Minkowski sum is commutative. For algorithms, see [Berg et al. 2008].
Since the Minkowski sum is dwarfed computationally by other computational challenges in this chapter, the algorithm implemented is unoptimized and runs in polynomial time (it is essentially the non-convex algorithm). The hulls of B are defined using polytopes and all vectors of the polytopes are added to all vectors of the other polytope to construct a new preliminary vector space $F_{\text{preliminary}}$, as in:

$$F_{\text{preliminary}} = \vec{b_1} + \vec{b_2}, \;\; b_1 \in B_1, b_2 \in B_2, \forall\, b_1, b_2. \tag{3.2}$$

The final flexibility region F is constructed from this using the convex hull algorithm

Quickhull [Barber et al. 1996]. All the flexibility regions defined in this chapter are convex and therefore this is permissible.
Non-controllable devices (such as traditional loads) can be included with controllable devices: they become another part of the Minkowski sum and translate F by the complex vector representing the non-controllable load at any point in time. This produces a minor benefit in that it further simplifies modeling in the distribution grid, but it is not of great consequence. A visualized description of Minkowski sums is given in appendix chapter C.

3.4. Aggregated Dynamic Behavior

The closed loop of a distributed device controlled for power generation or consumption generally observes first-order transfer function behavior (for simplicity here with unity gain and for either active or reactive power individually):

$$G_{i_d}(s) = \frac{1}{T_{i_d} \cdot s + 1}. \tag{3.3}$$

This observation results from the integral control used in many such generators, the assumed linear independence of active and reactive power, and can be found, for example, in [Keyhani et al. 2009; Mahmoud et al. 2015] and observed in [El-Sharkawi 2011]. T_{i_d} is time-invariant since it is based on the technical properties of the device and its controllers, not on changing environmental conditions which affect the flexibility region. More generally, if the open-loop power generation or consumption behavior of a distributed device follows any non-linear function

$$y = f(u), \tag{3.4}$$

with y being either the active or reactive power, then choosing the controller

$$\begin{aligned} u &= f^{-1}(v), \\ v &= \frac{1}{T} \int e \, \mathrm{d}e \end{aligned} \tag{3.5}$$

will lead to a closed-loop transfer function exhibiting first-order transfer function behavior with the control error $e = r - y$, where r is the reference signal of the active or reactive power, depending on which is being analyzed:

$$\begin{aligned} y &= f\left(f^{-1}\left(\frac{1}{T} \int e \, \mathrm{d}e\right)\right), \\ y &= \frac{1}{T} \int e \, \mathrm{d}e = \frac{1}{Ts} e = r \frac{1}{Ts + 1}. \end{aligned} \tag{3.6}$$

In practice $f^{-1}(v)$ is generally not a causal function, but causal approximations still yield closed-loop behavior which approximates a first-order transfer function. This implies that distributed generators can always be designed to behave as first-order transfer functions, though possibly at the cost of some dynamic performance.
At present, manufacturers are free to implement essentially whatever controller they want in their devices, and this information is usually proprietary. System identification is often the only way of gathering information on the dynamic behavior of individual devices. Since manufacturers are unlikely to relinquish knowledge on their DG controllers, grid codes would have to be changed to force manufacturers to use controllers that result in equation 3.3.
With the assumption that the device i_d can reasonably be characterized by the transfer function in equation 3.3, the bus has the power transfer function, either active or reactive and assuming they are perfectly decoupled, of the sum of these first-order transfer functions:

$$\begin{aligned} y &= \sum_{i_d=1}^{n_d} R_{i_d} G_{i_d}(s) \\ &= \frac{R_1(T_2 s+1)\cdots(T_{n_d} s+1) + \cdots + R_{n_d}(T_1 s+1)\cdots(T_{n_d-1} s+1)}{(T_1 s+1)(T_2 s+1)\cdots(T_{n_d} s+1)}. \end{aligned} \tag{3.7}$$

The second line derives from the first by making the denominator of all the transfer functions the same. The denominator of this transfer function will not generate instability, over- or undershoot: it has n_d all-negative, stable poles $s = -\frac{1}{T_{i_d}}$ and $m = n_d - 1$ zeros at $s = -\frac{1}{{}^0T_j}$ with n_d connected devices. The gains R_{i_d} depend on the reference values assigned to the different devices relative to the current output according to $R_{i_d} = r_{i_d} - y_{\text{curr},i_d}$, which can be confirmed using the steady state of $s = 0$.
However, this implies that the bus behavior is not necessarily measure-preserving under all conditions. Recall from classical control theory that, for example,

$$\begin{aligned} y =& r({}^0T s + 1)G(s) \\ =& r({}^0T)sG(s) + rG(s), \end{aligned} \tag{3.8}$$

meaning that a transfer function zero at $-\frac{1}{{}^0T}$ can be thought of as adding a derivative of the transfer function without the zero. Sufficiently large values of ${}^0T$ result in y temporarily exceeding r, generating overshoot, while negative values of ${}^0T$ can result in undershoot. The transient nature of derivatives invariably makes this behavior temporary and does not affect the steady state $s = 0$ where the term vanishes, but transient over- or undershoot could not be reflected by a first-order approximation. However, a first-order approximation for the bus would be ideal because it allows very inexpensive simulation at larger scales. Behavior which isn't measure-preserving (i.e. it over- and undershoots) is also more difficult for higher-level controllers, since an over- or undershoot in the power generation or consumption might violate operational safety limits. The bus controller should eliminate this behavior for these reasons.

Ideally the bus as a whole would behave similar to another first-order transfer element so that it can be approximated well as a first-order element. Since most of the undesirable behavior in equation 3.7 comes from the numerator, an ideal form of the transfer function for this bus would eliminate all the Laplace variables in the numerator and look like this:

$$y = \frac{\sum_{i_d=1}^{n_d} R_{i_d}}{(T_1 s + 1)(T_2 s + 1) \cdots (T_{n_d} s + 1)}. \tag{3.9}$$

It would simply have the final gain of the transition in the numerator. A way must be found to eliminate all the other coefficients from the numerator. We can multiply out equation 3.7 to arrive at the following equations:

$$\begin{aligned} y &= \frac{a_1 s^{n_d-1} + a_2 s^{n_d-2} + \cdots + a_{n_d-1} s + \sum_{i_d=1}^{n_d} R_{i_d}}{(T_1 s + 1)(T_2 s + 1) \cdots (T_{n_d} s + 1)}, \\ y &= \frac{\overbrace{a_1 s^{n_d-1} + a_2 s^{n_d-2} + \cdots + a_{n_d-1} s + 1}^{\text{Factorization}} - 1 + \sum_{i_d=1}^{n_d} R_{i_d}}{(T_1 s + 1)(T_2 s + 1) \cdots (T_n s + 1)}, \\ &= \frac{(h_1 s + 1)(h_2 s + 1) \cdots (h_m s + 1) - 1 + \sum_{i_d=1}^{n_d} R_{i_d}}{(T_1 s + 1)(T_2 s + 1) \cdots (T_{n_d} s + 1)}, \end{aligned} \tag{3.10}$$

h_j must be calculated using polynomial factorization (performed later using MATLAB's `numden`. For more algorithms, see [Hachenberger et al. 2020]). Due to this, all h_j depend on all R and T:

$$h_j = f_{\text{fac}}(R_1, R_2, \cdots, R_{n_d}, T_1, T_2, \cdots, T_{n_d}). \tag{3.11}$$

This might seem like a complex disadvantage, but it also means that the chosen reference functions for the connected devices directly influence the observed dynamic behavior through R. In most cases, there are an infinite number of ways to achieve some desired sum power flow by assigning relatively more or less generation or consumption to the various devices. An optimization algorithm could carefully choose appropriate R which bring all h_j to zero, which leads to the collapse of all factorized terms:

$$\begin{aligned} y &= \frac{(h_1 s + 1)(h_2 s + 1) \cdots (h_m s + 1) - 1 + \sum_{i_d=1}^{n_d} R_{i_d}}{(T_1 s + 1)(T_2 s + 1) \cdots (T_{n_d} s + 1)}, \\ y &= \frac{\sum_{i=1}^{n_d} R_{i_d}}{(T_1 s + 1)(T_2 s + 1) \cdots (T_{n_d} s + 1)}, \quad \Leftarrow \forall\, h_j = 0. \end{aligned} \tag{3.12}$$

How the optimization algorithm in the controller obtains such solutions for R will be the topic of the next section. For now, it will be assumed that it is possible. A first-order approximation G_Σ of a sum of first-order transfer functions can then be calculated using the sum-of-time-constants method (taken from [Kuhn 1995]) which weighs the time constants according to their contribution to the response:

$$\begin{aligned} T_\Sigma &= \sum_{i_d=1}^{n_d} T_{i_d} - \sum_{j=1}^{m} {}^0T_j \\ &= \frac{\sum_{i_d=1}^{n_d} R_{i_d} T_{i_d}}{\sum_{i_d=1}^{n_d} R_{i_d}} \\ R_\Sigma &= \sum_{i_d=1}^{n_d} R_{i_d} \\ \implies G_\Sigma &= \frac{R_\Sigma}{T_\Sigma \cdot s + 1}. \end{aligned} \tag{3.13}$$

This can be calculated from equation 3.10 or 3.7 by multiplying it out and factorizing again if the form using ${}^0T_j$ is used:

$$\begin{aligned} y &= \frac{a_1 s^{n_d-1} + a_2 s^{n_d-2} + \cdots + a_{n_d-1} s + \sum_{i_d=1}^{n_d} R_{i_d}}{(T_1 s + 1)(T_2 s + 1) \cdots (T_{n_d} s + 1)}, \\ &= \frac{({}^0T_1 s + 1)({}^0T_2 s + 1) \cdots ({}^0T_m s + 1)}{(T_1 s + 1)(T_2 s + 1) \cdots (T_{n_d} s + 1)}. \end{aligned} \tag{3.14}$$

Otherwise it can be calculated more efficiently using the controller output R_{i_d} and the device constants T_{i_d} as in equation 3.13.
Note that the approximation in equation 3.13 is measure-preserving and has neither undershoot nor overshoot (it is simply a first-order transfer function). The sum-of-time-constants method has the rather useful property of yielding an approximation which has the same integral absolute error in a step response as the original transfer function if the original is also measure-preserving in the sense that it has no over- or undershoot. This means that while a simulation of the aggregated bus (such as by the SPC controller or some other entity) might not follow precisely the same dynamic dynamic behavior as the distributed devices "in the wild," the integral of the control error of the response is the same. The approximation constants T_Σ and R_Σ can then be reported to the higher-level SPC controller by the bus controller to allow very computationally inexpensive simulation of the aggregate dynamic behavior of the bus. Since first-order transfer functions have an analytic solution (that being the exponential decay function), numerical simulations wouldn't be required either — the solution can be evaluated directly.
The next chapter will describe in more detail the controller which generates the signals that minimize h_j while following reference signals to maintain this first-order approximation of the bus.

3.5. Reference Signals

3.5.1 Reduced Complexity Control

The bus controller reports the aggregated flexibility region F of the bus to the SPC controller, which calculates a reference apparent power generation or consumption $\vec{r}_{S\to B}$ for

the bus based on grid-wide considerations such as power balance and the local voltages and sends $\vec{r}_{S\to B}$ to the bus controller. The bus controller then has the obligation to calculate individual reference signals $\vec{r}_{i_d}$ for the connected devices satisfying the constraints

$$\vec{r}_{S\to B} = \sum_{i_d=1}^{n_d} \vec{r}_{i_d} \qquad \wedge\ \vec{r}_{i_d} \in B_{i_d}\ \forall\ \vec{r}_{i_d}. \tag{3.15}$$

These constraints represent that the sum $\sum_{i=1}^{n} \vec{r}_{i_d}$ of the generation or consumption of the different devices must satisfy the requested generation or consumption $\vec{r}$ of the higher-level controller and that each reference signal must come from inside the respective device's flexibility region B_{i_d}. Despite these constraints, this problem generally does not have a single unique solution when more than one device is connected and $\vec{r}_{S\to B}$ is not on the hull of F. This is good: it allows assigning reference signals to the various devices subject to some kind of optimality. The coefficients h as described in the previous chapter need to be minimized to limit the complexity of the dynamic behavior of the bus and to approach the approximation in equation 3.13. Therefore an objective function is added to the controller which is to be minimized:

$$o_h = \sum_{j=1}^{m} |h_{P,j}| + \sum_{j=1}^{m} |h_{Q,j}|\,, \tag{3.16}$$

where h_P are the calculated transfer function coefficients along the real, active power axis while h_Q are the calculated transfer function coefficients along the imaginary, reactive power axis as defined in equation 3.12. Naturally it would be ideal if $h_j = 0$ could be guaranteed for all r, but solutions on the hull of the flexibility region can be unique and may not guarantee this condition (see [Fukuda 2004] for a variety of uniqueness and decomposition proofs). This is regrettable, but also unavoidable without shrinking the flexibility region F. Such intentional shrinking will be explored in a later section. Therefore the algorithm attempts to bring all the terms of h_j to zero instead of including it as an equality constraint that may not allow a solution.
This results in a non-linear optimization problem with both linear equality constraints ($\vec{r}_{S\to B} = \sum_{i_d=1}^{n_d} \vec{r}_{i_d}$) and non-linear inequality constraints ($\vec{r}_{i_d} \in B_{i_d}$). Two common algorithms used for such problems are sequential quadratic programming (SQP) and interior-point. Both will be tested in section 3.7.
There is guaranteed to be at least a unique solution to the constraints on the hull of F and normally a set of solutions for the optimization problem. This is because F is transmitted to the SPC controller before it sends a new bus reference signal and the device flexibility regions B are still used as constraints to the optimization problem.

3.5.2 Control Mode Comparisons

Two other optimization functions to generate $\vec{r}_{i_d}$ are defined here to demonstrate that the algorithm to reduce complexity provides a tangible difference in dynamic behavior. For

example, the algorithm might strive to share the reference generation or consumption proportionally across all connected devices (a form of load sharing):

$$o_l = \sum_{i_d=1}^{n_d} \left\| \vec{r}_{i_d} \oslash \vec{r}_{i_d,\max} \right\| \\ \wedge \vec{r}_{i_d,\max} \neq 0, \tag{3.17}$$

where $\oslash$ is the Hadamard operator representing element-wise division. Another possibility would be limiting the reactive power which is wasted when a device consumes reactive power generated by a device at the same bus:

$$o_c = \sum_{i_d=1}^{n_d} \left(\frac{\Im\left(\vec{r}_{i_d}\right)}{\Im\left(\vec{r}_{i_d,\max}\right)} \right)^2 \\ \wedge \vec{r}_{i_d,\max} \neq 0. \tag{3.18}$$

These control modes represent more conventional control goals in a power grid and they will be compared against function 3.16 for illustration. Functions o_l and o_c are not considered to be original. They are used only to better demonstrate the behavior of the o_h mode by comparing it against different functions.

3.6. Avoiding Unique Solution Vectors $\vec{r}_{i_d}$

3.6.1 Unique Solution Vectors

Consider the Minkowski sum of a rectangle and a semicircle in figure 3.4. A number of vector additions to the hull (the limit or border) of the Minkowski sum are indicated. These specific vector additions are unique — they are the only way of constructing vectors that reach those specific points in the PQ-plane. Attempting to change one of the two vectors of each addition and then compensating for this change using the other vector is impossible; it would violate the limit of that vector's vector space.
Since reference vectors $\vec{r}_{S\to B}$ that lie on the hull of the aggregated flexibility region F generally have unique solutions $\vec{r}_{i_d}$, they therefore do not allow any sort of optimization of the function 3.16: the optimization algorithm manipulates the coefficients h by assigning more or less power generation or consumption among the controlled devices (refer to equation 3.11). This is also described in more detail in appendix chapter C. As explained, the purpose of the optimization function is the minimization of the coefficients h in the transfer function that lead to transient under- and overshoot, so not being able to optimize this function means that the controller may not be able to satisfy one of its primary design goals.

3.6.2 Shrinking Vector Spaces

The uniqueness of these solutions is a fundamental feature of the Minkowski sum [Fukuda 2004] and of energetic flexibility in general; the vectors forming the hull of F are the

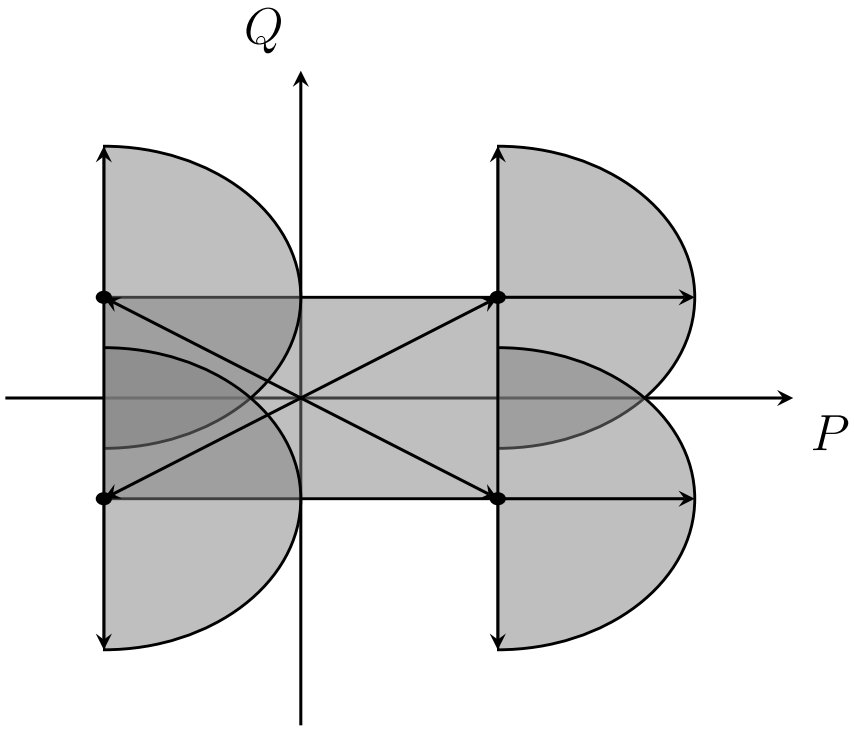

Figure 3.4: Vectors on Hull of Minkowski Sums

result of the vector addition of vectors forming the hulls B_{i_d}. Therefore the only way to avoid unique solutions is to reduce the size of the flexibility region F so that the hull of F is not presented as a permissible reference signal $\vec{r}_{S\to B}$ to the higher-level controller. In principle, this could be done before or after the the Minkowski sum F is calculated by either shrinking F directly or by shrinking B_{i_d} before addition. Shrinking B_{i_d} offers the advantage that all individual flexibility regions B_{i_d} can be shrunk by a uniform factor and no device is unduly impacted. The disadvantage is that the algorithm which reduces the size of the flexibility region has to be executed for each B_{i_d} instead of only once for F. Unlike the aggregation of the flexibility regions into F, which is perforce conducted using the Minkowski sum, this reduction can be performed using different mathematical operations that each offer different advantages in the context of this control problem. The aggregated region F will be used in the following equations since the operations would be analogous for B_{i_d}. More algorithms to reduce the flexibility region are possible and only two will be explored here for the sake of brevity.

3.6.3 Minkowski Difference

A simple solution would be the Minkowski difference (using the set complement $A^c = \overline{A}$ and taken from [Hadwiger 1950])

$$\begin{aligned} F_{\text{reduced}} &= F - L \\ F_{\text{reduced}} &= (F^c + (-L))^c, \end{aligned} \tag{3.19}$$

where L should be defined as a circular vector space whose radius gives the distance from the hull which F is uniformly reduced by to create F_{reduced}. This method behaves well for convex flexibility regions but not for non-convex shapes since the reduction distance from the hull is constant and risks entirely eliminating narrow non-convex features. A graphical example is given in figure 3.5. It is important to note that this operation is not isomorphic: this means that the original shape of F cannot be reconstructed from F_{reduced} even if L is known.

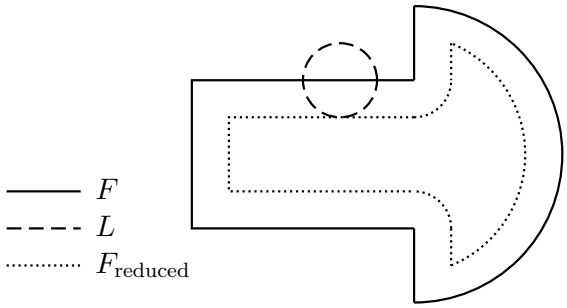

Figure 3.5: Reduction Using Minkowski Difference

3.6.4 Convex Decomposition & Rescaling

Rescaling for a convex polytope would calculate the centroid of the flexibility region, translate the centroid to the origin, scale the vectors of the hull by some factor $\lambda < 1$, and then translate the centroid back. This operation has the advantage of being isomorphic and relatively simple. However, it is not a safe operation for non-convex flexibility regions since it moves non-convex features with respect to the main centroid. This can result in non-convex features being present in areas outside the original flexibility region F with the catastrophic result that such reference vectors would not be tracked by the physical system. A non-convex flexibility region would first have to be decomposed into its elementary convex polytopes using algorithms such as [Chazelle et al. 1985], scaled, and then recombined along the decomposition vertices. This does not eliminate narrow features and is isomorphic, but it does not guarantee the removal of all vectors forming the hull of F either. An example is given in figure 3.6. Note that parts of the hulls of F and F_{reduced} are unfortunately identical.
Non-convexity in a flexibility region can arise, for example, from YΔ connections producing different operational envelopes [Lund et al. 2007], though generally the flexibility regions of distributed generators are convex and behave well.

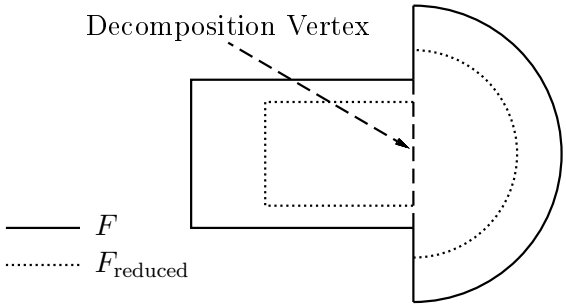

Figure 3.6: Reduction Using Convex Decomposition

3.7. Verification

3.7.1 Primary Control Mode o_h

Armed with the knowledge of the preceding chapters, an example bus can be analyzed and simulated in the time domain. The example will consist of a generator and a combination of battery and static VAR compensator. The small number of connected devices is chosen for graphical visiblity. Scalability will be shown later. The combined flexibility region is depicted in figure 3.7. The generator flexibility is modeled as a semicircle while the battery and static VAR compensator are lines on the real and imaginary axis, respectively. The Minkowski sum is depicted in bold black. The base values are listed in appendix table D.1.
Two reference transitions were chosen for visibility inside the flexibility region. Solutions to the computational problem of assigning reference signals for the state transitions according to section 3.5, equation 3.16 were calculated using sequential quadratic programming (SQP) and interior-point. Solutions were identical and the computational load is compared in appendix table D.3. SQP is substantially faster.
The time constant of the generator T_{gen}, the time constant of the battery T_{bat}, and the time constant of the static VAR compensator T_{var} are listed in appendix table D.4. The reference vectors $\vec{r}_{S\to B}$ are listed with their transition times in appendix table D.2. The calculated approximation constants for $T_{\Sigma,P}$ and $T_{\Sigma,Q}$ during those transitions can be found in appendix table D.4 as well. The solution vectors are depicted graphically using vector addition in figure 3.7.
The dynamic behavior of the system in the time domain is again shown in figures 3.8 and 3.9 for the active and reactive power generation or consumption of the bus. The bus begins the simulation at $t = 0\,\text{s}$ at a reference consumption of $\vec{r}_{S\to B} = [-3 + j2]$ and immediately receives a reference signal to transition to $\vec{r}_{S\to B} = [-2 - j5]$. At $t = 1\,\text{s}$ it receives another reference signal to transition to $\vec{r}_{S\to B} = [7 - j4]$. The plots have been split at $t = 1\,\text{s}$ for improved visibility of the transfer function behavior so that these two reference steps are displayed on their own scales and can be better compared to their approximations. The first-order approximations G_Σ calculated using equation 3.13 are shown as dash-dot lines together with the full-order response as a solid line. The

aggregate reference states for the transition of the whole bus are shown as a dotted line. These reference states are shown using small circles in figure 3.7. Note that since the controller enforces first-order lag behavior, the steady-state error will also tend towards zero for $\lim_{t\to\infty}$.

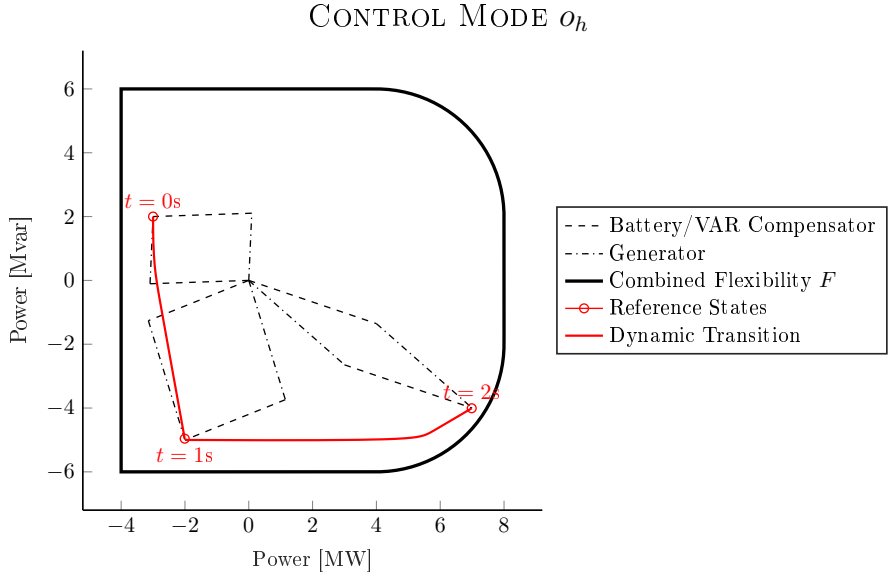

Figure 3.7: Dynamic Simulation (P/Q-plane) with Flexibility Region (o_h)

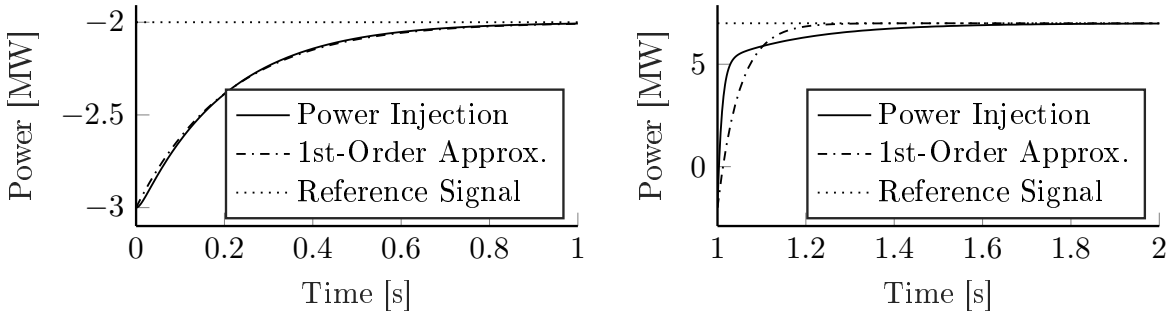

Figure 3.8: Dynamic Simulation (Active Power, o_h)

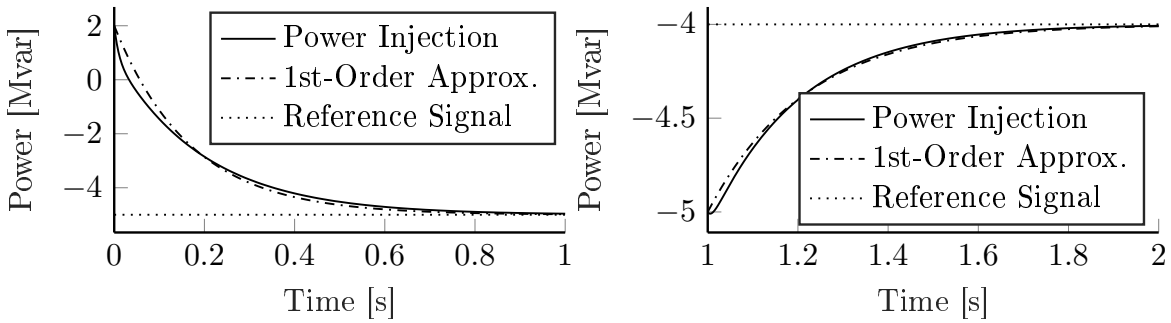

Figure 3.9: Dynamic Simulation (Reactive Power, o_h)

It can be seen from the simulation that the dynamic behavior of the bus contains no

overshoot and the approximation reported by the bus controller based on T_Σ is accurate. Note also that the reference signals given to the controller are quite close to the hull of F. The controller therefore has only limited ability to optimize h due to the problems with unique solutions outlined in chapter 3.6. Nevertheless the controller works as designed, although less ideal behavior would be expected from reference signals on the hull of F. All the design goals of the controller outlined in section 3.4 are therefore fulfilled and the controller works successfully.

3.7.2 Comparison Control Modes o_c, o_l

As explained in section 3.5, showing that the control mode o_h does not generate under- or overshoot is not meaningful without knowing that other modes will generate such behavior quite regularly. A comparison to the two other control modes described in chapter 3.5 will be made here. The behavior according to the alternate control modes described by equations 3.17 and 3.18 show over- and undershoot. The dynamic behavior of control mode o_l is shown in figure 3.10 in the P/Q-plane and in figures 3.11 and 3.12 in the time domain. The dynamic behavior of control mode o_c is shown in figure 3.13 in the P/Q-plane and in figures 3.14 and 3.15 in the time domain.
Both functions show substantial over- or undershoot in figures 3.12, 3.14, and 3.15. This degrades the accuracy of the T_Σ approximation and potentially endangers grid stability and reliability. Compare this undesirable behavior to the designed o_h mode, which suppresses it in figures 3.8 and 3.9. It is clear that the design goal of the controller in mode o_h – enforcing first-order transfer function behavior – is achieved.

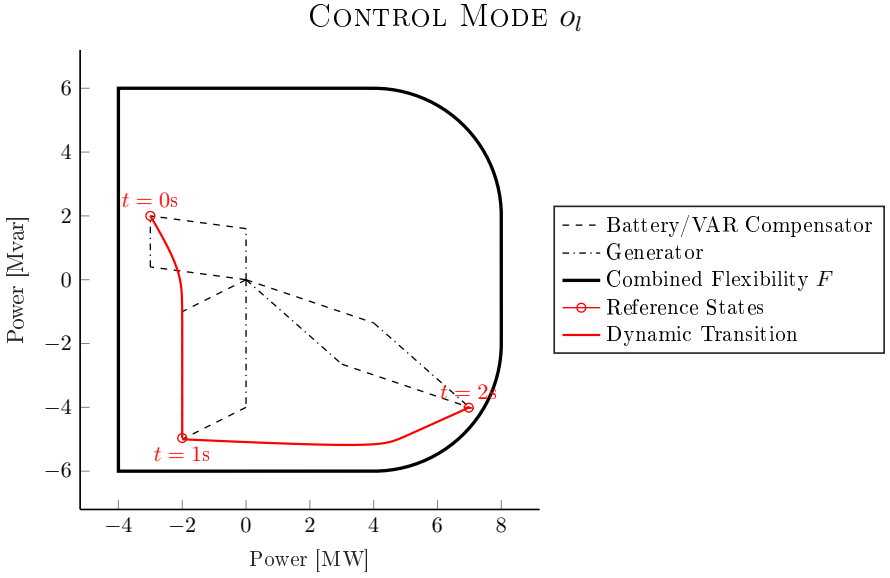

Figure 3.10: Dynamic Simulation (P/Q-plane) with Flexibility Region (o_l)

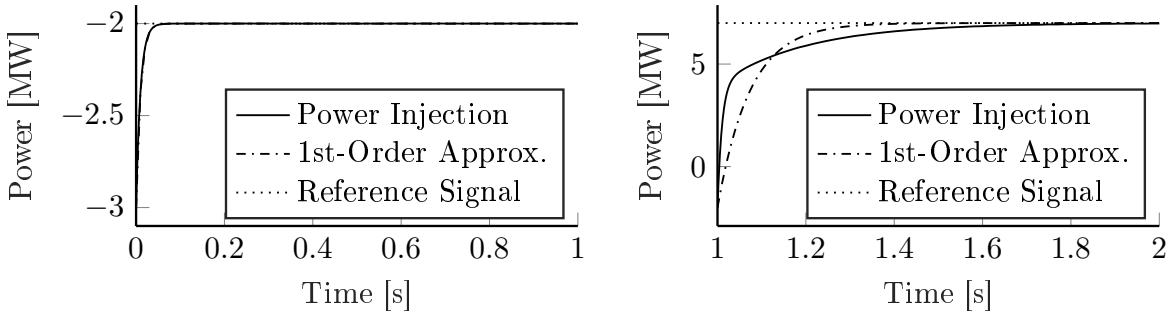

Figure 3.11: Dynamic Simulation (Active Power, o_l)

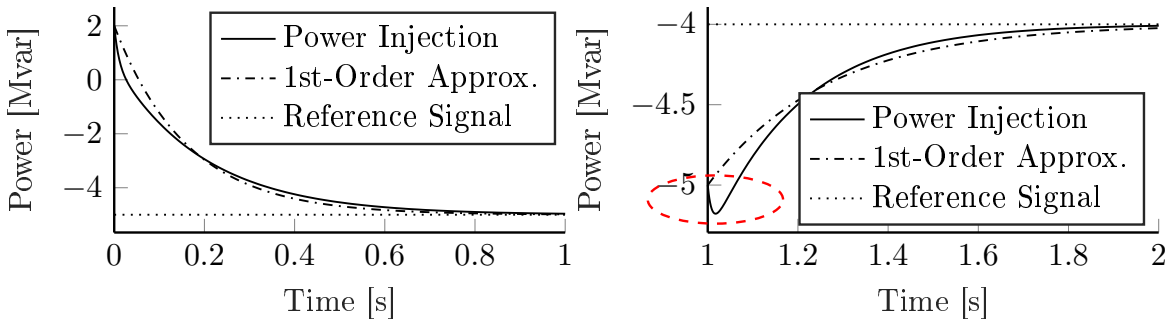

Figure 3.12: Dynamic Simulation (Reactive Power, o_l) – Note Undershoot

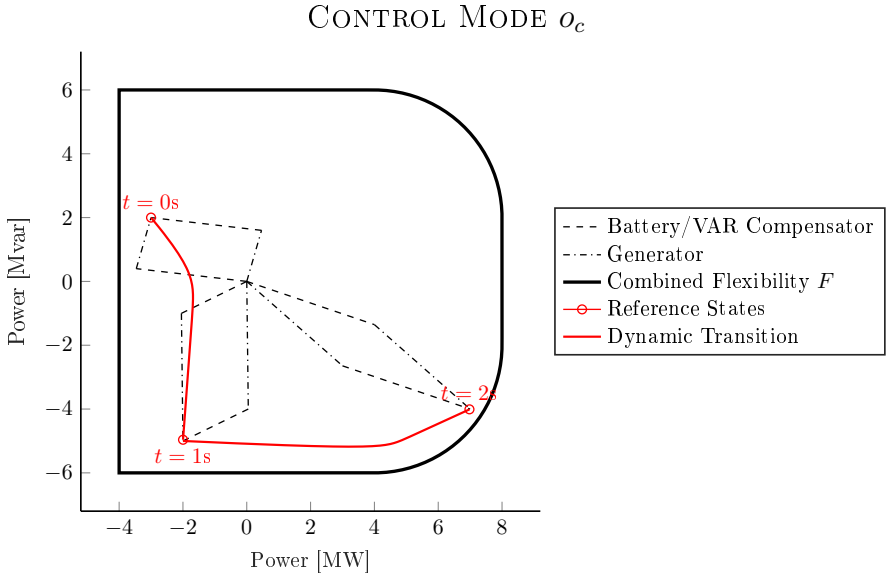

Figure 3.13: Dynamic Simulation (P/Q-plane) with Flexibility Region (o_c)

3.7.3 Scalability

The previous simulations were made using a bus with few devices to make a vector visualization of the bus behavior possible. It shall be demonstrated that the algorithm is also scalable. A bus with 30 random devices is simulated as it responds to a random reference step using mode o_h. The response is shown in figure 3.16 for the active power and

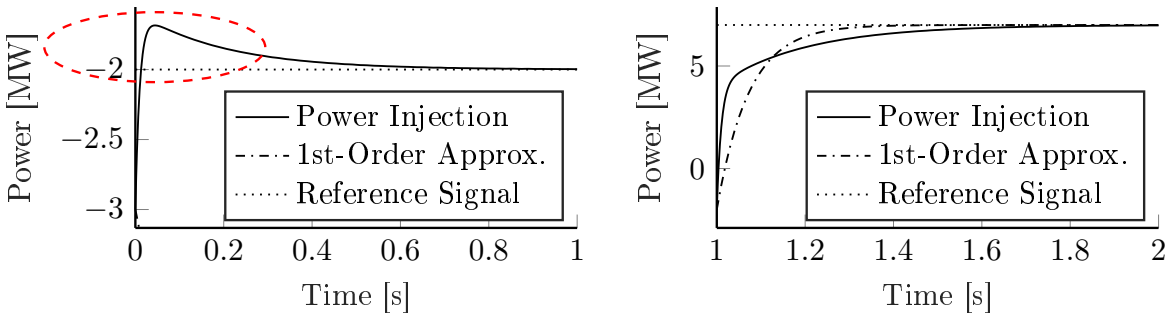

Figure 3.14: Dynamic Simulation (Active Power, o_c) – Note Overshoot

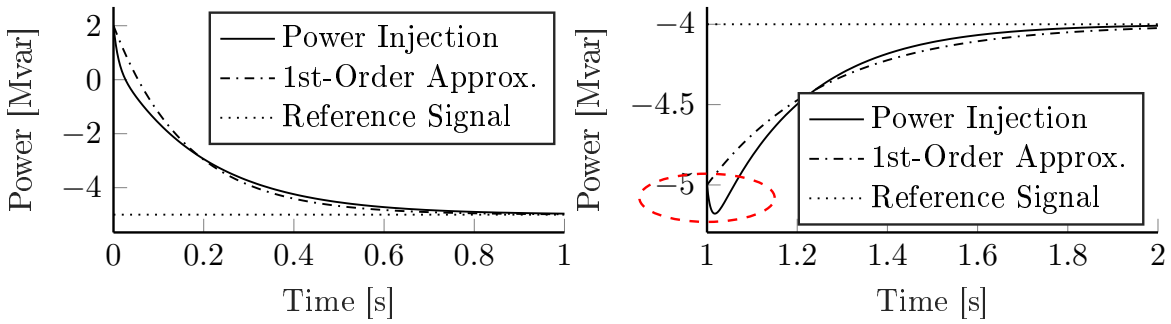

Figure 3.15: Dynamic Simulation (Reactive Power, o_c) – Note Undershoot

figure 3.17 for the reactive power. The calculation time for the Minkowski sum aggregation was 0.03 s and the calculation time for the optimization algorithm using SQP was 0.24 s. This shows that the algorithm is scalable. The symbolic factorization required to calculate the coefficients in equation 3.7, which are necessary for the optimization to run efficiently, becomes expensive for large buses and can require several minutes, but this needs to be calculated only once, not in real-time. The given computation times here and previously are relative to MATLAB running on an office computer. The shown first-order approximations were calculated as given in equation 3.13.

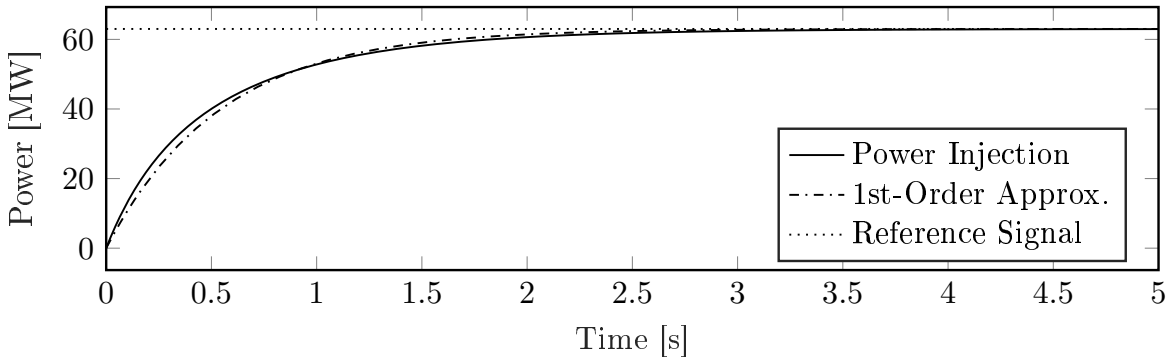

Figure 3.16: Dynamic Simulation (Active Power, Large Bus, o_h)

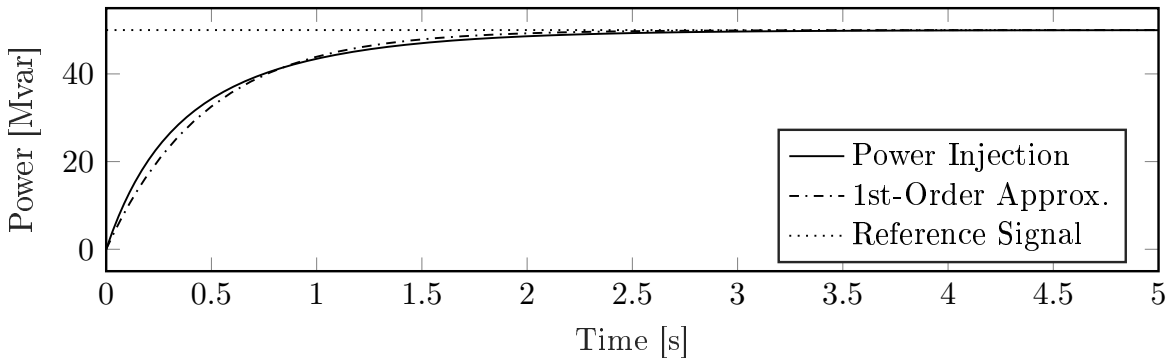

Figure 3.17: Dynamic Simulation (Reactive Power, Large Bus, o_h)

Chapter Summary

The bus controller described in this chapter controls a single bus in the medium- or low-voltage grid to which an array of distributed generators, flexible loads, storage devices, multi-modal interfaces or some other such controllable installations with diverse dynamic behavior are connected. It uses a constrained optimization problem to allocate reference signals to each connected device in such a way that the collective dynamic behavior of the power generation or consumption of the bus approximates a first-order transfer element with no under- or overshoot as well as satisfying the generation or consumption requested by the higher-level controller. The bus controller also respects the operational flexibility limits of each connected device.

The bus controller communicates what the time constant of its current first-order approximation is to the next higher-level controller, presumably the one controlling a Smart Power Cell in the distribution grid. It also communicates the aggregated flexibility region of the bus. The advantage of this is that for the higher-level controllers, the bus behaves as a single controllable device with first-order transfer function behavior using a single flexibility region. Whatever happens inside the bus does not have to be represented in more detail than that in the models or in the controller design of higher-level controllers.

The controller itself is computationally inexpensive and easily scalable to dozens of controllable devices, but the factorization of the coefficients for the optimization function becomes expensive with a large number of devices. However, this factorization is performed off-line and only once, so it doesn't represent a serious drawback.
The controller does not control the bus or the devices for voltage directly. The bus voltage is instead intended to be controlled by the higher-level SPC controller in the distribution grid by sending appropriate reference signals from the SPC controller to the bus controller. This disadvantage limits the bus controller to geographically close devices. The reasoning is that the bus controller already controls for two potentially opposing control goals (power flow and also limited complexity), so assigning bus voltage control to the SPC controller spreads dynamic complexity more evenly throughout the controller hierarchy. This is covered in the next chapter together with the other control goals of the SPC controller.

Internal Control of Smart Power Cells

The bus controllers of the previous chapter allow simplified, controlled behavior of the buses inside a Smart Power Cell, but most core functions of the Smart Power Cell are not handled by them. They merely follow the reference signals sent to them by the SPC in the most dynamically benign way possible. A controller in the Smart Power Cell is necessary to generate reference signals for the bus controllers based on reference signals sent to the SPC and based on the internal requirements of the SPC. The end goal of the Smart Power Cell is being a self-contained, stable entity inside the transmission grid that is controllable and dispatchable for the transmission system operator. The development of such a controller for the SPC as a whole is the subject of this chapter.

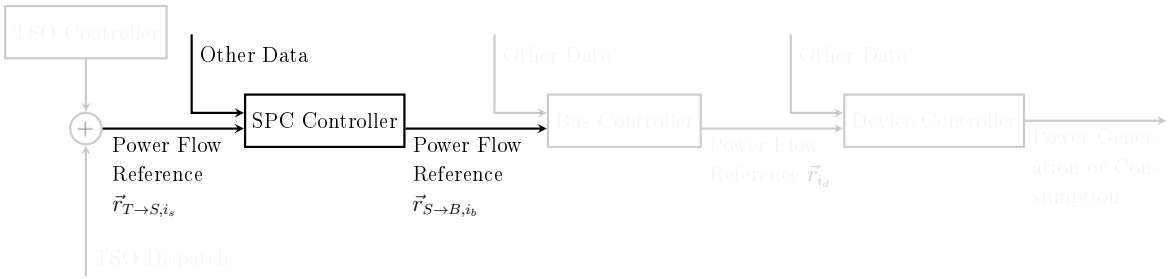

Figure 4.1: Controller Hierarchy Overview (Current Chapter in Bold)

Such a Smart Power Cell is interconnected with the transmission grid and other Smart Power Cells and by tracking reference signals for the power flow at these interconnections, the SPC follows the commands of the TSO. The location of the SPC controller inside the controller hierarchy is given in figure 4.1. A schematic depiction of the SPC controller inside an example grid is given in figure 4.2. The SPC controller provides an intermediate layer between the transmission system operator and the large numbers of bus controllers and connected devices (controllable generators, loads, storages, etc).

4.1. Design Goals of SPC Controller

The control variables of the SPC are its controlled buses. As described in chapter 3, these controlled buses are an accurate simplification of a variety of controlled generators,

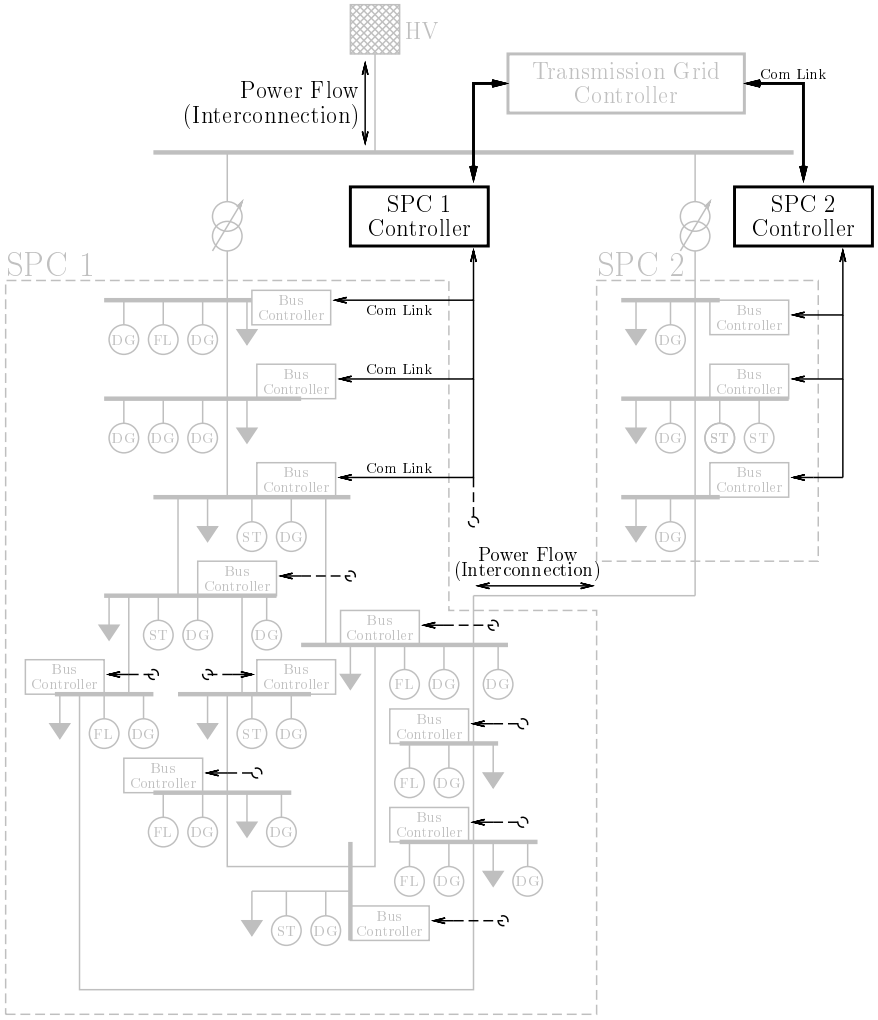

Figure 4.2: Location of SPC Controllers in an Example Grid with Distributed Generators (DG), Flexible Loads (FL), and Storages (ST)

loads, storages, multi-modal interfaces, et cetera connected to a bus in the SPC. The SPC controller then sends reference signals to these buses based on the following criteria:

1. Following reference signals for the power flow at the TSO-SPC interconnection sent to the SPC by the TSO.

2. Following reference signals for the power flow at any SPC-SPC interconnection(s) sent to the SPC by the TSO or DSO (in case regulations determine that medium-voltage interconnections between SPCs are the responsibility of the DSO).

3. Maintaining safe voltages at all buses inside the SPC.

Note that, as described here, it is the TSO or DSO which determines the reference signals for the power flow at the interconnections between an SPC and its neighboring SPCs. In practice, this might not be desirable if the grid operators have no interest in dispatching medium-voltage interconnections or no ability to do so. In such a case, interconnection power flow reference values could be calculated by the SPCs using an algorithm based

on consensus such as [Pourbabak et al. 2020], but this will not be explored further in this thesis and it is assumed that the grid operator responsible dispatches these interconnections.

4.2. State of the Art

The controller in this chapter is a direct descendant of the controller described in [Mayorga Gonzalez 2021]. It therefore deserves special mention. The previous controller used integral controllers at each bus to track the active and reactive power flow reference functions at the single interconnection with the transmission grid. For this it uses the generator connected to that bus. If a voltage violation is detected anywhere in the SPC, the controllers and their integrators are frozen everywhere. The controllers then await clearing of the voltage violation by the OLTC step transformer at the interconnection with the transmission grid. Several potential improvements exist:

1. The previous controller is only able to track the reference functions of a single interconnection with the transmission grid. It is not possible to track reference values for additional interconnections with other SPCs or other energy grids.

2. Voltage control is provided by freezing the controllers and awaiting action by the OLTC. This means that

   (a) the SPC must be interconnected through an OLTC with the transmission grid.

   (b) if the SPC is large and has buses very far away from the OLTC, the OLTC may not detect an existing voltage violation since it only observes the voltage at its own secondary winding and not elsewhere throughout the SPC. This leads to a general controller failure because the controllers remain frozen indefinitely due to a voltage violation which is never cleared. Depending on the size of the grid and the voltage differential between the OLTC bus and distant buses, this can create dangerous grid conditions.

These shortcomings will be improved on in this chapter. There are no other directly comparable controllers. Large-scale projects such as ELECTRA (see [Cabiati et al. 2018] for a summary) were wide-ranging and included many of the goals of the controller in this chapter (cellular approach, controlled interconnections, voltage control), but the different subsystems were not integrated for unified studies or developed in much depth. Other approaches like the receding horizon dispatch in [Jiang et al. 2019] share the same goals, but are not true continuous-time controllers. It is deeply questionable whether an algorithm based on 15 min dispatch is truly capable of managing the rapidly fluctuating conditions in a renewable power grid based on distributed generation. Other projects such as the consensus-based algorithm in [Kouveliotis-Lysikatos et al. 2022] include similar goals and suffer from the same shortcoming, i.e. it acts on iterative and comparatively slow timescales.

Reviews such as [Ghadi et al. 2019] identified a wide variety of algorithms for ADN operation, but the only continuous controllers capable of a fast response were those designed for local voltage control and fault ride-through using reactive power. Continuous controllers capable of providing ancillary services to the transmission grid, such as by following interconnection power flow reference values, did not exist. More recent reviews of the field of ADN control such as [Palensky et al. 2023] covered exclusively consensus- and optimization-based algorithms that provide dispatch functionality inside an ADN on long timescales using a variety of methods such as mixed-integer linear programming, stochastic programming, or multi-stage optimization. No further advances had been made to expand continuous control beyond local voltage management and to fill the research gap at short timescales described in section 1.4.

4.3. TSO-DSO Power Flow Control

The SPC becomes a controllable entity in its own right for higher-level controllers because it tracks reference signals for the active and reactive power flow at the interconnections with the transmission grid and neighboring SPCs. To explain the SPC controller, the final control function will be introduced first, and then its composition will be explained. The interconnection power flow control error is a vector with entries for m interconnections. For the active power, it is the vector

$$\vec{e}_P = \vec{r}_{T\to S,P} - \vec{y}_P = \begin{bmatrix} r_{P,1} \\ r_{P,2} \\ \vdots \\ r_{P,k} \\ \vdots \\ r_{P,m} \end{bmatrix} - \begin{bmatrix} y_{P,1} \\ y_{P,2} \\ \vdots \\ y_{P,k} \\ \vdots \\ y_{P,m} \end{bmatrix}, \tag{4.1}$$

where $\vec{y}_P$ are the power flow measurements $y_{P,k}$ at the m interconnections tracked by the SPC controller. Similarly, for the reactive power flow, the vector

$$\vec{e}_Q = \vec{r}_{T\to S,Q} - \vec{y}_Q = \begin{bmatrix} r_{Q,1} \\ r_{Q,2} \\ \vdots \\ r_{Q,k} \\ \vdots \\ r_{Q,m} \end{bmatrix} - \begin{bmatrix} y_{Q,1} \\ y_{Q,2} \\ \vdots \\ y_{Q,k} \\ \vdots \\ y_{Q,m} \end{bmatrix}, \tag{4.2}$$

contains the reactive power flow control errors $y_{Q,k}$ for the m tracked interconnections of one single SPC. The full control function of the SPC controller is, for the active power,

$$\begin{bmatrix} r_{S\to B,P,\text{Bus }1} \\ r_{S\to B,P,\text{Bus }2} \\ \vdots \\ r_{S\to B,P,\text{Bus }i_b} \\ \vdots \\ r_{S\to B,P,\text{Bus }n_b} \end{bmatrix} = \begin{bmatrix} K_1(s)\begin{bmatrix}\vec{D}_1 & K_U(e_{1,U})\cdot\mathfrak{H}(\vec{e}_P)\end{bmatrix}\cdot\begin{bmatrix}\vec{e}_P \\ e_{1,U}\end{bmatrix} \\ K_2(s)\begin{bmatrix}\vec{D}_2 & K_U(e_{2,U})\cdot\mathfrak{H}(\vec{e}_P)\end{bmatrix}\cdot\begin{bmatrix}\vec{e}_P \\ e_{2,U}\end{bmatrix} \\ \vdots \\ K_{i_b}(s)\begin{bmatrix}\vec{D}_{i_b} & K_U(e_{i_b,U})\cdot\mathfrak{H}(\vec{e}_P)\end{bmatrix}\cdot\begin{bmatrix}\vec{e}_P \\ e_{i_b,U}\end{bmatrix} \\ \vdots \\ K_{n_b}(s)\begin{bmatrix}\vec{D}_{n_b} & K_U(e_{n_b,U})\cdot\mathfrak{H}(\vec{e}_P)\end{bmatrix}\cdot\begin{bmatrix}\vec{e}_P \\ e_{n_b,U}\end{bmatrix} \end{bmatrix} \tag{4.3}$$

$$\vec{r}_{S\to B,P} = \begin{bmatrix} K_1(s)\left(\vec{D}_1\cdot\vec{e}_P + K_U(e_{1,U})\cdot\mathfrak{H}(\vec{e}_P)\cdot e_{1,U}\right) \\ K_2(s)\left(\vec{D}_2\cdot\vec{e}_P + K_U(e_{2,U})\cdot\mathfrak{H}(\vec{e}_P)\cdot e_{2,U}\right) \\ \vdots \\ K_{i_b}(s)\left(\vec{D}_{i_b}\cdot\vec{e}_P + K_U(e_{i_b,U})\cdot\mathfrak{H}(\vec{e}_P)\cdot e_{i_b,U}\right) \\ \vdots \\ K_{n_b}(s)\Big(\underbrace{\vec{D}_{n_b}}_{\text{Power Flow Controller}}\cdot\vec{e}_P + \underbrace{K_U(e_{n_b,U})\cdot\mathfrak{H}(\vec{e}_P)}_{\text{Voltage Controller, Ch. 4.4}}\cdot e_{n_b,U}\Big) \end{bmatrix},$$

and for the reactive power

$$\begin{bmatrix} r_{S\to B,Q,\text{Bus }1} \\ r_{S\to B,Q,\text{Bus }2} \\ \vdots \\ r_{S\to B,Q,\text{Bus }i_b} \\ \vdots \\ r_{S\to B,Q,\text{Bus }n_b} \end{bmatrix} = \begin{bmatrix} K_1(s)\begin{bmatrix}\vec{D}_1 & K_U(e_{1,U})\cdot\mathfrak{H}(\vec{e}_Q)\end{bmatrix}\cdot\begin{bmatrix}\vec{e}_Q \\ e_{1,U}\end{bmatrix} \\ K_2(s)\begin{bmatrix}\vec{D}_2 & K_U(e_{2,U})\cdot\mathfrak{H}(\vec{e}_Q)\end{bmatrix}\cdot\begin{bmatrix}\vec{e}_Q \\ e_{2,U}\end{bmatrix} \\ \vdots \\ K_{i_b}(s)\begin{bmatrix}\vec{D}_{i_b} & K_U(e_{i_b,U})\cdot\mathfrak{H}(\vec{e}_Q)\end{bmatrix}\cdot\begin{bmatrix}\vec{e}_Q \\ e_{i_b,U}\end{bmatrix} \\ \vdots \\ K_{n_b}(s)\begin{bmatrix}\vec{D}_{n_b} & K_U(e_{n_b,U})\cdot\mathfrak{H}(\vec{e}_Q)\end{bmatrix}\cdot\begin{bmatrix}\vec{e}_Q \\ e_{n_b,U}\end{bmatrix} \end{bmatrix} \tag{4.4}$$

$$\vec{r}_{S\to B,Q} = \begin{bmatrix} K_1(s)\left(\vec{D}_1\cdot\vec{e}_Q + K_U(e_{1,U})\cdot\mathfrak{H}(\vec{e}_Q)\cdot e_{1,U}\right) \\ K_2(s)\left(\vec{D}_2\cdot\vec{e}_Q + K_U(e_{2,U})\cdot\mathfrak{H}(\vec{e}_Q)\cdot e_{2,U}\right) \\ \vdots \\ K_{i_b}(s)\left(\vec{D}_{i_b}\cdot\vec{e}_Q + K_U(e_{i_b,U})\cdot\mathfrak{H}(\vec{e}_Q)\cdot e_{i_b,U}\right) \\ \vdots \\ K_{n_b}(s)\Big(\underbrace{\vec{D}_{n_b}}_{\text{Power Flow Controller}}\cdot\vec{e}_Q + \underbrace{K_U(e_{n_b,U})\cdot\mathfrak{H}(\vec{e}_Q)}_{\text{Voltage Controller, Ch. 4.4}}\cdot e_{n_b,U}\Big) \end{bmatrix}.$$

This is less complicated than it looks. To explain the terms, take row i_b:

$$r_{S\to B,P,\text{Bus } i_b} = K_{i_b}(s)\begin{bmatrix}\vec{D}_{i_b} & K_U(e_{i_b,U})\cdot\mathfrak{H}(\vec{e}_P)\end{bmatrix}\cdot\begin{bmatrix}\vec{e}_P \\ e_{i_b,U}\end{bmatrix}. \tag{4.5}$$

$r_{S\to B,P,\text{Bus } i_b}$ is the active power (P) reference signal transmitted by the SPC controller to the controllable bus i_b. $K_{i_b}(s)$ is a control function that is the topic of section 4.5. $\vec{D}_{i_b}$ is a row vector of length m for m tracked interconnections which rescales the power flow control errors $\vec{e}_P$ and $\vec{e}_Q$ based on the cable lengths from bus i_b to the interconnections using the vector

$$\vec{D}_{i_b} = \frac{\begin{bmatrix}\frac{1}{\text{sd}(i_b,1)+1} & \cdots & \frac{1}{\text{sd}(i_b,k)+1} & \cdots & \frac{1}{\text{sd}(i_b,m)+1}\end{bmatrix}}{\left\|\begin{bmatrix}\frac{1}{\text{sd}(i_b,1)+1} & \cdots & \frac{1}{\text{sd}(i_b,k)+1} & \cdots & \frac{1}{\text{sd}(i_b,m)+1}\end{bmatrix}\right\|}, \tag{4.6}$$

where sd is a shortest distance search function such as Dijkstra's algorithm on the undirected, weighted cable-length network graph of the SPC from bus i_b to interconnection k. This means that the SPC controller generates individual interconnection power flow reference values for each controllable bus based on their proximity to the different interconnections. The closer the bus is to an interconnection, the more it is affected by that control error relative to the other interconnection power flow control errors. The vector norm scales $\vec{D}_{i_b}$ to be unit length. $K_U(e_{i_b,U})\cdot\mathfrak{H}(\vec{e}_P)\cdot e_{i_b,U}$ is the voltage control parameter $K_U(e_{i_b,U})\cdot\mathfrak{H}(\vec{e}_P)$ (explained in section 4.4) multiplied with the local voltage control error $e_{i_b,U} = r_U - y_{i_b,U} = 1 - y_{i_b,U}$, measured in pu.
The vector multiplication means that the active power reference signal transmitted to bus i_b is

$$r_{S\to B,P,\text{Bus } i_b} = K_{i_b}(s)\left(\vec{D}_{i_b}\cdot\vec{e}_P + K_U(e_{i_b,U})\cdot\mathfrak{H}(\vec{e}_P)\cdot e_{i_b,U}\right), \tag{4.7}$$

meaning that the input of the control function $K_{i_b}(s)$ is the sum of all scaled power flow control errors $\vec{D}_{i_b}\cdot\vec{e}_P$ (for active power as an example) plus the local voltage control error multiplied with some functions that manipulate this voltage control error. The larger one of these terms, the more impact it has on the input to the control function $K_{i_b}(s)$ and on the reference signal transmitted to the bus i_b. If a term is zero, it has no effect at all and is ignored by the controller. This principle, the addition of multiple control errors in a carefully designed fashion to obtain a single control output, is analogous to state space controllers and it is where the inspiration for this controller is taken from. A somewhat more detailed explanation of multivariable control for the interested reader can be found in appendix chapter A.1 and the topic of state space controllers is covered well by literature such as [X. Liu 2018] using pole placement.

4.4. SPC Voltage Control

One of the unexplained terms which makes up the input to the control function $K_{i_b}(s)$ is the voltage control error $K_U(e_{i_b,U})\cdot\mathfrak{H}(\vec{e}_P)\cdot e_{i_b,U}$ (see equation 4.7). The term $K_U(e_{i_b,U})$

is shown in figure 4.3 and will be explained later. The other two terms are defined as

$$\mathfrak{H}(\vec{e}_P) = \max(|\vec{e}_P|) = \max\left(\begin{bmatrix} |e_{P,1}| \\ |e_{P,2}| \\ \vdots \\ |e_{P,m}| \end{bmatrix}\right), \tag{4.8}$$

$$e_{i_b,U} = 1 - y_{i_b,U}. \tag{4.9}$$

The function $\mathfrak{H}$ yields a scalar result: the largest absolute entry in the power flow control error vector. This is done because as shown here, the voltage control error $e_{i_b,U}$ is measured in pu and therefore usually has an order of magnitude around 10^{-2}. But the power flow control errors might be in kW or MW, i.e. 10^3 to 10^6. It would be almost meaningless to add the voltage control error to the power flow control errors in the way it is described in equation 4.7 without first rescaling the voltage control error to a more comparable order of magnitude.

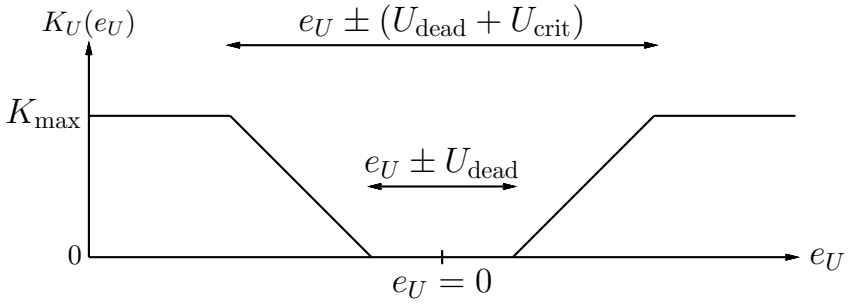

Figure 4.3: Voltage Controller Parameter $K_U(e_U)$

$K_U(e_{i_b,U})$ outputs another scalar, this time between 0 and $K_{\max}$. If the local voltage control error e_U is within a deadband, the function is zero and the whole voltage control term becomes zero. Outside the deadband is a symmetric voltage control band where the function increases linearly to $K_{\max}$ at some critical voltage. The function is shown in figure 4.3. It is intended that $20 > K_{\max} > 1$, but this does not have to be a very precise affair. An appropriate selection for $K_{\max}$ looks like this: recall that $\mathfrak{H}(\vec{e}_P) \cdot e_{i_b,U}$ yields a voltage control error of the same order of magnitude as the largest power flow control error and that $\vec{D}_{i_b}$ is always of unit length, so the sum of power flow control errors can never truly escape the rescaled voltage control error $\mathfrak{H}(\vec{e}_P) \cdot e_{i_b,U}$ in magnitude. Now consider the three regions of the function $K_U(e_U)$ in figure 4.3 and their relation to this power flow control error:

1. If the voltage control error is within the deadband, K_U is zero and the entire voltage control term becomes zero. Voltage control is disabled.

2. If the voltage control error is within the linearly increasing band, it scales the voltage control error between zero and $K_{\max}$. The final term of the voltage control

error rises quadratically with the unmodified voltage control error $e_{i_b,U}$ since both K_U and $e_{i_b,U}$ are linearly proportional to it, i.e.

$$K_U(e_{i_b,U}) \cdot \mathfrak{H}(\vec{e}_P) \cdot e_{i_b,U} \propto K_U(e_{i_b,U}) \cdot e_{i_b,U} \propto e_{i_b,U}^2. \tag{4.10}$$

3. If the voltage control error leaves the critical band, K_U becomes constant, though the error can still increase. In this band the voltage control error term is a large multiple of the power flow control error and increases linearly with $e_{i_b,U}$.

This is known as linear parameter-varying control. Books such as [Briat 2015] give an introduction the the topic. The controller responds linearly to the error, but the proportionality "constant" changes. The chief advantage in this particular formulation is that, because the parameter K_U increases from zero, it isn't necessary to derive the values with great care. They only have to be reasonably plausible. The system will stabilize itself somewhere on the ramps of K_U as long as the chosen value for $K_{\max}$ is not very small ($K_{\max} \ll 1$, which would lead to a systematically small voltage control error and insufficient voltage control) or very large ($K_{\max} \gg 20$, which would lead to oscillations in combination with other controllers). Even for very large values stability is conceivable, but strong oscillations would be expected. With a properly chosen $K_{\max} \approx 10$, the voltage control error will become much larger than the power flow control error somewhere on the ramp of $K_U(e_{i_b,U})$ and generate a strong controller response. However, temporary excursions above this point are possible due to delays in the infrastructure (generators, communications, controllers, etc), so the values for U_{dead} and particularly U_{crit} should be substantially smaller than the acceptable voltage variation to prevent excursion into unacceptable voltage bands. In later simulations, $U_{\text{crit}} = 0.06 = 6\%$ is used for a medium-voltage SPC where the voltage norm demands $\pm 10\%$ (as in DIN EN 50160).
$K_{\max}$ is also largely independent of the number of controlled interconnections m. Recall from equation 4.6 that all power flow control errors are multiplied with a vector of magnitude 1, so a larger number of controlled interconnections m leads to smaller coefficients for each interconnection and the magnitude of the sum of all power flow control error terms remains roughly the same. Since this can be guaranteed by equation 4.6 and the voltage control error term is scaled to the largest power flow control error by $\mathfrak{H}$, there is no scenario in which a large power flow control error would "overrule" a critical voltage control error despite a well-chosen $K_{\max}$.
This kind of parameter-varying behavior is also the working principle behind fuzzy controllers, although they are usually designed quite differently than the controller described here. Because of their mathematical similarity, they are explained a little more in appendix A.1.

4.5. $K_{i_b}(s)$ Control Function

As explained in the previous two sections, the term

$$\left[\vec{D}_{i_b} \quad K_U(e_{i_b,U}) \cdot \mathfrak{H}(\vec{e}_P)\right] \cdot \begin{bmatrix} \vec{e}_P \\ e_{i_b,U} \end{bmatrix} \tag{4.11}$$

is essentially just a sum of control errors, which is itself treated as a control error, albeit subjected to some elaborate rescaling. A control function is still necessary which provides some of the basic requirements of a controller, most importantly steady-state accuracy. Steady-state accuracy requires an integrator somewhere which integrates the controller for as long as it persists in an attempt to remove it. Intuitively one might decide to simply integrate all control errors until the errors go away, i.e.

$$K_1(s) = K_2(s) = \ \ldots\ = K_{i_b}(s) = \ \ldots\ = K_{n_b}(s) = K(s) = s^{-1}. \tag{4.12}$$

This does in fact work, but it has disadvantages. The rows of equations 4.3 and 4.4 are independent, so they could also be interpreted as separate controllers, one for each controlled bus i_b in the SPC. If different controllers target the same output variable, in this case the entries of the power flow control errors $\vec{e}_P$ and $\vec{e}_Q$, they will oscillate against each other if more than one of them contains an integrator. The voltage control errors, while not the same, are coupled as well. A rising voltage at one bus will also raise the voltage at nearby buses. In classic transmission grid control, where the frequency control error is targeted by many decentralized controllers, this is solved by only integrating the frequency control error for one single large power plant while the rest only target it using proportional control. This strategy is not trivially adaptable for the SPC. Changing environmental conditions and their influence on connected renewable generators mean that the control authority of each bus, that being the scale of its capacity to change its power generation or consumption to influence conditions in the grid, changes frequently and sometimes abruptly. A cloud passing over a large photovoltaic installation could turn a bus from having the most control authority to having the least. The SPC controller would constantly have to switch the integrator between its various buses so that the best-suited one performs this duty. If control authority is lost at one bus, only its replacement bus would integrate in its stead, thereby slowing the control reponse and potentially saturating the generation or absorption capacity of the controlled bus, which results in a steady-state error. These are very serious drawbacks.
Instead of attempting to shift the integrator between buses based on their control authority, a relatively recent improvement on PID controllers called fractional PID control will be used. Books such as [Indranil et al. 2013] give an introduction. Fractional PID controllers modify the PID control function

$$K(s) = K_P + K_I s^{-1} + K_D s^1 \tag{4.13}$$

by changing the exponents of the Laplace variable s to non-integer values:

$$K(s) = K_P + K_I s^{-\alpha} + K_D s^{\beta}, \qquad \alpha, \beta \in \mathbb{R}. \tag{4.14}$$

This has complex effects on the behavior of the controller. For the purpose of this chapter, it shall suffice to say that fractional derivatives produce a damping response to persistent oscillations such as those that arise from controller interactions. A more detailed introduction to fractional control is given in appendix chapter B. Since a fractional controller is able to suppress inter-controller oscillations, it eliminates the only serious argument against giving every row of equations 4.3 and 4.4 an integrator using

$$K_1(s) = K_2(s) = \ldots = K_n(s) = K(s) = K_I s^{-\alpha} + K_D s^{\beta}. \tag{4.15}$$

Two disadvantages exist in this approach, but they are of relatively little importance here:

1. Implementations of fractional controllers use computationally expensive numerical calculations to approximate fractional operators. These are not so expensive as to make implementation in microcontrollers or simulations impossible, but they are still orders of magnitude more expensive to calculate than simple PID controllers.

2. The synthesis of the fractional coefficients $\{K_I, K_D, \alpha, \beta\}$, especially α and β, is not analytically possible for most systems, unlike PID control for which well-established synthesis methods exist. Usually these coefficients are generated using metaheuristics, which is slow and yields results of dubious optimality.

The first disadvantage slows the simulation somewhat, but implementation on microcontrollers is still well within what is possible [Oprzędkiewicz et al. 2021; Muresan et al. 2013]. The second would ordinarily be serious, but it turned out to be quite easy to simply select appropriate values manually.
This explains all terms of equations 4.3 and 4.4. The rows i_b are individually transmitted to the controlled buses i_b as a reference signal for the bus controller of chapter 3.

4.6. Model Structure

With the SPC controller architecture described in general terms in the previous section, it is time to test it in a simulation. For this, a three-phase, medium-voltage test grid was created based on CIGRE's medium-voltage benchmark grid [Strunz et al. 2014] for renewable energy integration. It contains two medium-voltage SPCs. Both are connected to the high-voltage grid through OLTC (on-load, tap-changing) transformers and through a single medium-voltage cable to each other. To every bus is connected an uncontrolled load based on the benchmark grid values as well as an aggregated device (a combination of generators, storages, and flexible loads) controlled by the bus controller. A graphical illustration of the two SPCs, the cables connecting the buses, and the interconnections is given in figure 4.4. The cable parameters and lengths are listed in appendix tables D.8 and D.10. The active and reactive power values of the uncontrolled constant power loads at each bus are listed in appendix tables D.11 and D.12. Nominal system voltage is 20 kV in accordance with [Strunz et al. 2014]. The simulations are run

as 50 Hz RMS (phasor) simulations. The greyed-out elements in figure 4.4 were either described in previous chapters (as is the case for the bus controller and the aggregated devices) or are not the subject of this chapter (as is the case for the transmission grid controller).
In accordance with the results of chapter 3, the closed loop of each bus is modelled as a first-order transfer function. The time constants T_Σ of these transfer functions are randomized from 0.1 s to 1 s. The flexibility region of the aggregated devices is assumed to be a circle randomized from 1 MVA to 15 MVA. This greatly simplifies numerical controller behavior on the hull of the flexibility region.
For improved observability of certain controller interactions, voltage control using active power is disabled in the simulations (i.e. always $\mathfrak{H}(\vec{e}_P) = 0$). Voltage control is only provided using reactive power. The controller parameters are given in appendix table D.5 to D.7 together with the technical properties of the system. Two variants of the control function $K(s)$ are compared: a unity integral controller and the fractional controller described previously. The parameters are also in the appendix.

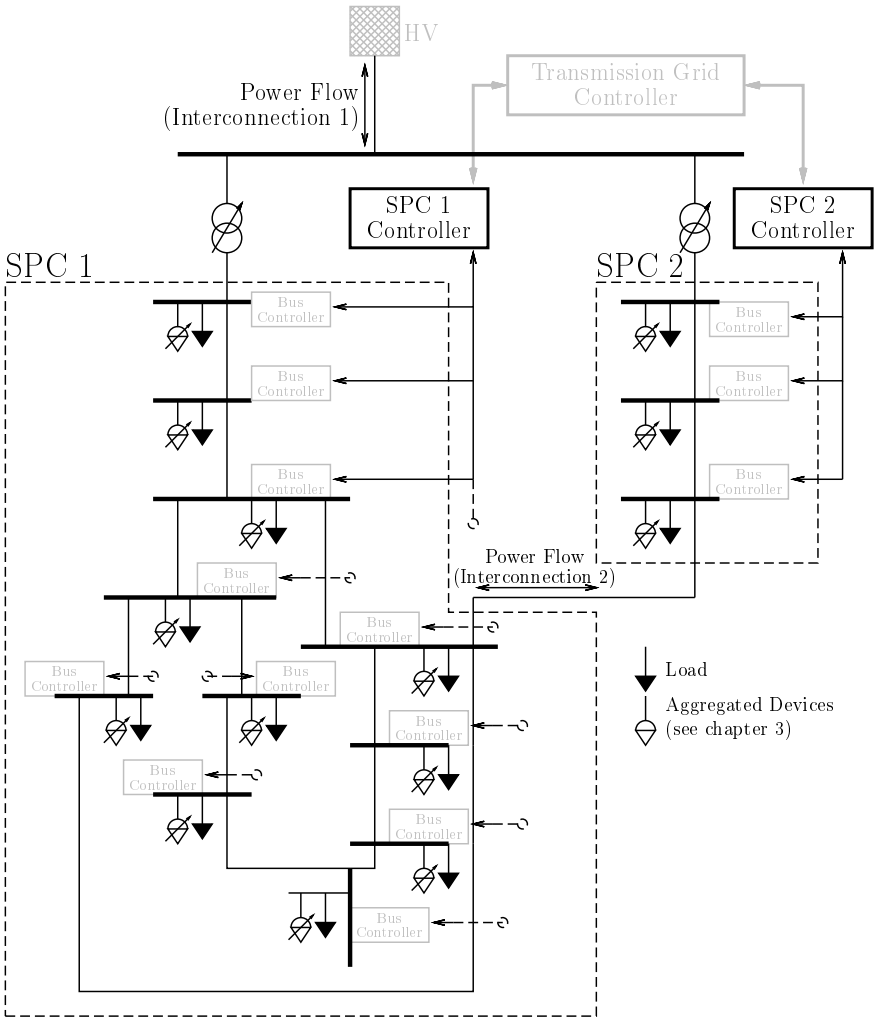

Figure 4.4: SPC Controller Test Grid

4.7. Simulation

The simulation lasts for 60 s and uses 1 ms time steps. Since the transmission grid controller is so far undefined, reference step functions must be selected randomly. The times and magnitudes of the reference steps are shown in appendix table D.9. The simulation results for the power flows at the interconnections for the I-controller are shown in figures 4.5 through 4.8, one for the active and reactive power flow at each interconnection. The bus voltages are depicted in figure 4.9. Around $t = 12\,\mathrm{s}$ the system reaches the end of the voltage deadband at some buses and uses reactive power to stabilize the voltage. This is clearly visible in the reactive power flows at the interconnections in figures 4.7 and 4.8. The controllers generally ignore the interconnection power flow reference signal here since the voltage control error is much larger than the power flow control error in equation 4.4. When the OLTC step transformer detects an overvoltage, it reduces the voltage, which allows the controllers to target the interconnection power flow control error again. The stepping behavior of the OLTC transformer is also the reason behind the power flow dips observable in the power flow behavior of both controllers around $t = \{16, 21, 26\}\mathrm{s}$. The interaction of the integral controllers from 10 s to 15 s produces considerable oscillations in the bus voltages and reactive power flows.
The fractional ID-controller is subjected to the same reference steps as the I-controller and shown in figures 4.10 through 4.13. The voltages are depicted in figure 4.14. The controller eliminates the undesirable oscillations present in the I-controller and shows very similar behavior otherwise. The argument for a fractional controller instead of an integer one is therefore compelling.

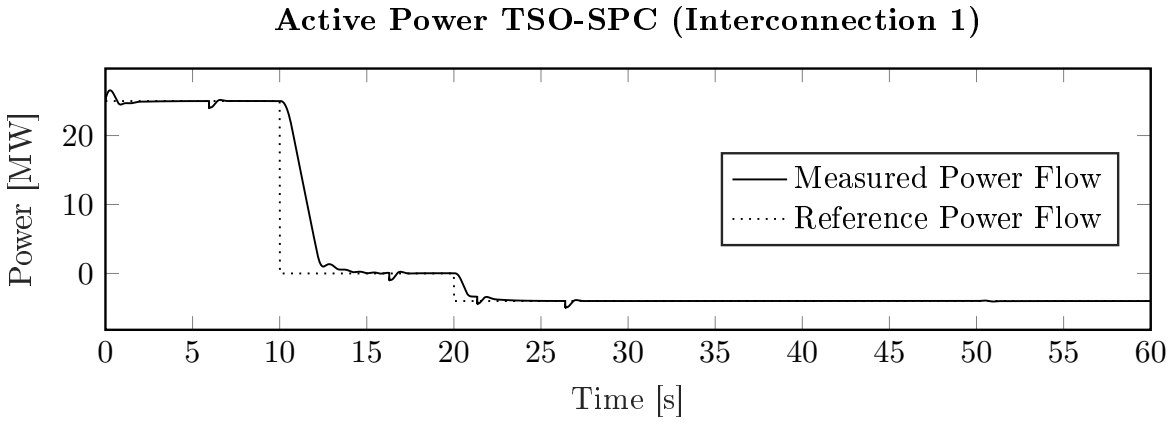

Figure 4.5: Active Power Exchange TSO-SPC (I-Controller)

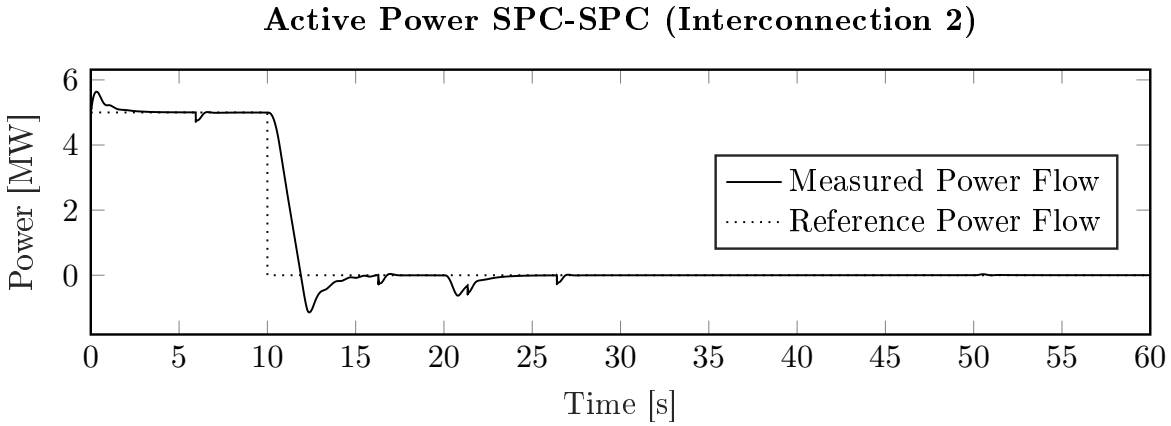

Figure 4.6: Active Power Exchange SPC-SPC (I-Controller)

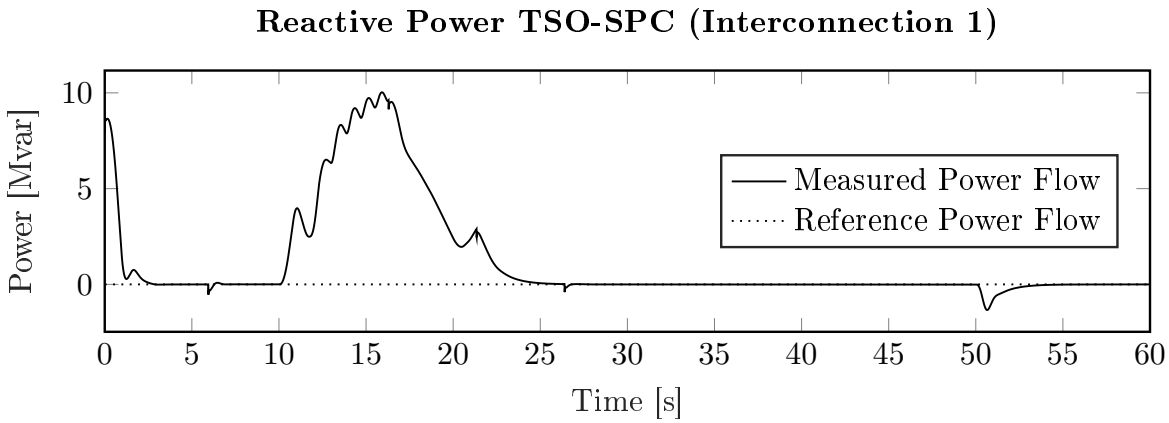

Figure 4.7: Reactive Power Exchange TSO-SPC (I-Controller)

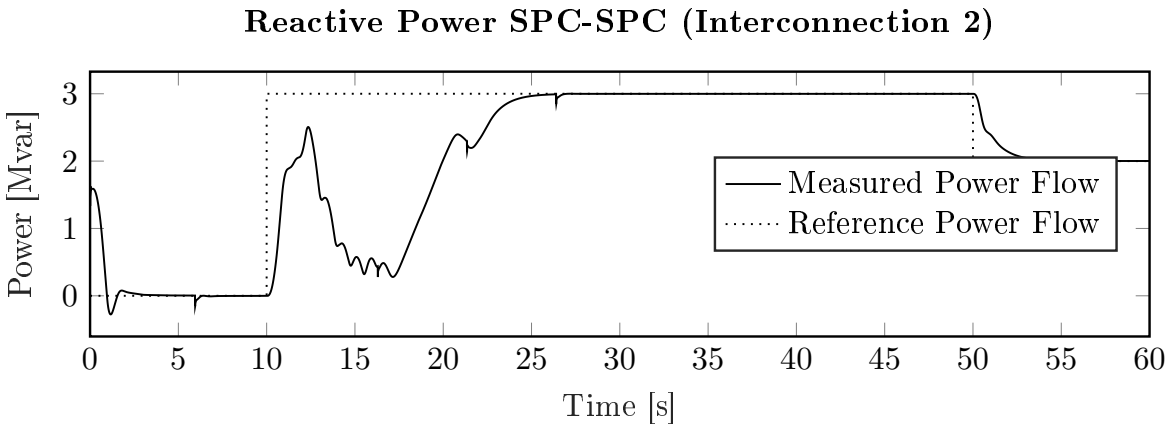

Figure 4.8: Reactive Power Exchange SPC-SPC (I-Controller)

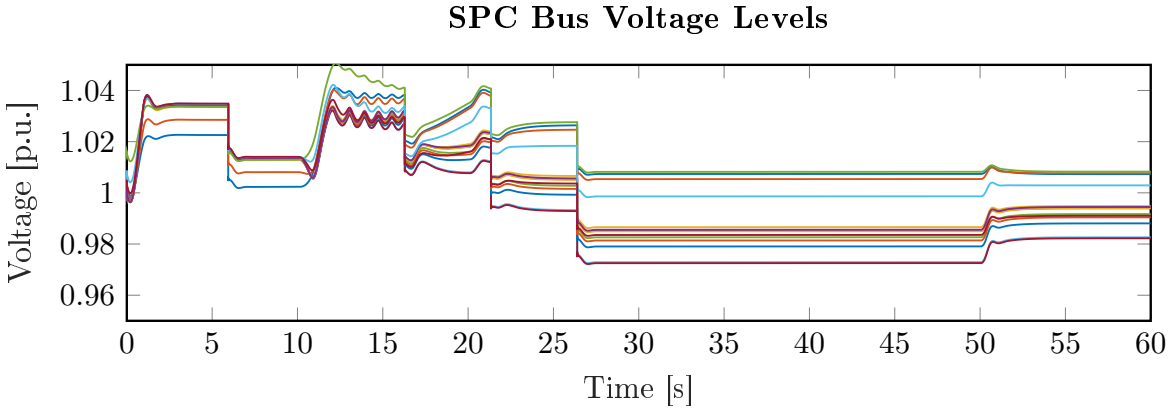

Figure 4.9: Bus Voltages in SPC (I-Controller)

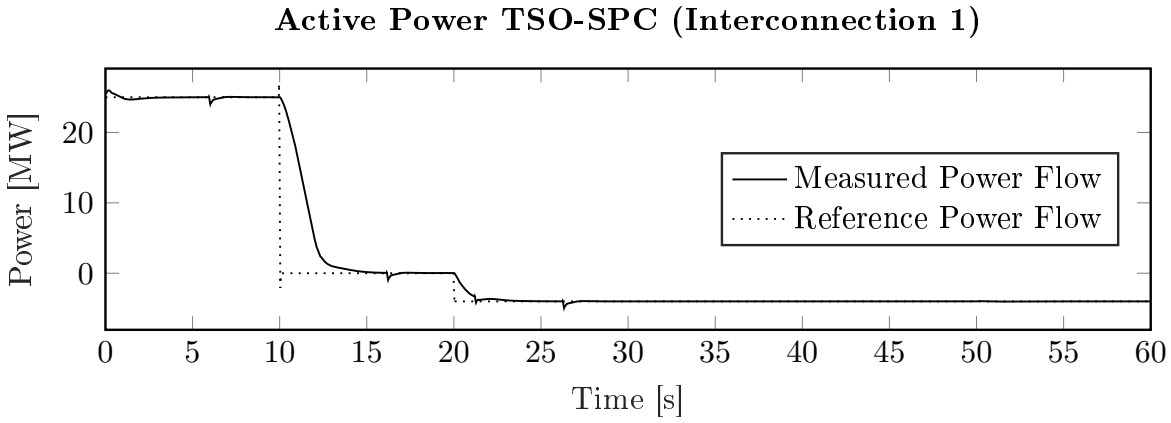

Figure 4.10: Active Power Exchange TSO-SPC (FID-Controller)

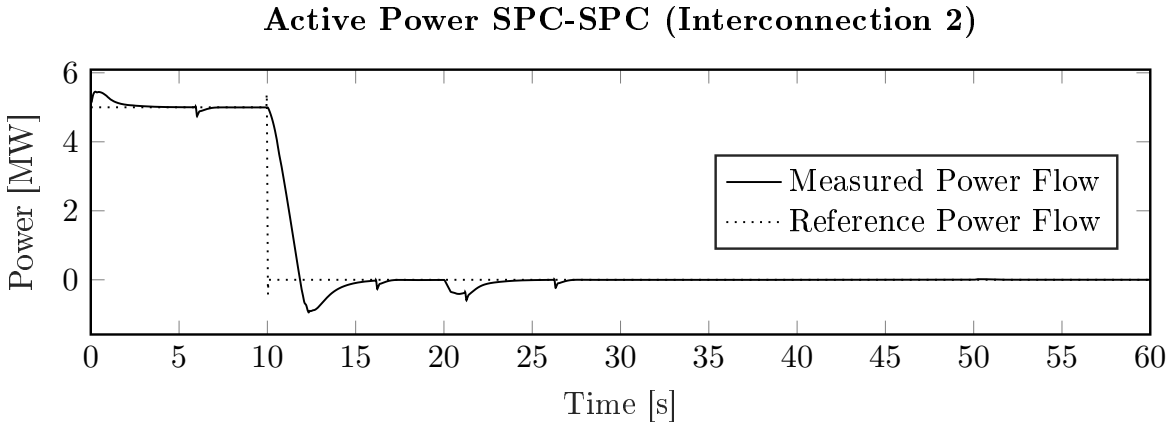

Figure 4.11: Active Power Exchange SPC-SPC (FID-Controller)

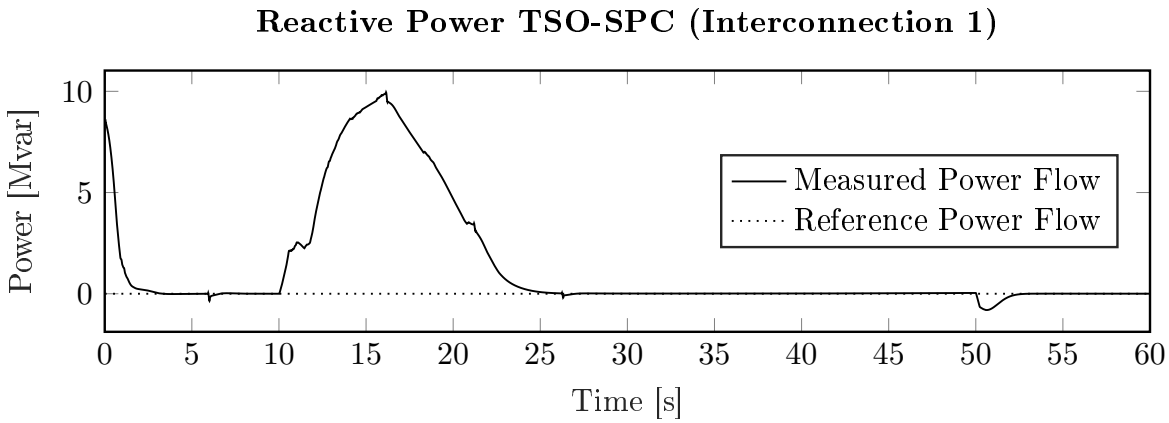

Figure 4.12: Reactive Power Exchange TSO-SPC (FID-Controller)

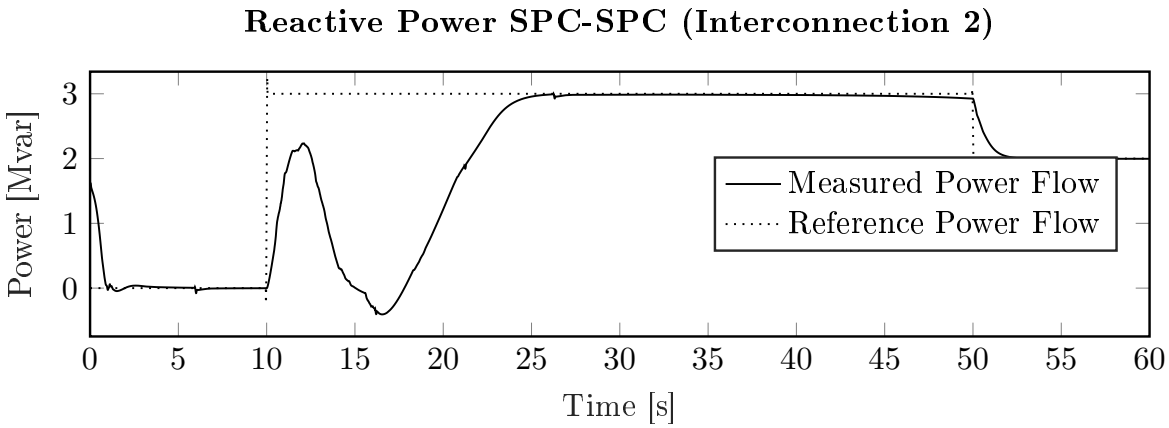

Figure 4.13: Reactive Power Exchange SPC-SPC (FID-Controller)

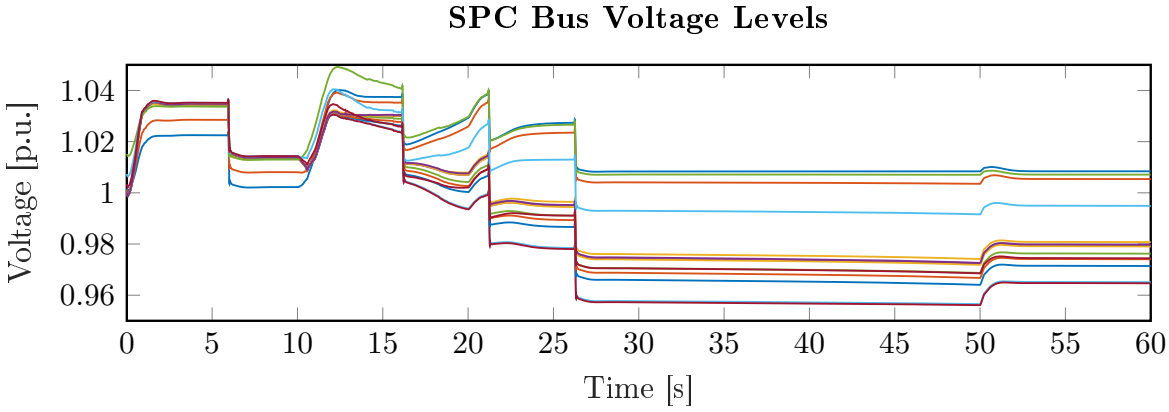

Figure 4.14: Bus Voltages in SPC (FID-Controller)

4.8. Alternate Controllers

It can be noted that the controller described in this chapter does not require a variety of signals reported to it by the lower-level bus controllers inside the SPC. Unused signals are

1. the flexibility regions F_{i_b} of the buses i_b in the SPC,
2. and the approximated time constant T_{Σ,i_b}.

The flexibility region F_{i_b} of the buses is not used because the SPC controller contains an integrator for every bus. Therefore the operational limits of all buses would automatically be reached if this is necessary for grid control and knowledge of the limits of F_{i_b} is not necessary, though it is implicitly used in the simulation to prevent controller windup. The approximated time constant T_{Σ,i_b} is not used for similar reasons: it provides no benefit to the controller described in this chapter since the controller makes no dynamic prediction. However, a part of the contribution of this work in accordance with chapter 1.6 is an easily adaptable and modular control structure. For example, a possible alternative to the controller described in this chapter would be model-predictive control (MPC). Model-predictive control simulates the response $y(t, u)$ of a model representing the controlled system over some limited horizon to various control inputs of u and selects the response which minimizes the control error $e = r - y$ over the optimization horizon. This process is then repeated and the next value for u is chosen, resulting in a piece-wise constant signal for u. This is illustrated in figure 4.15. MPC relies on computationally efficient models of the system because the effectiveness of the controller is limited by the computational feasibility of simulating the system often enough to obtain a good u in as short a time as possible to minimize the length of time that u is held for. MPC has found wide acceptance in complex but reasonably slow systems like certain types of chemical process control. MPC would also be a reasonable candidate for the SPC controller as well, and in this case would require the T_{Σ,i_b} of the various buses to calculate the response $y(t, u)$ as well as the limits F_{i_b}. In fact, since the first-order transfer functions using T_{Σ,i_b} have analytic solutions, a system approximation for MPC would execute very efficiently.

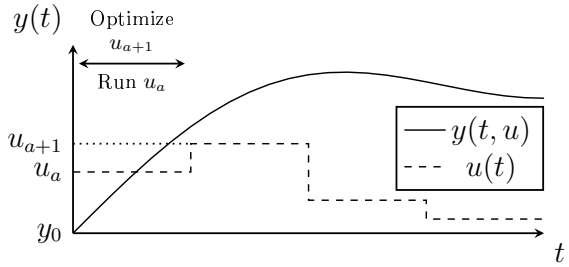

Figure 4.15: Model-Predictive Control

Chapter Summary

In this chapter, an SPC controller was described which receives reference signals for the active and reactive power flows at its interconnections with the transmission grid and neighboring SPCs and tracks them while maintaining voltages at all its buses. As its control variables, it uses aggregated devices at each bus that represent a controlled aggregation of generators, storages, and loads. This was covered in a previous chapter.

Mathematically, power flow control is provided using a scaled addition of control errors and voltage control is provided using a linear parameter-varying function. The control errors are inputs to a fractional control function which suppresses inter-controller oscillations and makes it possible to have multiple integrators targeting the same output variable. Simulations show the success of this approach compared to simple integral controllers.

In the next chapter, a simplified model for the SPC and its controller as described in this chapter will be designed and tested. This will allow representation of various SPCs as simplified models in the transmission grid and allow reasonably efficient simulations including a diverse set of SPCs.

Model Reduction of the SPC

Computational complexity is a constant struggle in the modeling, control, and simulation of power systems. The sheer size of the system means that simplifications must be made. The SPC and its controllers designed in the previous chapters is intended to be interconnected with other SPCs through the transmission grid in future chapters, but connecting six SPCs (the CIGRE high-voltage benchmark model having this number, for example) of ten or more buses in each SPC and their associated loads and generators to each other would lead to very expensive dynamic simulations without being a particularly large power system in the first place. Furthermore, there are controllers (notably model-predictive controllers) that rely on a reasonably cheap model of the system they are controlling. A TSO wishing to implement a model-predictive controller in the transmission grid (such as for voltage control) would struggle with the large computational burden of a full-scale SPC.
The subject of this chapter is the design of a model order reduction of the controlled SPC described in the previous chapter.

5.1. Design Goals of SPC Model-Order Reduction

The reduced model of the SPC is intended to be a drop-in replacement for any model which requires simulation of the SPC, but where knowledge of the internal states of the SPC are not directly necessary. For example, a TSO wishing to simulate the behavior of an SPC connected to the transmission grid would be interested in the power exported or imported by the SPC as a function of time, but how exactly the SPC accomplishes this is largely irrelevant to the TSO as long as it works. The internal controllers of the SPC are tasked with managing this. The model order reduction specifically maintains the following features:

1. Reduced computational cost.
2. Dynamic equivalence in terms of interconnection power flow; the tracking response of the full- and reduced-order models should show similar dynamic behavior for the active and reactive power flows at the interconnection(s).

5.2. State of the Art

Dynamic, reduced approximations of distribution grid models have a considerable history. Classic research on the subject such as [Karlsson et al. 1994] used the passive properties of distribution grids in historical power grids to define a combination of nonlinear blocks that represent an aggregate load. This approach loses accuracy in a distribution grid subject to the constantly changing conditions of distributed generators and their controllers. Arriving at a reduced model that reflects these characteristics is much more complex. As late as [Milanovic et al. 2013; Resende et al. 2013] the vast majority of methods to derive reduced models were based on uncontrolled, passive distribution grids that are unsuitable for active distribution grids in general and the Smart Power Cell in particular. Modern and more flexible approaches to arrive at reduced equivalents often use grey-box model identification. That is, they use a reduced structure arrived at by some heuristic consideration, usually expert knowledge, and calculate or optimize the parameters of the reduced structure to match model behavior [Glad 2021]. This approach was widely used in [Chaspierre 2020] using evolutionary algorithms for the parameter optimization, in [Conte et al. 2019] using constrained nonlinear optimization, and in [Fulgêncio et al. 2020] again using an evolutionary algorithm. These approaches are all similar to the approach presented in this chapter in that they optimized the power flow behavior at the interconnection with the transmission grid using the parameter vector of some reduced model arrived at using expert knowledge. However, there is still a large methodological difference coming from the exact definition of an active distribution network in the context of their research. The active distribution network approximated in [Chaspierre 2020] uses local controllers to control for voltage and frequency, [Conte et al. 2019] controlled locally for voltage and power factor, and [Fulgêncio et al. 2020] controlled only for local voltage. This means that none of the cited existing research defines an ADN that fulfills the requirements of the SPC; for example, it is not able to provide controlled behavior at the interconnection with other parts of the grid. Consequently, while the methods may be superficially similar to the method presented in this chapter, the underlying controller architecture to be approximated is fundamentally different and requires a somewhat different approach.

5.3. Grey-Box Model Order Reduction

As hinted in the state of the art, one way to categorize model order reductions is by the manner in which they derive their structure. A white-box model order reduction takes the mathematical representation of the system and, through analytic means, derives a reduced structure and parameters for this structure. For example, linear state space models can be reduced in size by simply eliminating low-energy, low-contribution states from the model through an analysis such as the Hankel singular values. There is a direct (but not necessarily isomorphic) relationship between the two models and any differences between the models can be analyzed analytically.

This is in stark contrast to a black-box model order reduction which obtains reduced model behavior without any direct and clear relationship between the two models. An example would be many algorithms based on machine learning. A neural network can be trained to produce output similar to a given system, but the reason for any deviations or lack thereof is almost impossible to trace back to the full-order model. A black-box model is obviously never isomorphic, meaning that it is impossible to return to the original model based on the reduced model and knowledge of the reduction algorithm.
A grey-box model order reduction refers to an approach which combines elements of both these approaches. It could be either a reduced model structure that is obtained analytically or which is directly derived from the full structure, but for which no adequate parameters are obtainable using analytic methods. It could also be a subset of parameters that is obtainable analytically but for which other parts of the model structure are unknown and must be approximated using black-box methods. For a wider introduction to different modeling techniques, see [Glad 2021] and the other articles in that book.
For the approach in this work, a grey-box model order reduction approach is chosen. It uses a reduced model structure determined using the intuition and the educated guess of the designer combined with a metaheuristic optimization of its parameters to produce dynamic behavior similar to the full system. The only analytic requirement of the reduced grid structure is that it has the same number of interconnections as the full model.
Reduced computational complexity is obtained by the reduction of the buses inside the model relative to the full-order model. Similarity of its controlled behavior is obtained by using the same controller to control the buses in the reduced grid as would be used to control the buses in the full-order grid. Consider the tracking response shown in the previous chapter in figures 4.12 through 4.14. Complexities in the tracking response are a result of voltage deadband violations and OLTC steps (which are also a result of voltage deadband violations). The number of buses and the parameters of the cables or lines connecting them are the primary way in which a properly optimized reduced model imitates this voltage behavior using its own buses, so the educated guess involved in the design of the reduced model's structure is a balance between computational reduction (fewer buses and cables) and the richness of the reduced grid's voltage behavior.
Two variants are depicted in figure 5.1. One has two buses and one interconnection with the high-voltage grid, the other has three buses and two interconnections, one with the high-voltage grid and another with another part of the medium-voltage grid. A larger number of interconnections should be reflected with a proportionally larger number of buses in the reduced structure so that there are buses located far away from the interconnection to reflect some of the voltage gradient phenomena that affect the full-order model. The more complex the effects of voltage phenomena on the tracking response at the interconnections, the more buses and cables should be kept in the reduced-order model.
The greyed-out elements in the figure are numerically identical between models. The two models use the same OLTC, equivalent controllers, and an identical representation of the wide-area grid.

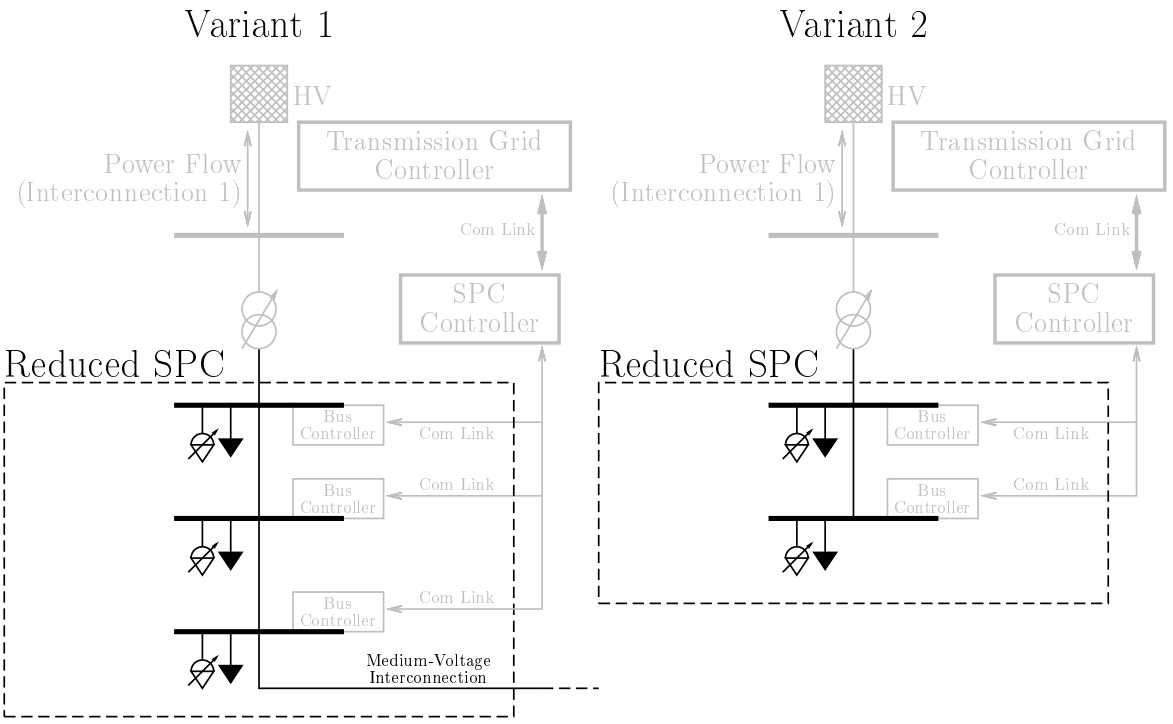

Figure 5.1: Reduced SPC Variants

5.4. Reduced Model

5.4.1 Reduced Model Structure

The purpose of this model order reduction is making large-scale models involving an interconnection of SPCs more computationally feasible. The high-voltage model recommended by CIGRE for renewable energy integration benchmarks does not include any medium-voltage interconnections between SPCs, only interconnections through the transmission grid. For this reason, a simple two-bus model is chosen as a model-order reduction of the SPC 1 covered in the previous chapter in figure 4.4. The second SPC and the medium-voltage interconnection between the two SPC is omitted.
The full SPC model and the reduced SPC model are shown again in figure 5.2, the full SPC being on the left, having 11 buses and being identical to SPC 1 from the previous chapter except for the omission of the medium-voltage cable connecting it to SPC 2. Just as shown in figure 5.1, the greyed-out elements are identical in both models and were described in previous chapters or they are not the subject of this chapter yet (in the case of the transmission grid controller).

5.4.2 Reduced Model Parameters

The reduced SPC model shown in figure 5.2 contains 3 dynamic elements with adjustable parameters that determine the simulation behavior: two loads, one connected to each bus, and one cable connecting the two buses. The cable is a π-section cable with 7

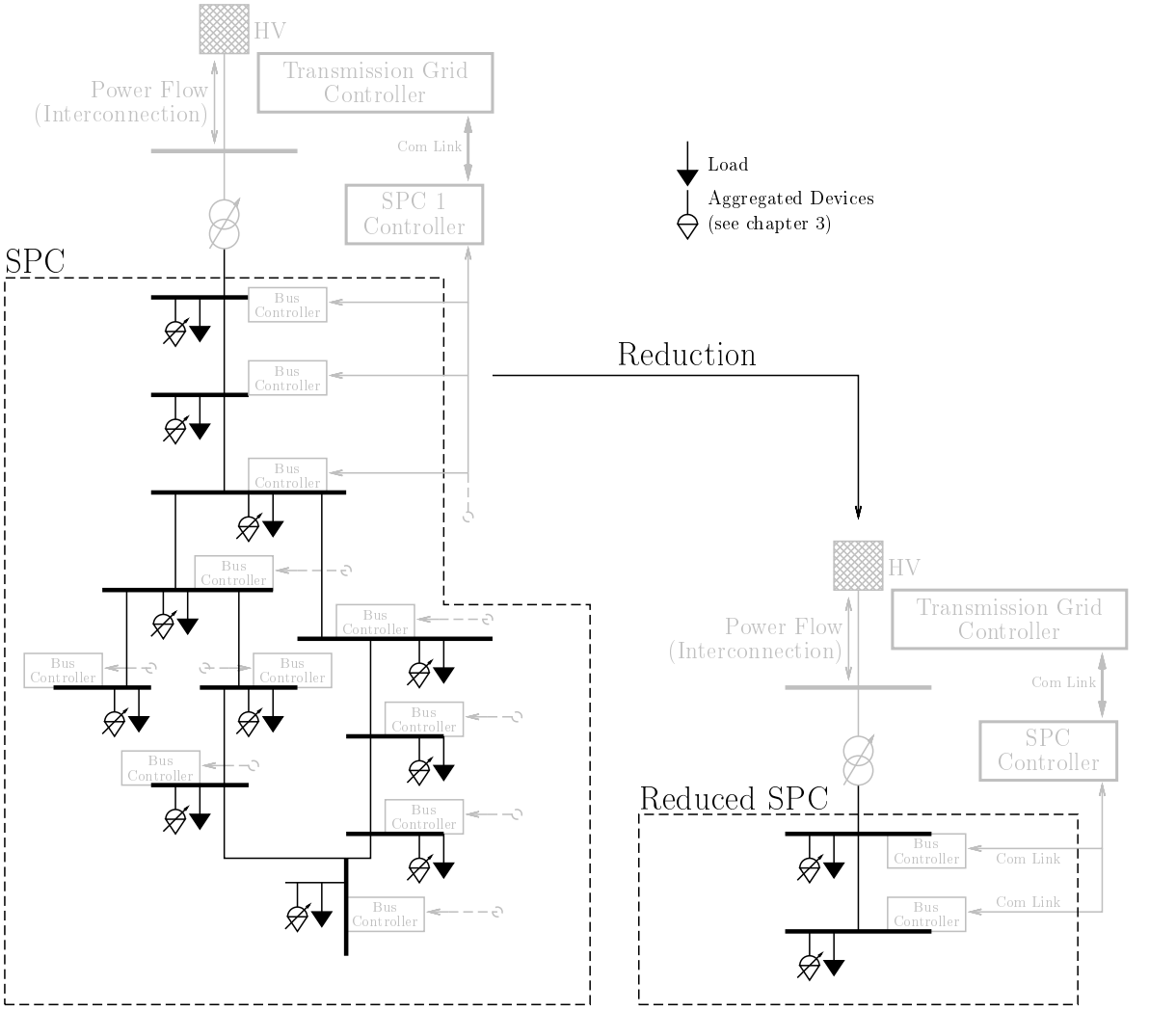

Figure 5.2: Single-Interconnection SPC Reduction

parameters (just as in the previous chapter) and the loads are constant-power loads. π-section cables use resistance, inductance and capacitance parameters per unit length that reflect the inductive and capacitive coupling between the phases and ground as well as between the terminals of the cable. Their name derives from the circuit diagram of the n-phase cable, which resembles the letter π. More details regarding the cable model can be found in [MATLAB 2023a n.d.]. This results in 11 parameters subject to the grey-box parameter optimization stored in the parameter vector $\vec{O}$:

Positive-Sequence Resistance per km r'_+
Zero-Sequence Resistance per km r'_0
Positive-Sequence Inductance per km l'_+
Zero-Sequence Inductance per km l'_0
Positive-Sequence Capacitance per km c'_+
Zero-Sequence Capacitance per km c'_0
Cable Length L.

Load 1 Active Power P_1
Load 2 Active Power P_2
Load 1 Reactive Power Q_1
Load 2 Reactive Power Q_2

The optimization function is

$$\varepsilon(\vec{O}) = \sum_{t_i=0}^{t_i=T_{\text{end}}} (y_{P,\text{full}}(t_i) - y_{P,\text{red}}(t_i))^2 + (y_{Q,\text{full}}(t_i) - y_{Q,\text{red}}(t_i))^2, \tag{5.1}$$

where y_P and y_Q are the active and reactive power flows at the interconnection with the transmission grid for the full and reduced grid respectively. These parameters are iteratively improved by the optimization by simulating the reduced model using the parameter vector $\vec{O}$ and updating it until the quality of the solution does not appear to improve anymore (called a plateau). A block diagram of this process is shown in figure 5.3.

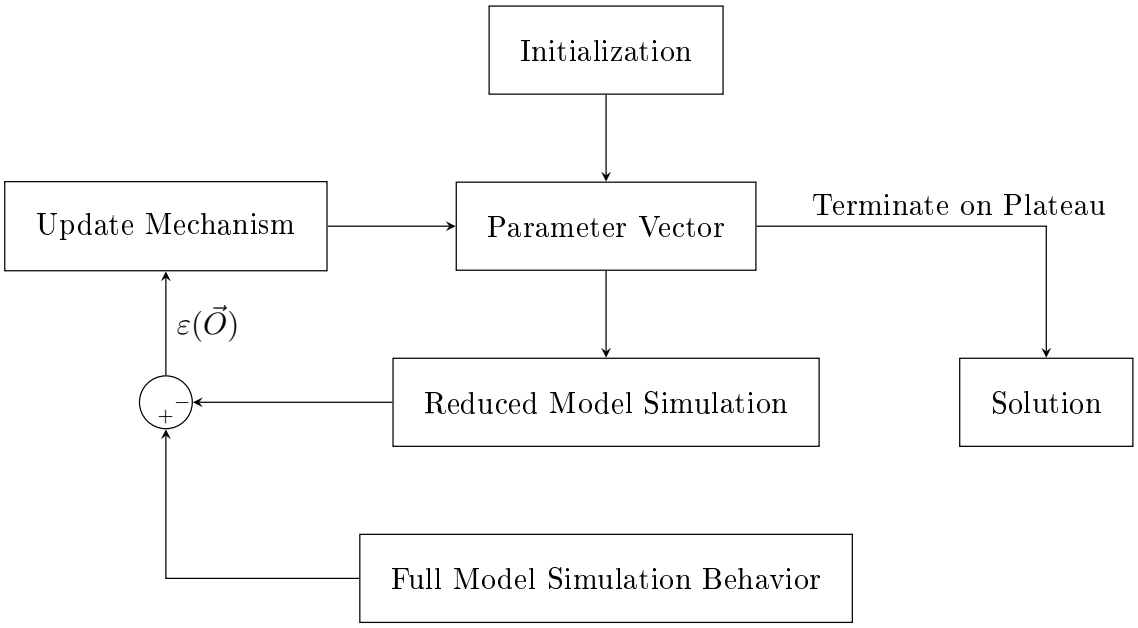

Figure 5.3: Optimization Block Diagram (Generalized Form)

There are two main things to consider when the update mechanism is chosen. The optimization function ε as it is described here lacks an analytic gradient, ruling out many algorithms. The problem is also most likely not convex, and investigating the convexity would be mathematically elaborate. These questions can be avoided by using the most general class of optimization algorithms relying on the least amount of knowledge about the system: metaheuristics. Among the metaheuristics, it would be possible to use discrete optimization algorithms, such as genetic algorithms, by defining a discrete encoding of the continuous parameter space, but a more direct approach is using a continuous algorithm such as Particle Swarm Optimization (PSO) or Simulated Annealing. Since the solution space is assumed to be very large and of somewhat unclear extent (it being unclear what range of parameters can be excluded from the search space), PSO is chosen over Simulated Annealing since it is population-based and likely traverses a large search space more efficiently. For a substantial introduction to the topic of metaheuristics and arguments in favor of the various algorithms, see [Talbi 2009].
Particle Swarm Optimization initializes its population (of size S) of candidate solutions

randomly and simulates all of them to obtain their optimality ε. It then generates a difference vector (similar to a velocity) for each candidate solution such that

$$\begin{aligned}\vec{v}_{p,\text{new}} = (&\omega \cdot \vec{v}_{p,\text{last}} \\ &+ \gamma_p \cdot r_p \cdot (\vec{O}_{\text{best,ptcl}} - \vec{O}_{\text{current,ptcl}}) \\ &+ \gamma_g \cdot r_g \cdot (\vec{O}_{\text{best,global}} - \vec{O}_{\text{current,ptcl}})) \cdot r_r,\end{aligned} \tag{5.2}$$

where $\vec{O}_{\text{best,ptcl}}$ is the best solution which the individual candidate solution itself has seen in the past, $\vec{O}_{\text{best,global}}$ is the best solution which any individual candidate solution in the population has seen, and $\vec{v}_{p,\text{last}}$ is the solution's difference vector before the update to the vector. $\omega \cdot \vec{v}_{p,\text{last}}$ can be thought of as an inertia component. $\{r_p, r_g\}$ are diagonal matrices of uniformly distributed random variables on the interval $[0, 1]$ and $\{\omega, \gamma_p, \gamma_g\}$ are weights given to the influence of the respective components described earlier. The difference vector then updates the parameter vector after each iteration such that $\vec{O}_{\text{new}} = \vec{O}_{\text{old}} + \vec{v}_p$ and the new optimality of the candidate solution is calculated using simulation. In addition to these classic PSO components, a random variable r_r was added which had a chance of 0.89 to take the value $r_r = 1$, a chance of 0.1 to take the value $r_r = 10$, and a chance of 0.01 to take the value $r_r = 100$. This provides simple reset behavior to aid in exploration by greatly scaling the difference vector. Due to the large size and unclear extent of the search space, the initialization is also performed over the range described in appendix table D.14 (the left column shows the cable length and its positive- and zero-sequence impedance and the right column shows the active and reactive power consumption of the loads) and the coefficients $\{\omega, \gamma_p, \gamma_g\}$ as well as the population size S are in appendix table D.13.
Properties of the reduced model not subject to optimization but which could be optimized if necessary are:

1. The integrator coefficient K_I of the controllers. It is set to 5.5 because the number of buses is reduced by a factor of $\frac{11}{2} = 5.5$. Integrators are linear elements, so this results in identical integration.

2. The apparent power generator limits. The two available generators use the mean generator limit of the full grid, each multiplied by 5.5. This means the aggregated generator flexibility regions of the two models are the same.

5.5. Simulation

The parameter optimization of the reduced model is run according to the method described above to generate a reduced 2-bus model which reflects the dynamic behavior of the 11-bus model corresponding to SPC 1 of the previous chapter at lower computational cost. The parameters for the cable length, positive- and zero-sequence impedances, and the constant-power loads as yielded by the optimization algorithm are given in appendix table D.15. A simulation comparison of the reduced model and the full model is given

in figures 5.4 through 5.6 for the active and reactive power flow at the interconnection with the transmission grid as well as the behavior of the OLTC step transformer.

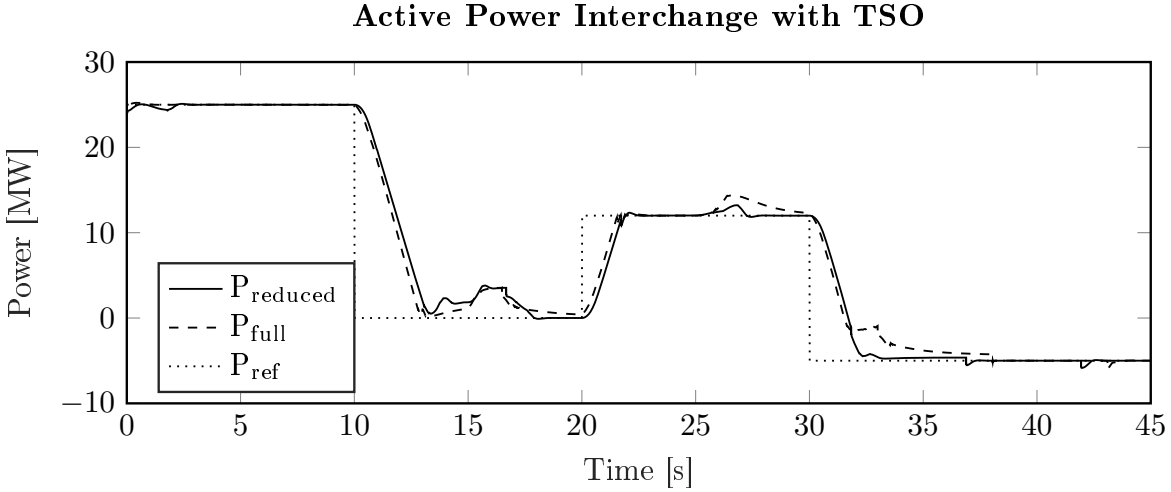

Figure 5.4: Model Comparison (Interconnection Active Power Flow)

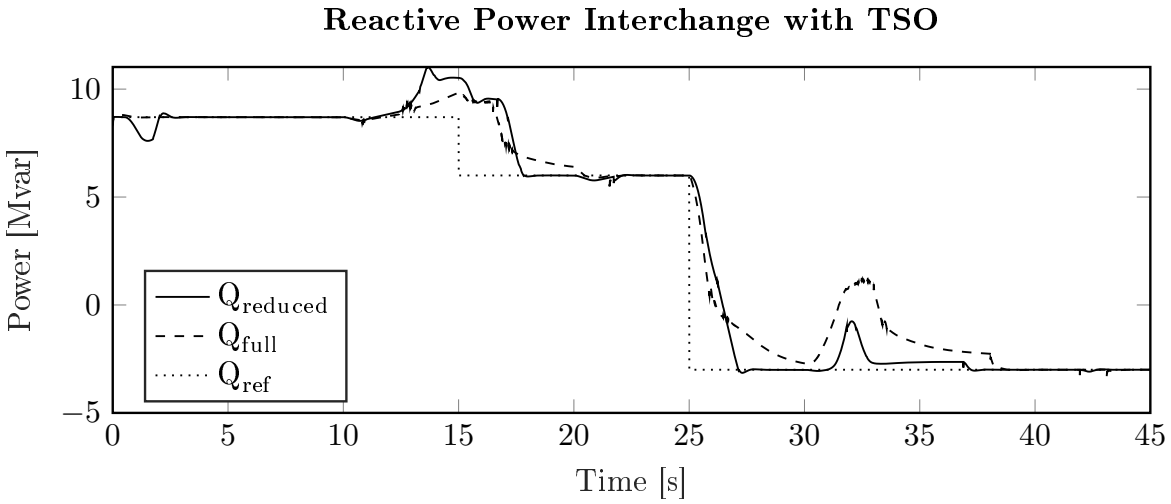

Figure 5.5: Model Comparison (Interconnection Reactive Power Flow)

The two grids follow the same reference signals sent by the transmission grid controller and show similar behavior. Of particular interest is the model behavior around 15 s and 35 s. Here the full model abandons tracking the power flow reference signals and uses its generators to stabilize the voltage. This behavior is described in more detail in the previous chapter. The reduced model shows similar behavior at the same time, implying that the voltage behavior of the reduced model is also similar. This is further supported by the very similar OLTC stepping behavior shown in figure 5.6. This is a notable accomplishment since it is primarily the voltage behavior which produces more complex controller tracking. However, comparing bus voltages directly is not very meaningful since there is no direct correspondence between the models and the transmission grid controller is not intended to have knowledge of the internal states of the SPC anyway. The relative computational cost of the reduced model compared to the full model is

approximately 15% or an 85% reduction.

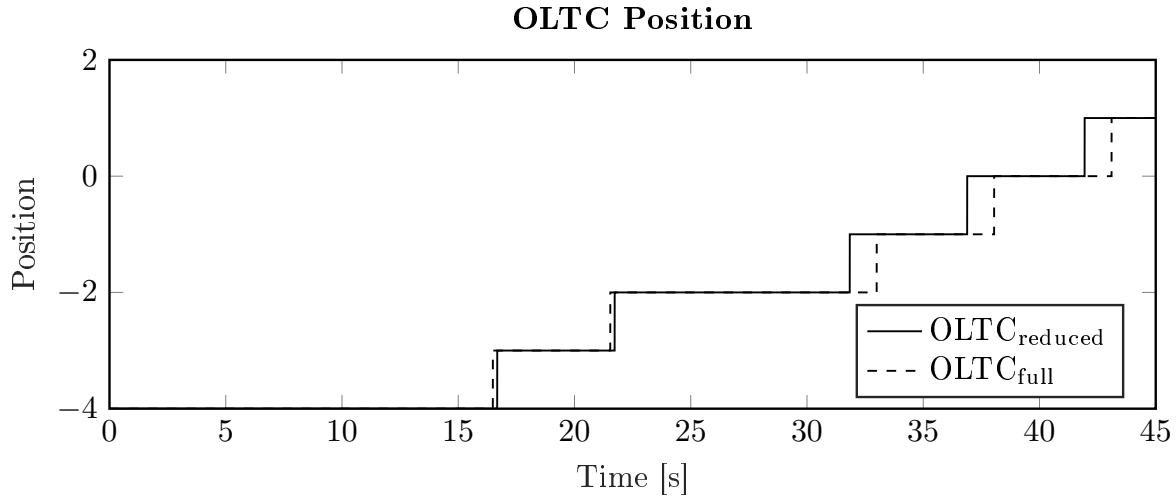

Figure 5.6: Model Comparison (OLTC Steps)

5.6. Validation

Although proven to function correctly, the behavior of the reduced model should be analyzed over a wider range of reference functions. This will be done using reference steps from generator curtailment to various reference points in the PQ-plane and storing the tracking delay between the transmission of the reference step and fulfillment of that reference step:

$$\begin{aligned}
\tau_{p,q} &= \max(t_p, t_q) \\
t_p &= |e_P| < \varepsilon_P \\
&\quad \wedge \left|\frac{de_P}{dt}\right| < \varepsilon_P, \\
e_P &= r_{T\to S,P} - y_P, \\
\varepsilon_P &= |P_{\text{ref}} \cdot 1\%| + 10\,\text{kW}
\end{aligned}
\qquad
\begin{aligned}
t_q &= |e_Q| < \varepsilon_Q \\
&\quad \wedge \left|\frac{de_Q}{dt}\right| < \varepsilon_Q, \\
e_Q &= r_{T\to S,Q} - y_Q, \\
\varepsilon_Q &= |Q_{\text{ref}} \cdot 1\%| + 10\,\text{kvar}.
\end{aligned}
\tag{5.3}$$

Here, e_P and e_Q are the interconnection power flow control errors and ε represents some (fairly small) tolerance. 10 kW and 10 kvar are added to ε so that for reference values of 0 (i.e. power balancing) there is still a non-zero tolerance. 10 kW corresponds to a 1% tolerance at 1 MW, which is the first non-zero simulation point. The controller is judged to have successfully tracked a reference power flow when both its absolute control error $|e|$ and the absolute control error derivative $\left|\frac{de}{dt}\right|$ fall below the tolerance margin ε. The derivative of the control error is used to exclude oscillations around the reference step. The earliest time by which a reference value is tracked is stored as the delay t. The final tracking delay τ stored for some combination of active and reactive power flow reference

values is then simply the maximum of the two delays t. The tracking delays for the two models are shown in figure 5.7 for the full model and 5.8 for the reduced model using isolines. The two models have similar tracking delays and track reference signals in a similar feasible region.

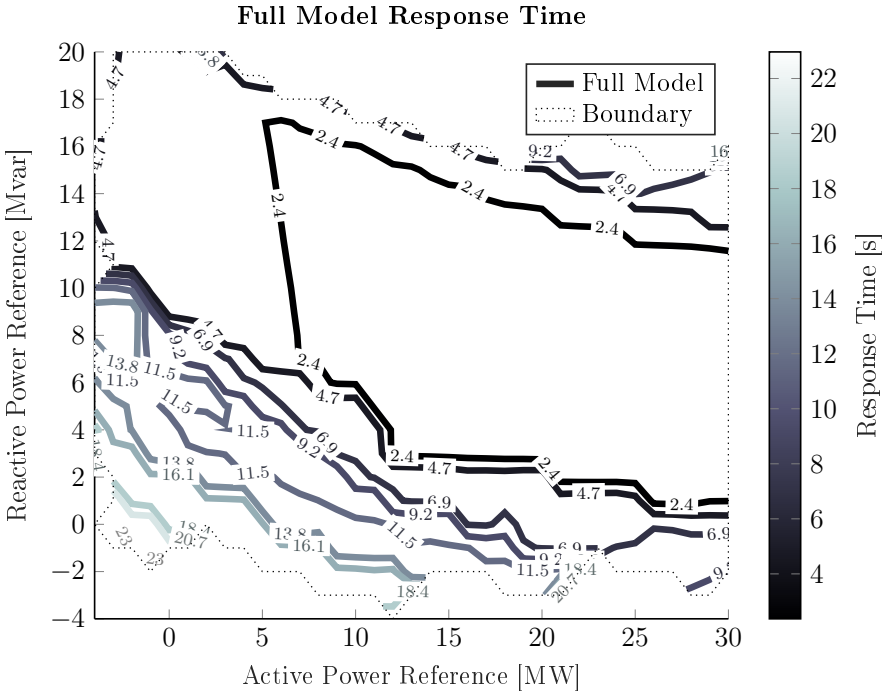

Figure 5.7: Full Model Tracking Delay Depending on P_{ref} and Q_{ref}

To quantify the difference of the two models, a tracking delay inaccuracy 2-D matrix is defined as

$$\boldsymbol{T} = \boldsymbol{\tau}_{\mathbf{red}} - \boldsymbol{\tau}_{\mathbf{full}}, \tag{5.4}$$

where $\boldsymbol{\tau}_{\mathbf{red}}$ and $\boldsymbol{\tau}_{\mathbf{full}}$ are the matrices containing the response times of the reduced and full model for the queried reference power flows in the P/Q-plane. The subtraction necessitates that the matrices are of equal size and that they query the same reference values for the active and reactive power flow.
The tracking inaccuracies are shown using isolines in figure 5.9. The SPC can be expected to spend most of its time in the central areas of the feasible region and would transition through these areas most of the time. The tracking inaccuracy of the reduced grid in these areas is very low and generally close to 0. Towards the edges of the feasible region, the tracking inaccuracy becomes larger, reducing the predictive capabilities of the reduced model. However, the flexibility regions have a similar size and shape, so despite the difference in tracking delay prediction, the fundamental capacity of the grid to follow the reference signal is still correctly modeled. The flexibility regions of the generators of the full grid were randomly sized to roughly coincide with SPC apparent power balancing. The values are given in appendix tables D.16 and D.17.

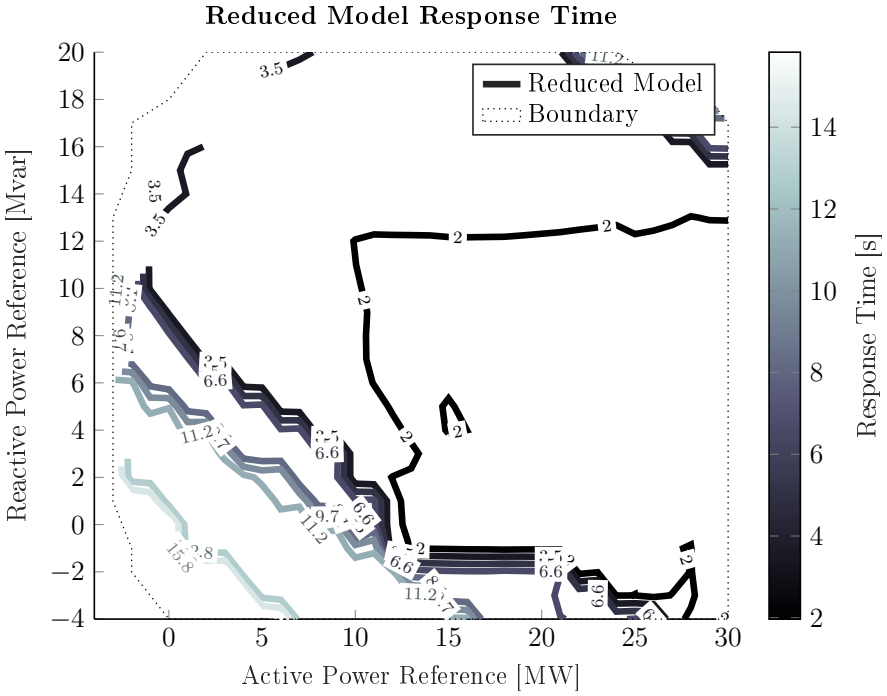

Figure 5.8: Reduced Model Tracking Delay Depending on P_{ref} and Q_{ref}

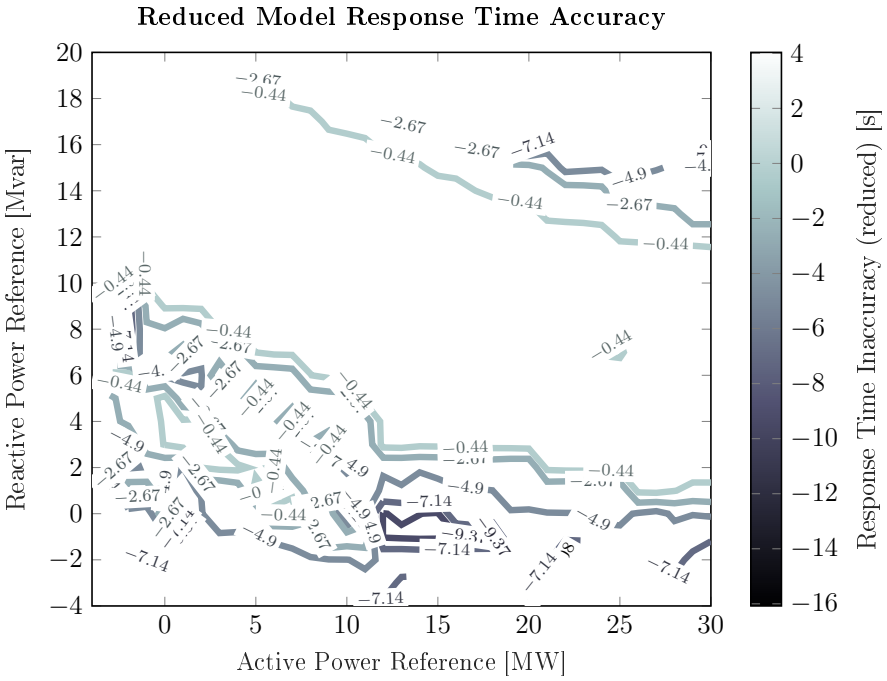

Figure 5.9: Inaccuracy Matrix $\boldsymbol{T}$ (according to eq. 5.4)

5.7. Upstream Signals

The SPC sends status signals upwards in the controller hierarchy just as it received signals from those lower in the hierarchy. There are obvious signals that should be reported upwards without concrete knowledge of the algorithm in the higher-level controller. The following signals should give broad coverage for a variety of complex higher-level controllers:

1. The parameters and structure of the reduced-order model derived in this chapter.
2. The flexibility region of the SPC.

Dynamic simulations are common in the operation of the transmission grid and communicating the parameters and structure of the reduced-order models derived in this chapter is essential for automated simulations. The flexibility region of the SPC must be calculated first. Principally, there are three ways to calculate it:

1. Aggregating F_{i_b} transmitted upwards by the buses using the Minkowski sum described in chapter 3 and appendix C.
2. Aggregating using power flow calculation sampling.
3. Aggregating using simplified power flow calculation sampling.

The first of these, aggregating F_{i_b}, is largely identical to the approach in chapter 3, where the device flexibility regions B were aggregated into the bus flexibility region F_{i_b}. This approach works well if all devices are connected to a single bus, but it does not work well for the SPC's flexibility region because it only aggregates energetic flexibility: it doesn't necessarily mean that the operating point is safe (bus voltages, cable currents, etc) for the SPC. In chapter 3 this was not considered problematic because the devices prior to aggregation were not thought to be dispersed enough to have appreciably different voltage levels.
Aggregating using power flow calculation sampling would perform the following steps:

1. Generate an operating point for all the devices from the different bus flexibility regions F_i.
2. Run power flow and determine safety.
3. Generate new operating point and iterate.
4. Discard unfeasible operating points and generate convex hull out of feasible ones to construct the SPC flexibility region.

Generating a new operating point can either be random or using some kind of heuristic search. Random sampling was used in [Mayorga Gonzalez 2021], for example. This

approach yields high-fidelity results for the flexibility region, but constructing a well-defined flexibility region requires many iterations and power flow calculations, which could be too slow for the higher-level controller.
Much time can be saved by using corrected linear approximations such as those developed in [D. Contreras 2021], making the calculation of the flexibility region both very fast and accurate.

Chapter Summary

This chapter described a reduced model of the SPC based on grey-box parameter optimization using metaheuristics. The reduced model is simple and only contains a few buses, just enough as are necessary to have as many interconnections as the full SPC model and as many as are necessary to produce adequate voltage gradients for appropriate control behavior. This was demonstrated in simulations using a two-bus, single-interconnection reduced model. Approximately 85% of the computational cost could be saved while providing a good approximation of the full model within most of the flexibility region away from the hull.
With a functional reduced model available, SPCs can be interconnected at acceptable computational cost through the transmission grid and their behavior investigated in the next chapter.

Interconnected Smart Power Cells

With an accurate reduced model having been established for the SPC in the previous chapter, a transmission grid-level controller can be designed for these SPCs and the reduced models can be connected in a model representing a section of the transmission grid to investigate the behavior of interconnected SPCs.

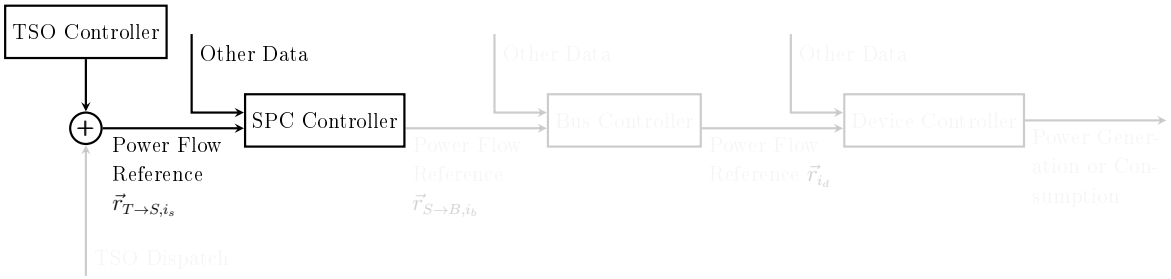

Figure 6.1: Controller Hierarchy Overview (Current Chapter in Bold)

The content of this chapter in the context of the controller hierarchy is shown in figure 6.1. Recall from chapter 4 that the SPC controller follows reference signals $\vec{r}_{T\to S}$ for the interconnections of the SPC while maintaining internally stable operation. For an adequate investigation of interconnected SPC behavior, it is not enough to invent these reference functions $\vec{r}_{T\to S}$ as was done in chapter 4 to test the controllers. They must be generated by an appropriate control mechanism that responds to conditions in the transmission grid.

6.1. Design Goals and Limitations of TSO Controller

6.1.1 Limitations

Power system control at the transmission grid level has a long history (unlike advanced distribution grid control) and covers a diverse range of methods and goals. Only a part of this field can be taken into account in this chapter.
Frequency control is historically tied to active power balance because of the rotational energy stored in spinning synchronous generators. The result is a global, coupled control problem for both frequency and active power and the frequency control error can be used as a proxy for the active power balance control error, which is much more

complex to measure. This behavior can be replicated in power electronics for better coexistence with conventional generation (see i.e. [J. Liu et al. 2016]), but as the power grid changes, it is unclear whether this will continue to be necessary or beneficial and whether a fundamental relationship between frequency and active power will continue to exist indefinitely. Furthermore, the simulation models in this work have been based on constant 50 Hz phasor models that fundamentally do not reflect this relationship in the interest of simulation speed. For these reasons, frequency control is not a part of the control problem in this chapter.
Scheduling and dispatch are discontinuous, long-term control actions that interact with dispatchable generation units to make sufficient capacity available for grid stability. They do this by sending a piece-wise constant setpoint signal to dispatchable units at regular time steps (such as 15 min) and by deciding which units to schedule for operation hours or days in advance. These dispatch algorithms (such as Optimal Power Flow, see modern versions in [W. Zhang et al. 2017]) would change somewhat in a grid dominated by renewable generation since the emphasis placed on weather and storage forecasts would be much larger. A variety of publications have already examined this problem and reviews have identified solid progress [Hasan et al. 2019]. It is for this reason that scheduling and dispatch algorithms for the renewable power grid were not identified as an urgent area of research in chapter 1. That aside, such adaptations of the dispatch algorithms are beyond the scope of this work also because they work on timescales of minutes and hours. The controllers designed for the SPC in the previous chapters act on millisecond to second timescales and running the simulation long enough to allow meaningful interaction with dispatch algorithms would be unfeasibly expensive computationally. The continuous controllers described in this chapter shift the operating point according to their control laws in response to changes in the grid and are not intended to replace scheduling and dispatch. This is also depicted in the chapter overview in figure 6.1.

6.1.2 Design Goals

The transmission grid-level controller designed in this chapter is intended to respond to disturbances by sending appropriate reference signals to the SPCs it controls. Since frequency control is not possible here, the focus will be voltage control and power balance aspects. The location of the transmission grid controller is again depicted in figure 6.2 along with the reduced SPC model derived in the previous chapter. With this in mind, the simulation will investigate the loss of most of an SPC's generation capacity and the response of the controllers to the resulting voltage drop.

6.2. State of the Art

Transmission grid dispatch is generally based on optimal power flow (OPF) or other optimization-based algorithms, such as the security-constrained OPF used in North America; see [Guo et al. 2013]. Purely continuous-time control has existed, but a general

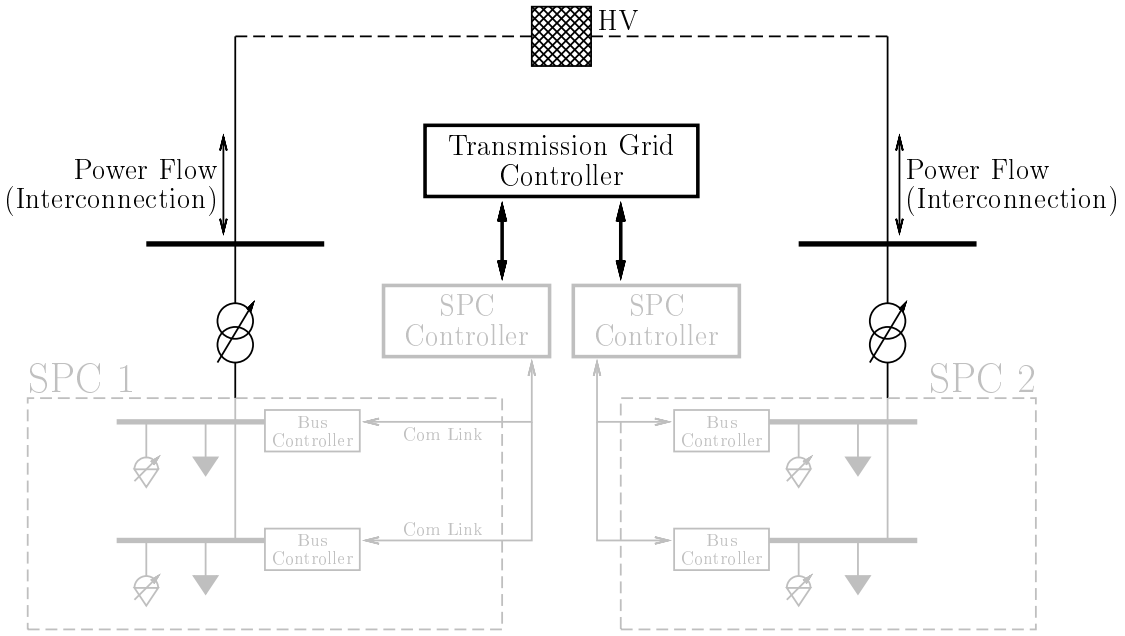

Figure 6.2: Location of Transmission Grid Controllers

movement towards OPF can be observed (for example in France, see [Ilic et al. 1995; Lefebvre et al. 2000]).

A combination of OPF-style dispatch and continuous control as used in the traditional grid offers reduced controller oscillations on long timescales and the possibility of running the system closer to the grid limits. The chief disadvantage of OPF is its struggle with fast dynamics (see [Mei et al. 2008]) due to its slow iterations and open-loop nature. There have been attempts to expand the capabilities of automatic control to return to it some of the authority given to OPF in recent decades. Pilot voltages and area partitioning were widely used for many years but struggle with shifting control authority in the grid due to renewable generation [Lu et al. 2018]. Attempts to correct this such as [Yan et al. 2016] using iterative genetic algorithms are generally complex and only feasible with large installations.

Since the Smart Power Cells would exist in large parts of the distribution grid to bundle their renewable generation, many buses in the transmission grid become controllable and can provide voltage control functionality at the high-voltage side when given appropriate reference signals for the active and reactive power flow at the interconnection. In a way, this makes voltage control at the high-voltage side for SPCs easier than it currently is: voltage control is largely a local control problem, so the more widely dispersed and homogeneous relative to the load the generation capacity is, the better it is for voltage control.

To provide voltage control, different algorithms exist, with the most popular varieties based on either $\cos\varphi(P)$ or $Q(U)$ control. $\cos\varphi(P)$ control defines a characteristic curve that adjusts the setpoint of a generator using its power factor based on the active power generation. In the majority of cases and for most applications, $Q(U)$ control performs better [Schultis et al. 2019]; it can be thought of as a proportional controller

with deadband behavior around the nominal voltage (the size of the deadband depending on the voltage level and application, but generally in the range of 3 % to 10 %. The voltage control in this chapter is based on this general principle as well, though not realized as a proportional controller.

6.3. Model Structure

6.3.1 Transmission Grid Model

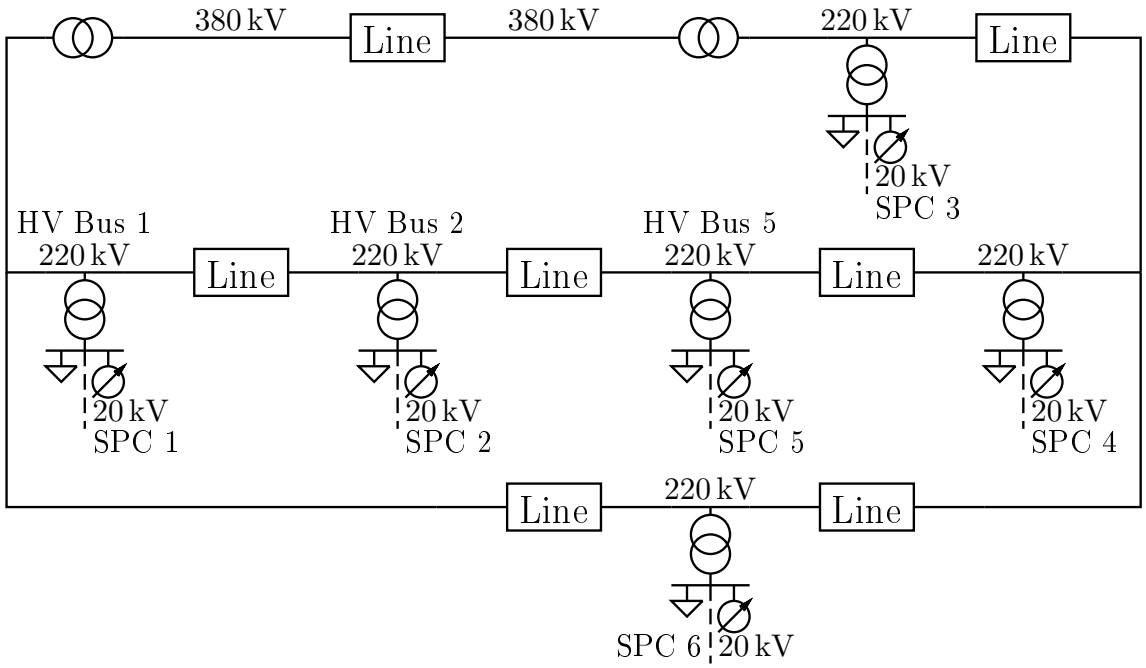

Figure 6.3: Model Transmission Grid Structure

The structure of the transmission grid connecting the SPCs is based on CIGRE's 6-bus high-voltage benchmark grid in [Strunz et al. 2014] for renewable generator integration, with some modifications to the line lengths. It is depicted schematically in figure 6.3. SPCs are assumed to be in close physical proximity in the future, and so the line lengths of the model are reduced by a factor of 10, consequently ranging from 10 km to 100 km. The slack bus is connected to high-voltage (HV) Bus 2, separated by another power line (not shown) 750 km long. This is intended to reflect a weak wide-area synchronous grid with limited ability to stabilize the SPCs.

6.3.2 SPC Models

Each connected SPC is based on the reduced model derived in chapter 5. Unique reduced grids were generated by modifying the parameters of the solution in appendix table D.15 randomly by up to ±10%.

The generators connected to the two buses $j = i_b = \{1, 2\}$ of each SPC $i_s = \{1, 2, 3, 4, 5, 6\}$ have a flexibility region in the PQ-plane for active and reactive power generation modelled as a circle of maximum apparent power $F_{i_s j}$. It is assumed that this circular shape arises from a variety of generators and storages being represented by a single, virtual generator according to the aggregation in chapters 3 and 5. $F_{i_s j}$ is randomly initialized between 16 MVA to 24 MVA. Bus 1 of SPC 4 is initialized as $F_{41} = 8\,\text{MVA}$ to make the simulation more interesting since it means that only fairly little generation capacity remains in SPC 4 after the loss of generation capacity at bus 2. The power balance of each SPC model lies at around 35 MVA, subject to the randomization described earlier.

6.4. Controller

6.4.1 Control Function

The transmission grid controller developed for this work generates the single-interconnection power flow reference values $r_{T\to S,P,i_s}$ and $r_{T\to S,Q,i_s}$ transmitted to each SPC controller i_s with a focus on providing a fast response to severe disturbances of generation capacity. Redispatch would further intervene at its iteration points, but this is much slower and will be ignored here. The general form of the controller for each reference signal is:

$$\begin{aligned} e_{U,i_s} &= (r_{U,i_s} - y_{U,i_s}) \\ e_{f,U,i_s} &= f(e_{U,i_s}) \\ r_{T\to S,P/Q,i_s} &= \frac{1}{s} e_{f,U,i_s} C, \\ e_{P/Q,i_s} &= r_{T\to S,P/Q,i_s} - y_{P/Q,i_s} \end{aligned} \tag{6.1}$$

where C is a non-zero scalar of dimension $\text{W}\,\text{pu}^{-1}$ or $\text{var}\,\text{pu}^{-1}$, respectively. An appropriate order of magnitude for C can be calculated by either taking it as the inverse of the voltage sensitivity index ($C = (\text{VSI})^{-1}$) or by estimating it using a DC approximation for the connected SPC, as in $C \approx \frac{U^2}{R}$, with R as the average sum line resistance of the distribution grid. It is not necessary to derive this constant very accurately because the controller integrates the controller error and will eventually provide the necessary power to stabilize the voltage. This sets the controller apart from $Q(U)$ control, which requires a more carefully chosen proportionality constant to return the voltage to the deadband.

6.4.2 Alternate Controllers

The transmission grid controller described here does not use any of the signals sent to it by the SPCs and requires no knowledge other than the HV-side bus voltage, though knowledge of the aggregated flexibility region of the SPC would be beneficial to prevent controller windup and is assumed for the simulation. As described in previous sections

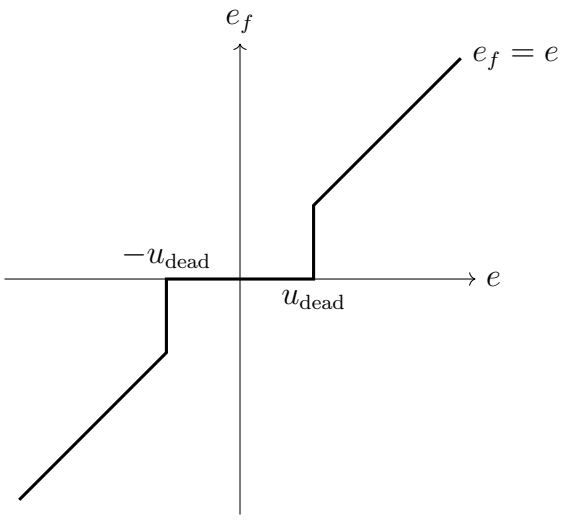

Figure 6.4: Voltage Deadband

that discussed unused signals, specifically sections 4.8 and 5.7, the control structure is meant to be adaptable and to not rely on specific algorithms that may or may not require or provide certain signals. Model-predictive control (MPC) is once more an appealing alternative to the described controller, although at this control layer the simulation of the reduced models of the SPC is still relatively slow (certainly when compared to the approximation of the controlled bus in chapter 3). This would make running a well-performing MPC very difficult. A different model-order reduction that provides faster reduced models would be preferable, perhaps based on machine learning.

6.5. Simulation

6.5.1 Simulation Parameters

The HV voltage deadband u_{dead} was chosen as $\pm 1\%$. C was estimated at $100\,\text{Mvar}\,\text{pu}^{-1}$. Only reactive power is used for voltage control and the active power flow interconnection reference signal is set to 0 (power balance, no import or export) for all connected SPCs. The medium-voltage (MV) controller parameters are the same as given in chapter 5. The bus flexibility limits are given in appendix table D.18 and the HV line lengths and parameters are given in appendix tables D.19 and D.20. The MV SPC reduced model parameters are in appendix table D.15.

6.5.2 Simulation Results

SPC 4 is subjected to a total loss of generation capacity at $t = 5\,\text{s}$ at bus 2 and the grid response is observed. The HV-side bus voltage of SPC 4 can be seen in figure 6.5. A sharp drop is visible when the generation capacity is lost. This is to represent, for example, some weather phenomenon that severely affects the renewable generators in that area. Voltage restoration in the high-voltage grid by the other SPCs is swift

and returns to within the deadband within one second. The voltage restoration induces oscillations in the response of the integral controller structure, but these are greatly dampened in the response of the FPID controller structure.
The active and reactive power flow at the interconnection of SPC 4 are depicted in figures 6.10 and 6.11, showing that the SPC loses roughly 15 MW of generation when its capacity at bus 2 is lost (a positive power flow at the interconnection being in the direction of the distribution grid). Naturally, bus 1 of SPC 4 attempts to correct this, but since the flexibility region was initialized at only 8 MVA, it has insufficient capacity to do anything. The noise in the reactive power flow is of a numerical nature only and doesn't represent a physical process. The controller repeatedly attempts to extract more reactive power generation from its only remaining generator than it can supply, which causes jitter at the edge of the flexibility region.
Due to the large size of the model and its many generators, only a few other buses can be depicted graphically. The active and reactive power flows at the interconnection of SPC 1 with the transmission grid can be seen in figures 6.6 and 6.7. Note that a positive power flow is in the direction of the distribution grid, so the reduction in response to the generation capacity loss in SPC 4 corresponds to an increase in the generation in SPC 1. This can be seen more clearly in figures 6.8 and 6.9 showing the active and reactive power generation of SPC 1, bus 2 (without accounting for the connected load). The controller oscillations of the I-controller structure are also clearly visible. These are also suppressed by the fractional controller.
Different reference values for the interconnections and different setpoints for the generators being generated by the transmission grid controller for the SPCs arise from the complex interaction of the SPC controller layer with the transmission grid controller layer. Changes in the generation in one SPC induce changes in the HV-side voltage of other SPCs and prompt these to shift their injection as well. Even though both simulations were performed with identical physical parameters, this controller interaction is enough to substantially shift the steady state operating point depending on which controller structure is used. Initializing both models completely identically would be extremely complex because of the decaying and saturating nature of fractional controller states, and therefore it was not attempted.
Simulation time on an office computer running MATLAB/Simulink was approximately 5 min, with little difference between the I-controller and the FPID controller. The relatively complex mathematics underlying fractional derivatives are insignificant compared to the general size of the model and such a controller could be implemented in a physical system.

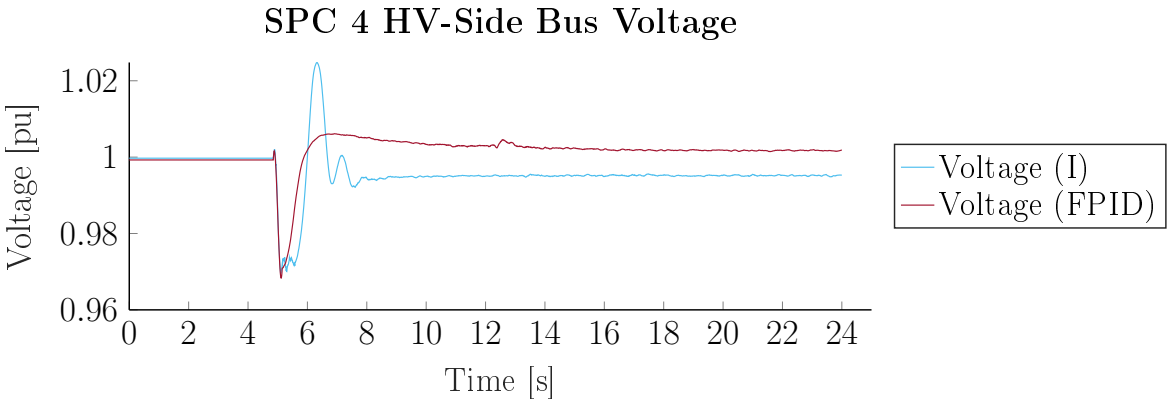

Figure 6.5: HV-side Bus 4 Voltages

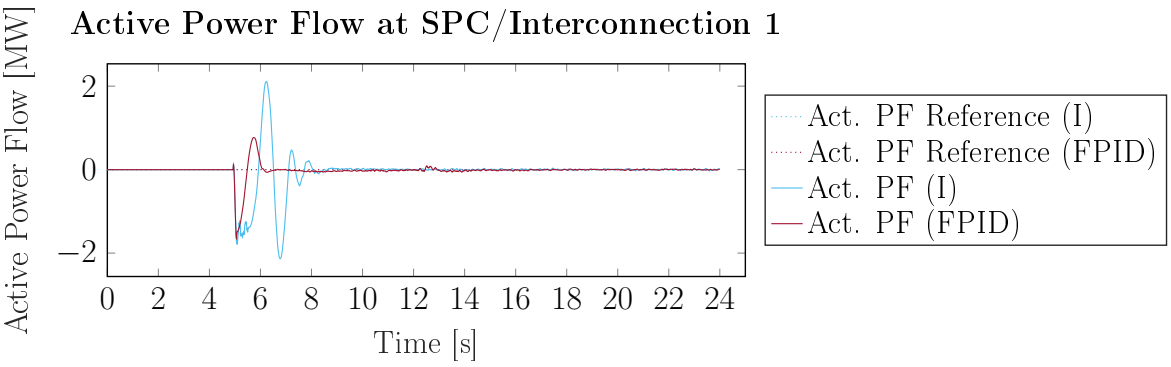

Figure 6.6: SPC-TSO 1 Interconnection Active Power Flow ($y_{P,1}$)

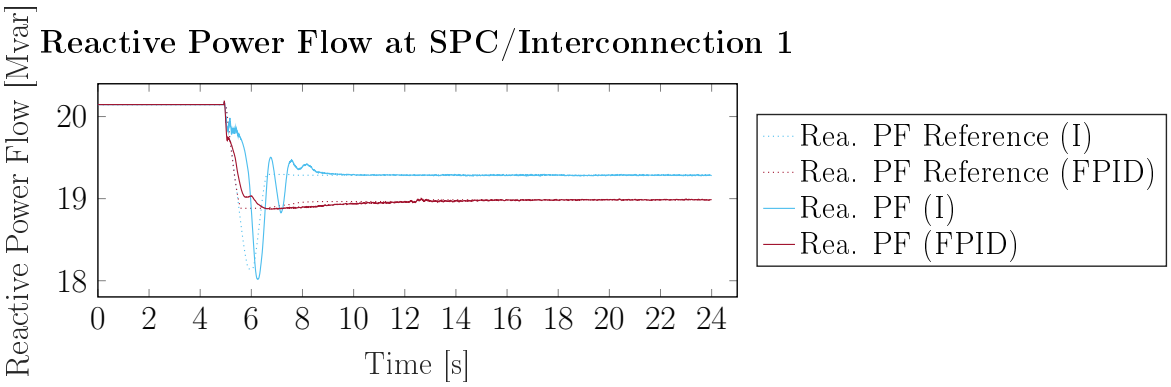

Figure 6.7: SPC-TSO 1 Interconnection Reactive Power Flow ($y_{Q,1}$)

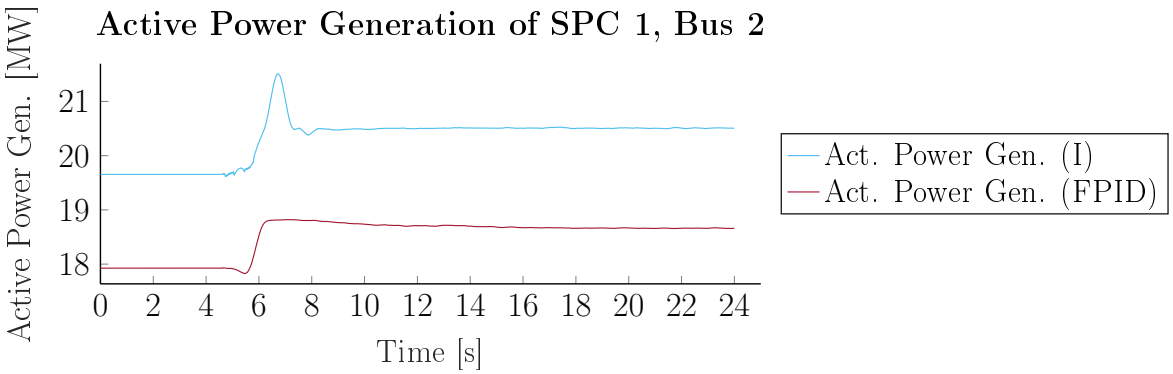

Figure 6.8: SPC 1 Bus 2 Active Power Generation (P_{12})

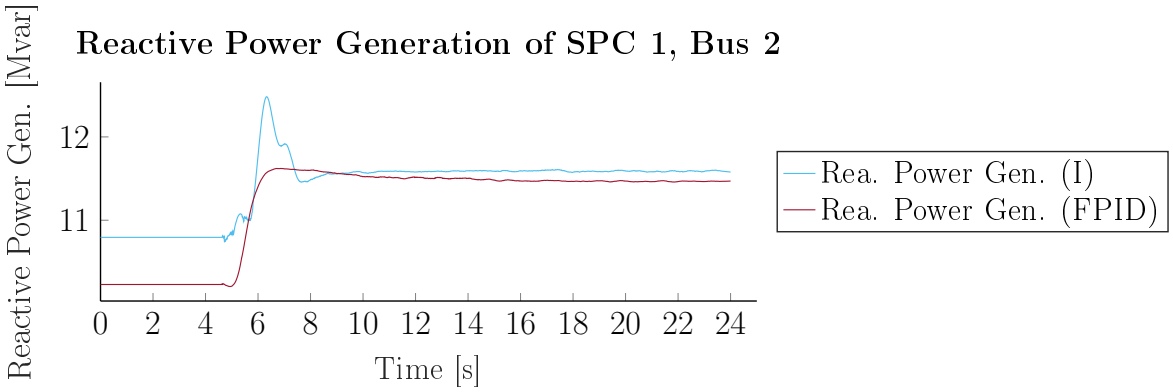

Figure 6.9: SPC 1 Bus 2 Reactive Power Generation (Q_{12})

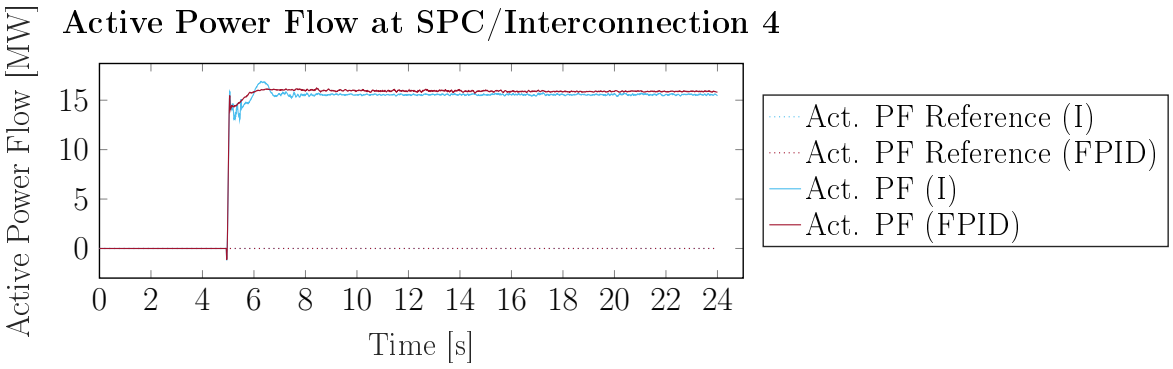

Figure 6.10: SPC-TSO 4 Interconnection Active Power Flow ($y_{P,4}$)

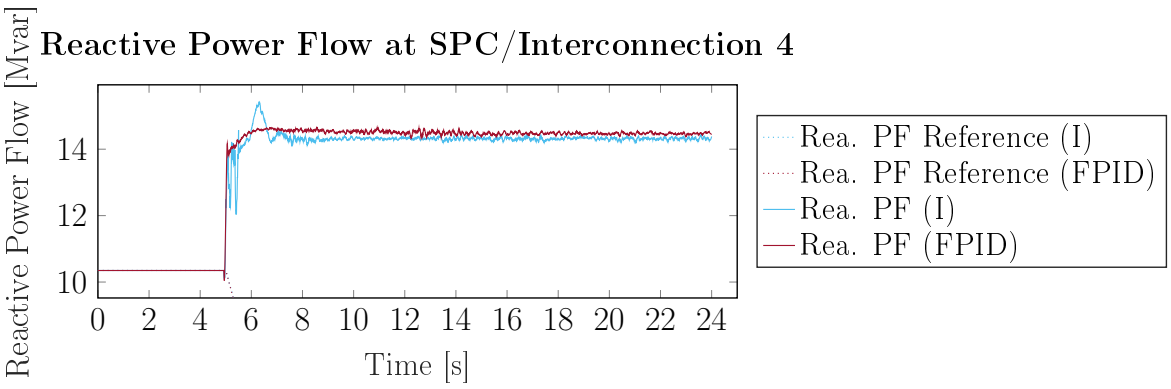

Figure 6.11: SPC-TSO 4 Interconnection Reactive Power Flow ($y_{Q,4}$)

Chapter Summary

This chapter described a voltage controller for the high-voltage buses in the transmission grid. It controls the voltage at these buses by sending reference power flow signals to the SPCs for the interconnections with the transmission grid in accordance with the SPC controller described in chapter 4. The simplified models of the SPC are based on the work in chapter 5 to make simulation more computationally feasible. The controllers were tested by simulating a large loss of generation capacity (for example, after a weather event) in one of the SPCs and thereafter successfully returned bus voltages to the tolerance band. The FPID controller described in chapter 4 suppresses oscillations compared to the integral controller. The simulation shows the fundamental interoperability of SPCs and their ability to support each other.

Conclusions

In this work, a control architecture for cellular grids was described based on the concept of the Smart Power Cell (SPC). The controller hierarchy spans multiple voltage levels, including a medium- or low-voltage bus controller, a medium-voltage SPC controller, and a high-voltage controller for the interconnection of SPCs. The controllers make themselves controllable for the next higher-level controller, leading to a hierarchical structure. Model-order reductions were also developed side-by-side with the controllers for the buses in the SPC and for the SPC as a whole to generate adequate reduced models for simulation and control. The work also made a substantial effort to standardize the hierarchy and its signal flows while maintaining modularity and flexibility.
In chapter 3, bus controllers were developed that control the controllable devices (generators, flexible loads, storage installations, etc) connected to the bus in order to fulfill the desired reference power flows from the higher-level controller while maintaining as simple dynamic behavior as possible. The controllers accomplish this using transfer function considerations and simplifications as well as a constrained optimization problem to assign appropriate setpoints to the various controlled devices. Simulation studies were carried out for validation and show good tracking and benign dynamic behavior. This chapter also explored the aggregation of bus generator flexibility using Minkowski sums.
These controllers were integrated into the Smart Power Cell in chapter 4 and a multiple-input, multiple-output controller was developed for the Smart Power Cell to track reference signals for the interconnections of the SPC with the transmission grid, other SPCs, and other energy grids while respecting voltage limits inside the SPC. To this end, the SPC controller used linear parameter-varying control for the voltage profile inside the SPC and a vector formulation broadly inspired by state space control for its tracked interconnections. Special attention was paid to reducing controller oscillations using fractional control. Simulation studies were carried out for validation and show the success of the controller in producing acceptable voltages, suppressing oscillations, and following power flow reference signals for the interconnections.
A reduced-order model was developed for the controlled (closed-loop) SPC model in chapter 5 to provide a dynamic approximation at lower computational cost. The reduced model approximated the power flow and voltage control behavior of the full model using metaheuristic optimization of a grey-box model structure. Simulation studies were carried out for validation over a large range of interconnection power flow reference values to show the similarity of the closed-loop behavior at the interconnections as characterized by the tracking delay and the similarity of the flexibility region of the full- and

reduced-order model. Large computational savings of around 85% could be obtained. With a comparatively computationally inexpensive model having been constructed from all the previous chapters, an interconnection of SPCs was constructed in chapter 6 and high-voltage voltage controllers developed which controlled the voltages at the high-voltage side of the SPCs in response to severe disturbances of generation capacity. The controllers were able to stabilize the voltage and limit controller oscillations.
The research questions described in section 1.5 were

1. the modeling and control of the various generators, loads, and storage elements in the SPC,
2. the internal control of the SPC and its ability to support other SPCs,
3. the reduction of the computational complexity of the SPC models,
4. the control of an interconnection of SPCs and the investigation of their behavior.

The results outlined above contributed substantially to all these research question and the contributions proposed in section 1.6 are considered fulfilled. The simulation results validate the developed hierarchical, modular control structure. It could be shown that large-scale complexity reduction is possible by integrating controller design and model-order reduction into a single process. The modularity and adaptability of the proposed controllers is also apparent in the discussions of their signal flow: none of them rely on specific algorithms in other layers and they generally produce more status signals than are necessary for the algorithms in this work to allow the drop-in implementation of other algorithms that might require these signals.

Outlook

Due to the flexibility and modularity of the controller architecture, there are many possible alternatives at different levels that could be investigated. Some of these have been mentioned in this work, such as replacing the SPC or TSO controller with model-predictive control. In fact, model-predictive control (MPC) could also be used for the bus controller. MPC can include complex optimality criteria besides control error, and including the desired first-order transfer function closed-loop behavior appears feasible. The SPC model order reduction can be improved upon. Machine learning has shown remarkable potential for the approximation of complex systems and some early forays have been published. The main drawback to this approach is that machine learning generally struggles to accurately learn discontinuous switching behavior such as OLTC transformers, and this switching behavior is important for the voltage profile. However, such a model approximation would run very quickly, much faster than the 85% reduction developed in this work using a grey-box model.
The interactions of the SPC architecture with traditional dispatch algorithms such as OPF are also worth investigating. This faces two hurdles. Simulating an interconnection of SPCs on timescales long enough to make dispatch relevant is still computationally burdensome using grey-box models. Additionally, for proper dispatch algorithms, economic data is integral. The concept of aggregation and reduction of complexity means that it would be counterproductive to allow market access to all the generators in the SPC individually. Instead, the SPC should participate in the energy market as a single entity. How exactly the SPC determines its own cost of generation remains a non-trivial question because of the possible need for the SPC controller to use non-optimal generators in support of SPC bus voltages. That said, the signal flow in the controller hierarchy can easily be expanded to include economic data for aggregation and control.
Other questions exist regarding the planning of the SPC, primarily in terms of sizing. In general, it is less the balance of load and generation of the SPC that affects its feasibility and more its physical and electrical size in terms of line or cable lengths. Since the OLTC transformers are essential for expanding the flexibility region of the SPC and assisting the SPC controller with voltage control, a large physical size of the SPC will make it difficult to properly utilize the flexibility of buses that are electrically distant from the OLTC transformers. Those buses would regularly be in voltage control mode and contribute relatively little to interconnection power flow control. A methodology should be developed to estimate the optimal size of an SPC for a variety of SPC topologies.
Presently, in this work, multi-modal interfaces are assumed to behave as storage elements of infinite capacity. The flow of hydrogen into the gas grid or out of it is assumed to be

insignificant relative to the capacity of the network. This may not be realistic depending on the scenario. Likewise, the limits of the gas grid are not being considered. Gas grids are also subject to constraints like node pressure and gas flows through pipes at far slower velocities of around $20\,\mathrm{m\,s^{-1}}$ to $100\,\mathrm{m\,s^{-1}}$, depending on the type of pipeline, compared to the near-light-speed of electric power transmission. Simulations of the gas grid would therefore play out on very different timescales. This is worth investigating, but designing a combined model capable of simulation at such vastly different timescales is a very complex task.

Bibliography

Barber, C. Bradford, David P. Dobkin, and Hannu Huhdanpaa (1996). "The quickhull algorithm for convex hulls". In: *ACM Transactions on Mathematical Software* 22.4, pp. 469–483.

Berg, M. d., O. Cheong, M. v. Kreveld, and M. Overmars (2008). *Computational Geometry*. Springer-Verlag Berlin Heidelberg, pp. 296–297.

Blasi, Thaís M., Thelma S. P. Fernandes, Alexandre R. Aoki, and Fabrício H. Tabarro (2021). "Multiperiod Optimum Power Flow for Active Distribution Networks With Provisioning of Ancillary Services". In: *IEEE Access* 9, pp. 110371–110395.

Briat, Corentin (2015). *Linear Parameter-Varying and Time-Delay Systems*. Heidelberg: Springer Verlag.

Cabiati, M., C. Tornelli, and L. Martini (2018). "The ELECTRA Web-of-Cells control architecture concept for the future power system operation". In: *2018 AEIT International Annual Conference*, pp. 1–6.

Cady, Stanton T., Alejandro D. Domínguez-García, and Christoforos N. Hadjicostis (2015). "A Distributed Generation Control Architecture for Islanded AC Microgrids". In: *IEEE Transactions on Control Systems Technology* 23.5, pp. 1717–1735.

Chaspierre, Gilles (Dec. 2020). "Reduced-order modelling of active distribution networks for large-disturbance simulations". PhD thesis.

Chazelle, B. and D. P. Dobkin (1985). "Optimal Convex Decompositions". In: *Machine Intelligence and Pattern Recognition* 2 (2), pp. 63–133.

Chen, Gang, Frank L. Lewis, E. Ning Feng, and Yongduan Song (2015). "Distributed Optimal Active Power Control of Multiple Generation Systems". In: *IEEE Transactions on Industrial Electronics* 62.11, pp. 7079–7090.

Conte, F., F. D'Agostino, and F. Silvestro (2019). "Operational constrained nonlinear modeling and identification of active distribution networks". In: *Electric Power Systems Research* 168, pp. 92–104.

Contreras, D. A. and K. Rudion (2019). "Time-Based Aggregation of Flexibility at the TSO-DSO Interconnection Point". In: *2019 IEEE Power & Energy Society General Meeting (PESGM)*, pp. 1–5.

Contreras, Daniel (Oct. 2021). "Estimation of Flexibility Potentials in Active Distribution Networks". PhD thesis.

Dittmar, Rainer (2017). *Advanced Process Control*. Berlin, Boston: De Gruyter Oldenbourg.

Fukuda, K. (2004). "From the zonotope construction to the Minkowski addition of convex polytopes". In: *Journal of Symbolic Computation* 38 (4), pp. 1261–1272.

Fulgêncio, Nuno, Carlos Moreira, Leonel Carvalho, and João Peças Lopes (2020). "Aggregated dynamic model of active distribution networks for large voltage disturbances". In: *Electric Power Systems Research* 178, p. 106006.

Ghadi, M. Jabbari, Sahand Ghavidel, Amin Rajabi, Ali Azizivahed, Li Li, and Jiangfeng Zhang (2019). "A review on economic and technical operation of active distribution systems". In: *Renewable and Sustainable Energy Reviews* 104, pp. 38–53.

Ghosh, Sudipta, Sukumar Kamalasadan, Nilanjan Senroy, and Johan Enslin (2016). "Doubly Fed Induction Generator (DFIG)-Based Wind Farm Control Framework for Primary Frequency and Inertial Response Application". In: *IEEE Transactions on Power Systems* 31.3, pp. 1861–1871.

Giuntoli, Marco and Davide Poli (2013). "Optimized Thermal and Electrical Scheduling of a Large Scale Virtual Power Plant in the Presence of Energy Storages". In: *IEEE Transactions on Smart Grid* 4.2, pp. 942–955.

Glad, S. Torkel (2021). "Modeling of Dynamic Systems from First Principles". In: *Encyclopedia of Systems and Control*. Ed. by John Baillieul and Tariq Samad. Springer International Publishing, pp. 1286–1291.

Grüne, Lars and Jürgen Pannek (2017). *Nonlinear Model Predictive Control*. Heidelberg: Springer Verlag.

Guo, Qinglai, Hongbin Sun, Mingye Zhang, Jianzhong Tong, Boming Zhang, and Bin Wang (2013). "Optimal Voltage Control of PJM Smart Transmission Grid: Study, Implementation, and Evaluation". In: *IEEE Transactions on Smart Grid* 4.3, pp. 1665–1674.

Hachenberger, Dirk and Dieter Jungnickel (2020). "Factorization of Univariate Polynomials over Finite Fields". In: *Topics in Galois Fields*. Cham: Springer International Publishing, pp. 241–295.

Hadwiger, H. (1950). "Minkowskische Addition und Subtraktion beliebiger Punktmengen und die Theoreme von Erhard Schmidt". In: *Mathematische Zeitschrift* 53 (3), pp. 210–218.

Hasan, Kazi Nazmul, Robin Preece, and Jovica V. Milanović (2019). "Existing approaches and trends in uncertainty modelling and probabilistic stability analysis of power systems with renewable generation". In: *Renewable and Sustainable Energy Reviews* 101, pp. 168–180.

Ilic, M.D., Xiaojun Liu, G. Leung, M. Athans, C. Vialas, and P. Pruvot (1995). "Improved secondary and new tertiary voltage control". In: *IEEE Transactions on Power Systems* 10.4, pp. 1851–1862.

Indranil, P. and D. Saptarshi (2013). *Intelligent Fractional Order Systems and Control*. Heidelberg: Springer Verlag.

Jenkins, N., J. Ekanayake, and G. Strbac (2010). *Distributed generation*. London: Institution of Engineering and Technology.

Jiang, Yibao, Can Wan, Jianhui Wang, Yonghua Song, and Zhao Yang Dong (2019). "Stochastic Receding Horizon Control of Active Distribution Networks With Distributed Renewables". In: *IEEE Transactions on Power Systems* 34.2, pp. 1325–1341.

Karagiannopoulos, Stavros, Jannick Gallmann, Marina González Vayá, Petros Aristidou, and Gabriela Hug (2020). "Active Distribution Grids Offering Ancillary Services in Islanded and Grid-Connected Mode". In: *IEEE Transactions on Smart Grid* 11.1, pp. 623–633.

Kardakos, Evaggelos G., Christos K. Simoglou, and Anastasios G. Bakirtzis (2016). "Optimal Offering Strategy of a Virtual Power Plant: A Stochastic Bi-Level Approach". In: *IEEE Transactions on Smart Grid* 7.2, pp. 794–806.

Karlsson, D. and D.J. Hill (1994). "Modelling and identification of nonlinear dynamic loads in power systems". In: *IEEE Transactions on Power Systems* 9.1, pp. 157–166.

Karthikeyan, Nainar, Jayakrishnan Radhakrishna Pillai, Birgitte Bak-Jensen, and John W. Simpson-Porco (2019). "Predictive Control of Flexible Resources for Demand Response in Active Distribution Networks". In: *IEEE Transactions on Power Systems* 34.4, pp. 2957–2969.

Keyhani, A., M.N. Marwali, and M. Dai (2009). *Integration of Green and Renewable Energy in Electric Power Systems*. Wiley.

Kontis, Eleftherios O., Theofilos A. Papadopoulos, Mazheruddin H. Syed, Efren Guillo-Sansano, Graeme M. Burt, and Grigoris K. Papagiannis (2019). "Artificial-Intelligence Method for the Derivation of Generic Aggregated Dynamic Equivalent Models". In: *IEEE Transactions on Power Systems* 34.4, pp. 2947–2956.

Kouveliotis-Lysikatos, Iasonas, Despina I. Koukoula, Aris L. Dimeas, and Nikos D. Hatziargyriou (2022). "Plug-and-Play Algorithms for the Efficient Coordination of Active Distribution Grids". In: *Proceedings of the IEEE* 110.12, pp. 1927–1939.

Kroposki, Benjamin, Andrey Bernstein, Jennifer King, Deepthi Vaidhynathan, Xinyang Zhou, Chin-Yao Chang, and Emiliano Dall'Anese (2020). "Autonomous Energy Grids: Controlling the Future Grid With Large Amounts of Distributed Energy Resources". In: *IEEE Power and Energy Magazine* 18.6, pp. 37–46.

Kuhn, U. (1995). "Eine praxisnahe Einstellregel für PID-regler". In: *Automatisierungstechnische Praxis* 5, pp. 10–16.

Kundur, Prabha (1994). *Power System Stability and Control*. 1st ed. McGraw Hill.

Lefebvre, H., D. Fragnier, J.Y. Boussion, P. Mallet, and M. Bulot (2000). "Secondary coordinated voltage control system: feedback of EDF". In: *2000 Power Engineering Society Summer Meeting (Cat. No.00CH37134)*. Vol. 1, 290–295 vol. 1.

Li, Xialin, Zhiwang Li, Li Guo, Jiebei Zhu, Yizhen Wang, and Chengshan Wang (2019). "Enhanced Dynamic Stability Control for Low-Inertia Hybrid AC/DC Microgrid With Distributed Energy Storage Systems". In: *IEEE Access* 7, pp. 91234–91242.

Li, Yin, Lingling Fan, and Zhixin Miao (2019). "Stability Control for Wind in Weak Grids". In: *IEEE Transactions on Sustainable Energy* 10.4, pp. 2094–2103.

Liu, Jia, Yushi Miura, and Toshifumi Ise (2016). "Comparison of Dynamic Characteristics Between Virtual Synchronous Generator and Droop Control in Inverter-Based Distributed Generators". In: *IEEE Transactions on Power Electronics* 31.5, pp. 3600–3611.

Liu, Xiangjie (2018). *Systems Control Theory*. Berlin, Boston: De Gruyter.

Lu, Yidan and Kevin Tomsovic (2018). "Wide Area Hierarchical Voltage Control to Improve Security Margin for Systems With High Wind Penetration". In: *IEEE Transactions on Power Systems* 33.6, pp. 6218–6228.

Lund, T., P. Sørensen, and J. Eek (2007). "Reactive power capability of a wind turbine with doubly fed induction generator". In: *Wind Energy* 10 (4), pp. 379–394.

MacDougall, Pamela, Bob Ran, George B. Huitema, and Geert Deconinck (2016). "Predictive control for multi-market trade of aggregated demand response using a black box approach". In: *2016 IEEE PES Innovative Smart Grid Technologies Conference Europe (ISGT-Europe)*, pp. 1–6.

Mahmoud, M. and F. Al-Sunni (2015). *Control and Optimization of Distributed Generation Systems*. Springer-Verlag Berlin Heidelberg.

MATLAB 2023a (n.d.). *Three-Phase PI Section Line*. URL: `https://de.mathworks.com/help/sps/powersys/ref/threephasepisectionline.html`.

Mayorga Gonzalez, D. (2021). "The Smart Power Cell Concept". PhD thesis. TU Dortmund.

Mei, Shengwei, Yixin Ni, Gang Wang, and Shengyu Wu (2008). "A Study of Self-Organized Criticality of Power System Under Cascading Failures Based on AC-OPF With Voltage Stability Margin". In: *IEEE Transactions on Power Systems* 23.4, pp. 1719–1726.

Meng, Xin, Jinjun Liu, and Zeng Liu (2019). "A Generalized Droop Control for Grid-Supporting Inverter Based on Comparison Between Traditional Droop Control and Virtual Synchronous Generator Control". In: *IEEE Transactions on Power Electronics* 34.6, pp. 5416–5438.

Milanovic, Jovica V., Koji Yamashita, Sergio Martínez Villanueva, Sasa Ž. Djokic, and Lidija M. Korunović (2013). "International Industry Practice on Power System Load Modeling". In: *IEEE Transactions on Power Systems* 28.3, pp. 3038–3046.

Mitra, Parag, Deepak Ramasubramanian, Anish Gaikwad, and Jason Johns (2020). "Modeling the Aggregated Response of Variable Frequency Drives (VFDs) for Power System Dynamic Studies". In: *IEEE Transactions on Power Systems* 35.4, pp. 2631–2641.

Müller, F. L., O. Sundström, J. Szabó, and J. Lygeros (2015). "Aggregation of energetic flexibility using zonotopes". In: *54th IEEE Conference on Decision and Control (CDC)*, pp. 6564–6569.

Muresan, Cristina I., Eva H. Dulf, Roxana Both, Andrei Palfi, and Mircea Caprioru (2013). "Microcontroller Implementation of a Multivariable Fractional Order PI Controller". In: *2013 19th International Conference on Control Systems and Computer Science*, pp. 44–51.

Muuß, Fridolin, Nasser G.A. Hemdan, Michael Kurrat, Daniel Unger, and Bernd Engel (2015). "Dynamic virtual reactive power plant in active distribution networks". In: *2015 IEEE Eindhoven PowerTech*, pp. 1–6.

Nguyen, Thai-Thanh and Hak-Man Kim (2021). "Cluster-Based Predictive PCC Voltage Control of Large-Scale Offshore Wind Farm". In: *IEEE Access* 9, pp. 4630–4641.

Oprzędkiewicz, Krzysztof, Maciej Rosół, and Jakubżegleń Włodarczyk (Feb. 2021). "The Frequency and Real-Time Properties of the Microcontroller Implementation of Fractional-Order PID Controller". In: *Electronics* 10, p. 524.

Othman, Mahmoud M., Mohamed H. Ahmed, and Magdy M. A. Salama (2020). "A Coordinated Real-Time Voltage Control Approach for Increasing the Penetration of Distributed Generation". In: *IEEE Systems Journal* 14.1, pp. 699–707.

Ouammi, Ahmed, Hanane Dagdougui, and Roberto Sacile (2015). "Optimal Control of Power Flows and Energy Local Storages in a Network of Microgrids Modeled as a System of Systems". In: *IEEE Transactions on Control Systems Technology* 23.1, pp. 128–138.

Palensky, Peter, Qixin Chen, and Marcos J. Rider (2023). "Guest Editorial: Special Section on Active Distribution Networks: Markets, Operations, Planning, and Regulation". In: *Journal of Modern Power Systems and Clean Energy* 11.1, pp. 1–2.

Pourbabak, Hajir, Qais Alsafasfeh, and Wencong Su (2020). "A Distributed Consensus-Based Algorithm for Optimal Power Flow in DC Distribution Grids". In: *IEEE Transactions on Power Systems* 35.5, pp. 3506–3515.

Resende, F. O., J. Matevosyan, and J. V. Milanovic (2013). "Application of dynamic equivalence techniques to derive aggregated models of active distribution network cells and microgrids". In: *2013 IEEE Grenoble Conference*, pp. 1–6.

Riaz, S. and P. Mancarella (2019). "On Feasibility and Flexibility Operating Regions of Virtual Power Plants and TSO/DSO Interfaces". In: *2019 IEEE Milan PowerTech*, pp. 1–6.

Schultis, D.-L., A. Ilo, and C. Schirmer (2019). "Overall performance evaluation of reactive power control strategies in low voltage grids with high prosumer share". In: *Electric Power Systems Research* 168, pp. 336–349.

Schwab, Adolf (2012). *Elektroenergiesysteme*. 3rd ed. Heidelberg: Springer.

El-Sharkawi, M. A. (2011). "Dynamic equivalent models for wind power plants". In: *IEEE Power and Energy Society General Meeting*, pp. 1–5.

Singh, M., A. Allen, E. Muljadi, and V. Gevorgian (2014). "Oscillation damping: A comparison of wind and photovoltaic power plant capabilities". In: *2014 IEEE Symposium on Power Electronics and Machines for Wind and Water Applications*, pp. 1–7.

Stevens, B. L., F. L. Lewis, and E. N. Johnson (2015). *Aircraft Control and Simulation: Dynamics, Controls Design, and Autonomous Systems*. 3rd ed. Hoboken: Wiley.

Stoustrup, Jakob (2019). "Distributed Control of Power Grids". In: *Smart Grid Control: Overview and Research Opportunities*. Ed. by Jakob Stoustrup, Anuradha Annaswamy, Aranya Chakrabortty, and Zhihua Qu. Cham: Springer International Publishing, pp. 85–98.

Strbac, G. (Mar. 2007). "Virtual power plant and system integration of distributed energy resources". In: *IET Renewable Power Generation* 1 (1), 10–16(6).

Strunz, K., Ehsan Abbasi, Robert Fletcher, Nikos Hatziargyriou, Reza Iravani, and Géza Joos (Apr. 2014). *TF C6.04.02 : TB 575 – Benchmark Systems for Network Integration of Renewable and Distributed Energy Resources*.

Talbi, El-Ghazali (2009). *Metaheuristics: From Design to Implementation*. Hoboken: Wiley.

Usman, Muhammad and Florin Capitanescu (2023). "Three Solution Approaches to Stochastic Multi-Period AC Optimal Power Flow in Active Distribution Systems". In: *IEEE Transactions on Sustainable Energy* 14.1, pp. 178–192.

Various Wikipedia Authors (2022). *Fractional calculus*. URL: https://en.wikipedia.org/wiki/Fractional_calculus (visited on 06/23/2022).

Waffenschmidt, Eberhard (2022). "Swarm Grids—Distributed Power Grid Control for Distributed Renewable Power Generation". In: *Renewable Energy Based Solutions*. Ed. by Tanay Sıdkı Uyar and Nader Javani. Cham: Springer International Publishing, pp. 149–165.

Waffenschmidt, Eberhard, Majid Nayeripour, Silvan Rummeny, and Christian Brosig (2020). "Electricity Grids for 100% Renewable Energy: Challenges and Solutions". In: *Accelerating the Transition to a 100% Renewable Energy Era*. Ed. by Tanay Sıdkı Uyar. Cham: Springer International Publishing, pp. 131–154.

Weber, Harald and Salaheddin Al Ali (2016). "Influence of huge renewable Power Production on Inter Area Oscillations in the European ENTSO-E-System". In: *IFAC-PapersOnLine* 49.27. IFAC Workshop on Control of Transmission and Distribution Smart Grids CTDSG 2016, pp. 12–17.

Yan, Wei, Wei Cui, Wei-Jen Lee, Juan Yu, and Xia Zhao (2016). "Pilot-Bus-Centered Automatic Voltage Control With High Penetration Level of Wind Generation". In: *IEEE Transactions on Industry Applications* 52.3, pp. 1962–1969.

Yi, Zhongkai, Yinliang Xu, Wei Gu, and Zhongyang Fei (2021). "Distributed Model Predictive Control Based Secondary Frequency Regulation for a Microgrid With Massive Distributed Resources". In: *IEEE Transactions on Sustainable Energy* 12.2, pp. 1078–1089.

You, Shutang, Gefei Kou, Yong Liu, Xuemeng Zhang, Yi Cui, Micah J. Till, Wenxuan Yao, and Yilu Liu (2017). "Impact of High PV Penetration on the Inter-Area Oscillations in the U.S. Eastern Interconnection". In: *IEEE Access* 5, pp. 4361–4369.

Zaferanlouei, Salman, Venkatachalam Lakshmanan, Sigurd Bjarghov, Hossein Farahmand, and Magnus Korpås (2022). "BATTPOWER application: Large-scale integration of EVs in an active distribution grid – A Norwegian case study". In: *Electric Power Systems Research* 209, p. 107967. ISSN: 0378-7796.

Zellulares Energiesystem (2019). Frankfurt am Main: VDE ETG Energietechnik.

Zhang, Congyue, Xiaobo Dou, Lin Wang, Yunfei Dong, and Yu Ji (2023). "Distributed Cooperative Voltage Control for Grid-Following and Grid-Forming Distributed Generators in Islanded Microgrids". In: *IEEE Transactions on Power Systems* 38.1, pp. 589–602.

Zhang, Wang, Yan Xu, ZhaoYang Dong, and Kit Po Wong (2017). "Robust Security Constrained-Optimal Power Flow Using Multiple Microgrids for Corrective Control of Power Systems Under Uncertainty". In: *IEEE Transactions on Industrial Informatics* 13.4, pp. 1704–1713. DOI: 10.1109/TII.2016.2644738.

Zhang, Yu, Nikolaos Gatsis, and Georgios B. Giannakis (2013). "Robust Energy Management for Microgrids With High-Penetration Renewables". In: *IEEE Transactions on Sustainable Energy* 4.4, pp. 944–953.

Publications

Hinners, Holm, Sergio F. Contreras, and Johanna Myrzik (2022). "Aggregate dynamic modelling and optimal control in cellular electric energy systems". In: *IET Generation, Transmission & Distribution* 16.2, pp. 282–292.

Hinners, Holm, Sergio F. Contreras, and Johanna Myrzik (2023). "Automatic Transmission Grid Control of Active Distribution Networks". In: *IFAC World Congress 2023*.

Hinners, Holm, Daniel Mayorga Gonzalez, and Johanna Myrzik (2019a). "Model Order Reduction of Active Distribution Networks with TSO-DSO Interconnection Power Flow Control". In: *2019 IEEE Milan PowerTech*.

Hinners, Holm, Daniel Mayorga Gonzalez, and Johanna Myrzik (2019b). "The Smart Power Cell Concept - A Novel Architecture for a CO2-Neutral, Power-Electronics-Based, Decentralized, Hybrid and Multimodal AC-DC Power". In: *International ETG-Congress 2019; ETG Symposium*.

Hinners, Holm, Daniel Mayorga Gonzalez, Johanna Myrzik, and Christian Rehtanz (2019). "Multivariable control of active distribution networks for TSO-DSO-coordinated operation in wide-area power systems". In: *at - Automatisierungstechnik* 67.11, pp. 904–911.

Hinners, Holm and Johanna Myrzik (2021). "Validation and Flexibility Region of the Model Order Reduction of an Active Distribution Grid". In: *2021 IEEE Madrid PowerTech*, pp. 1–6.

Liemann, Sebastian, Lia Strenge, Paul Schultz, Holm Hinners, Johannis Porst, Marcel Sarstedt, and Frank Hellmann (2021). "Probabilistic Stability Assessment for Active Distribution Grids". In: *2021 IEEE Madrid PowerTech*, pp. 1–6.

Supervised Theses

Supervised Bachelor Theses

- Winkler, Kora (2020). "Modellbildung und Literaturrecherche zu Power-to-Heat".
- Sampson, Lisa (2020). "Systemidentifikation und Reglersynthese für allgemeine verteilte Erzeugungsanlagen zur Regelung des Leistungsflusses an Netz-schnitt-stellen".
- Bödecker, Henning (2021). "Dynamisches Verhalten von Power-to-Gas Systemen".

Supervised Master Theses

- Miller, Markus (2021). "Electrical Model-Order Reduction as an Inverse Problem".

Basics of Advanced Control

The fundamentals of control theory, such as PID controllers, are single-input, single-output (SISO) controllers. In more mathematical terms, they map the input error scalar e to an output control scalar u:

$$u = f(e), \tag{A.1}$$

where, in the case of a PID controller, this expands to:

$$u(t) = K_P e(t) + K_I \int e(t)\,dt + K_D \frac{d}{dt} e(t), \tag{A.2}$$

$$u = K_P e + K_I \frac{1}{s} e + K_D s e. \tag{A.3}$$

This type of controller has obvious advantages. They are intuitively comprehensible to a trained human observer and they are simple to synthesize and simple to implement on a microcontroller. They are also usually reasonably robust when designed conservatively in the sense that they maintain some degree of stability under parameter variation and disturbance. But this controller also has many obvious disadvantages such as limited degrees of freedom, no support for multiple input or output variables, and local operator behavior.

The purpose of this chapter is to provide an extremely brief introduction to concepts that exist in more advanced control theory. It is not intended to impart the knowledge of how to use any of these methods or describe their advantages and disadvantages in detail; there is no space for that. However, it is hoped that the reader will understand the basic concepts a little and remember how much progress has been made in control theory in the last 50 years, the impact this can have on our lives, and perhaps recognize the potential usefulness for their own work.

A.1. A Few Basics of Multivariable Control

In many systems, SISO control is not enough because different variables interact to such a strong degree that designing controllers individually for them is nearly impossible. It might be desirable or necessary to have more than one input value and more than one control variable (i.e. the actuators) in a single controller. This is equivalent to the map of some vector of input error scalars $\vec{e}$ to an output control vector $\vec{u}$:

$$\vec{u} = f(\vec{e}). \tag{A.4}$$

This is the fundamental idea behind multiple-input, multiple-output (MIMO) control. A wide variety of algorithms exist to arrive at the function $f()$ with radically different philosophies behind them, such as state-space control, model-predictive control, control-Lyapunov functions, etc. Not all of these algorithms are of practical relevance. For example, control-Lyapunov functions in particular are notoriously difficult to obtain and not often used in practical systems, at least for now.
The possibly simplest approach is that taken by state space controllers. Instead of an algorithm to generate proportional control scalars K_P for a PID-controller, we could look for an algorithm that generates control matrices $\mathbf{K_P}$ for a dynamic system with n errors and m actuators:

$$\begin{aligned} \vec{u} &= \mathbf{K_P}\vec{e}, \\ \begin{bmatrix} u_1 \\ u_2 \\ \vdots \\ u_m \end{bmatrix} &= \begin{bmatrix} k_{11} & k_{12} & \dots & k_{1n} \\ k_{21} & k_{22} & & \\ \vdots & & \ddots & \\ k_{m1} & & & k_{mn} \end{bmatrix} \begin{bmatrix} e_1 \\ e_2 \\ \vdots \\ e_n \end{bmatrix}. \end{aligned} \tag{A.5}$$

Different algorithms exist that generate such a poportional response matrix $\mathbf{K_P}$ based on the time-invariant linear matrix representation of dynamic systems ($\dot{x} = \mathbf{A}x + \mathbf{B}u, y = \mathbf{C}x + \mathbf{D}u$). Additional algorithms exist which can then be used to expand the controller into a state-space PID controller:

$$\begin{aligned} \vec{u} &= \mathbf{K_P}\vec{e}, \\ \vec{u} &= \mathbf{K_P}\vec{e} + \mathbf{K_I}\frac{1}{s}\vec{e} + \mathbf{K_D}s\vec{e}. \end{aligned} \tag{A.6}$$

State-space control is mature and has, for example, been widely used in manned and unmanned aircraft flight control. Its chief disadvantage is the need for a good state-space representation of the system and the implicit necessity of obtaining through measurement or inference a full control error vector $\vec{e}$ (the controlled system is usually no longer stable if some measurements are unavailable). This becomes unrealistic for systems of high dimension such as a power system. A dynamic, medium-voltage SPC model has dozens of states, possibly exceeding 100, and it is not feasible to measure all of these states to provide a full error vector to the state-space controller. It is for this reason that the controller presented in chapter 4 is merely inspired by the mathematical formulation in equation A.5 and doesn't attempt to implement such a state-space controller algorithm directly.

A.2. A Few Basics of Nonlinear Control

Both PID controllers and state-space controllers are linear controllers for linear systems. In practice, almost all systems are to varying degrees nonlinear, meaning that they cannot be represented using a linear transfer function or a linear state-space. Instead of linear differential equations which are used to derive the transfer function or the state-space, nonlinear systems are usually based on nonlinear differential equations. Various approaches exist to generate controllers for a nonlinear system. It is the purpose of this section to describe some which are either relevant to this thesis or which might interest the reader.
A simple and intuitive solution to the problem of controller synthesis might be to take the nonlinear differential equations

$$\dot{\vec{x}} = f(\vec{x}, \vec{u}), \tag{A.7}$$

and then linearizing them around some operating point $\{\vec{x}_0, \vec{u}_0\}$. These linear differential equations can then be rearranged into a linear state-space to be used with linear design techniques. Obviously this controller would only generate a stable response as long as the system is somewhat close to the operating point for which it was linearized (and not necessarily even then, depending on the nature of the nonlinearities). However, the system could be linearized around many different operating points and the controllers pre-generated and saved. As the system changes, controllers are then selected for the control response based on which operating point is closest and therefore which controller is most applicable. This technique is called *gain scheduling* because its original formulation calculated various PID controller *gains* (K_P, K_I, K_D) for various operating points and *scheduled* them for the control response based on the measured behavior of the system. Gain scheduling is almost as old as modern control theory itself and has a long history of success.
A radically different approach is taken by fuzzy control. Instead of deriving a controller through mathematical consideration of the system, the controller is based on logical rules and definitions derived by a human expert. Consider the following rules for a generator:

When **[voltage]** is **[too low]**, produce **[more] [reactive power]**.
When **[voltage]** is **[too high]**, produce **[less] [reactive power]**.

What's missing now are more mathematical definitions for the terms **[too low]**, **[too high]**, **[more]**, and **[less]** that allow an implementation in a controller. For this, we define fuzzy truth values that express the validity of these statements along a numerical axis using values between 0 and 1. For the voltage, we might define an area of acceptable voltage (neither too high nor too low, meaning both of them have a fuzzy truth of 0), areas where the voltage begins to become too high or too low (a fuzzy truth between 0 and 1), and areas where it is definitely too high or too low (a fuzzy truth of 1):

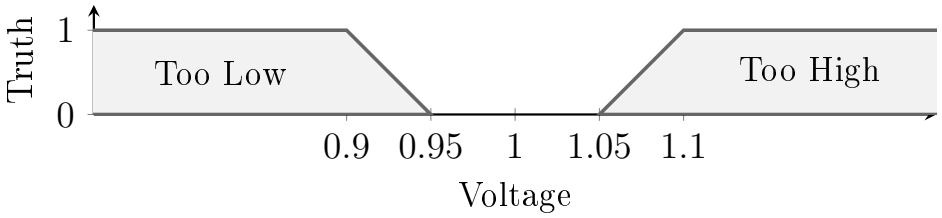

Similarly, we should define what we understand by "more" and "less" as a change of the current power generation (precise units omitted in this example, but necessary for implementation):

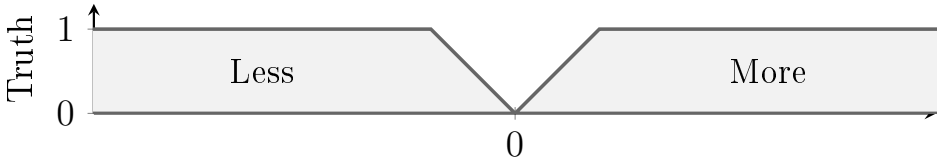

In this SISO case, the truth values are easily mapped to each other since they cannot be true at the same time and a numerical output is obtained for the controller, but this approach works for MIMO systems and systems with extremely complex rules as well. Multiple inputs and outputs can overlap; these are then "defuzzied" using the geometric centroid of the output truth polygon.

Fuzzy control has distinct advantages if the system is large and difficult to model adequately for a traditional controller synthesis, but can be intuitively understood quite well by a human expert and heuristic control laws defined. The system must also be somewhat insensitive to parameter variation because otherwise it becomes difficult for the expert to select appropriately defined fuzzy sets. In many cases, fuzzy control is much more stable than one would naively expect: for example, if our definition of "less" makes the controller a little too aggressive in its attempts to correct the voltage, it will oscillate between "less" and "more" for a while before stabilizing. Even if an output or input fuzzy set is imperfectly defined, the system will tend to oscillate towards a stable operating point because the aggressiveness of the controller changes based on the state of the system.

Ultimately, fuzzy control can be thought of as linear parameter-varying control with the controller parameters varying between fixed numbers depending on the fuzzy truth of the various defined statements. Since it can be equivalently converted to a conventional, linear controller whose parameters vary and tend towards zero for small errors, oscillations and instability are generally better than in a controller who immediately reacts aggressively to an error.

The disadvantages include its somewhat slower and less aggressive performance, the time-consuming trial-and-error nature of its derivation, and the lack of a robust mathematical basis to estimate stability margins and parameter uncertainty.

Basics of Fractional Calculus

FRACTIONAL CALCULUS is a field of mathematics concerned with obtaining a meaningful result for non-integer powers $\alpha \in \mathbb{R}$ of the differentiation $\frac{d}{dx}$

$$\left(\frac{d}{dx}\right)^{\alpha}, \tag{B.1}$$

or of the integration $f(x) = \int_0^x f(y)dy$. If the operator acts on a function that can be transformed using the Laplace transform, this simplifies to

$$s^{\alpha}, \quad \alpha \in \mathbb{R}, \tag{B.2}$$

where a positive real α yields a fractional differential operator and a negative real α yields a fractional integrator. The normal mathematical rules are intended to apply, so the multiplication of two half-derivatives $s^{\frac{1}{2}} \cdot s^{\frac{1}{2}}$ yields a normal, classical derivative s. The history of these fractional operators is surprisingly long, with the first speculations on their existence dating back to Guillaume de l'Hôpital and Gottfried Wilhelm Leibniz in the 17th century and a maturing understanding developed by Joseph Liouville and Oliver Heaviside in the 19th century.

B.1. Half-Derivative Example

As an example, consider the function $f(x) = x$ (based on [Various Wikipedia Authors 2022]) and let us assume that we wish to calculate the half-derivative

$$\frac{d^{\frac{1}{2}}}{dx^{\frac{1}{2}}}. \tag{B.3}$$

We begin with a generalized function and derivative:

$$\frac{d^a}{dx^a}x^k = \frac{k!}{(k-a)!}x^{k-a}, \tag{B.4}$$

for some a-th *integer* order derivative on the power function x^k. Other than the factorial, which is only defined for non-negative integers, there is nothing keeping us from having

non-integer exponents a for this expression. It turns out that such a generalization of the factorial is possible:

$$\frac{d^a}{dx^a}x^k = \frac{\Gamma(k+1)}{\Gamma(k-a+1)}x^{k-a}, \tag{B.5}$$

where Γ is the (well-established) gamma function which provides an extension of the factorial for real (and complex) numbers:

$$\Gamma(z) = \int_0^\infty x^{z-1}e^{-x}\,dx, \;\; \mathbb{R}(z) > 0. \tag{B.6}$$

With $k = 1, a = \frac{1}{2}$ we obtain

$$\begin{aligned} \frac{d^{\frac{1}{2}}}{dx^{\frac{1}{2}}}x &= \frac{\Gamma(2)}{\Gamma(\frac{3}{2})}x^{\frac{1}{2}}, \\ &= \frac{1}{\frac{\sqrt{\pi}}{2}}x^{\frac{1}{2}}, \\ &= \frac{2}{\sqrt{\pi}}\sqrt{x}. \end{aligned} \tag{B.7}$$

Repeating the process gives

$$\begin{aligned} &\frac{d^{\frac{1}{2}}}{dx^{\frac{1}{2}}}\frac{2}{\sqrt{\pi}}x^{\frac{1}{2}}, \\ =&\frac{2}{\sqrt{\pi}}\frac{\Gamma(\frac{3}{2})}{\Gamma(1)}x^0, \\ =&\frac{2}{\sqrt{\pi}}\frac{\sqrt{\pi}}{2}x^0, \\ =&1, \end{aligned} \tag{B.8}$$

meaning that after two half-derivatives, we correctly reach a full derivative $\frac{d}{dx}x = 1$. Using the Laplace transform and the operator $s^{\frac{1}{2}}$ yields the same result as above using convolution and the gamma function again.
Now consider the constant value $x^0 = 1$ for $x > 0$. As a Heaviside step function located at $x = 0$, its derivative is the Dirac delta. But its half-derivative is

$$\begin{aligned} \frac{d^{\frac{1}{2}}}{dx^{\frac{1}{2}}}x^0 &= \frac{\Gamma(0+1)}{\Gamma(0-\frac{1}{2}+1)}x^{0-\frac{1}{2}}, \\ &= \frac{1}{\sqrt{\pi}}x^{-\frac{1}{2}}, \\ &= \frac{1}{\sqrt{\pi}}\frac{1}{\sqrt{x}}, \end{aligned} \tag{B.9}$$

meaning that it merely decays to zero at infinity; it is no longer a local operator like an integer-order derivative and instead depends on the entire history of the function, not just its local evaluation.

B.2. Usefulness in Control Theory

The value of having a fractional integrator is limited. For integrators of s^α with α between 0 and -1 there is no full integer-order integration and the contents of the fractional integrator saturate even in the presence of a constant input; this is undesirable in most control systems since it defeats the purpose of having an integrator, which is steady-state accuracy. For values of $\alpha < -1$ there would be some combination of full- and fractional-order integrators, which can be useful in certain situations to prevent controller windup, but requires very careful parameter selection. However, fractional-order derivatives of α between 0 and 1 can be very useful because, as shown in equation B.9, a non-integer derivative is no longer local and will remain non-zero in the absence of an input (albeit decaying). It will also maintain its sign for some time after the sign of a normal derivative would change.
Consider the sawtooth function and its (half-)derivative in figures B.1-B.3.
An ordinary derivative yields Dirac deltas for $x = \{0, 10, 20 \dots\}$ and constant (negative) values inbetween. The half-derivative decays instead, remaining positive for some time. Also note that the response of the half-derivative at $x = 0$ is slightly different from the response at $x = 10$ – this is correct behavior because the fractional derivative has memory and at $x = 0$ this memory is initialized empty, so the half-derivative responds differently here as compared to later where the memory contains function behavior from the past. In fact, although it appears as though the half-derivative responds with periodic recurrence at $x = \{10, 20 \dots\}$, these responses are *all* slightly different from each other as well. They would only be identical if the sawtooth function (and the half-derivative's memory) reached infinitely far into the past. However, due to the decaying influence of past values, this difference is so small that it becomes invisible at the figure's scale after the first period of the sawtooth function.
Inter-controller oscillations in control theory often occur because a delay exists between the response of one controller and the detection of this response in the control error by a different controller. This causes controllers to react strongly to an error that has had the opportunity to grow larger than it would have if a single controller with more immediate detection were available. Inter-controller oscillations around the reference value result in frequent changes to the sign of the derivative of the control error. The half-derivative dampens the controller response because it "remembers" that the control error had a different sign not long ago, as can be seen in the sign changes of the half-derivative in figure B.3. This reduces or eliminates the tendency of an integral controller to oscillate against other integrators.
By way of a simple demonstration, consider the block diagram in figure B.4. The two identical controllers $K(s)$ receive the same reference signal r and target the same output variable y. One controller is delayed by a unity first-order transfer transfer function. Both controllers then act on the system which is also a unity first-order transfer function. The three controllers compared here for $K(s)$ are

$$K_I = 2\frac{1}{s}, \tag{B.10}$$

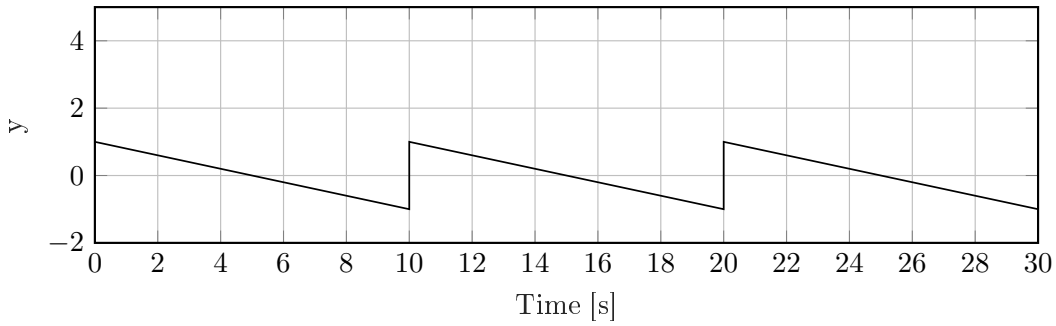

Figure B.1: Sawtooth Function

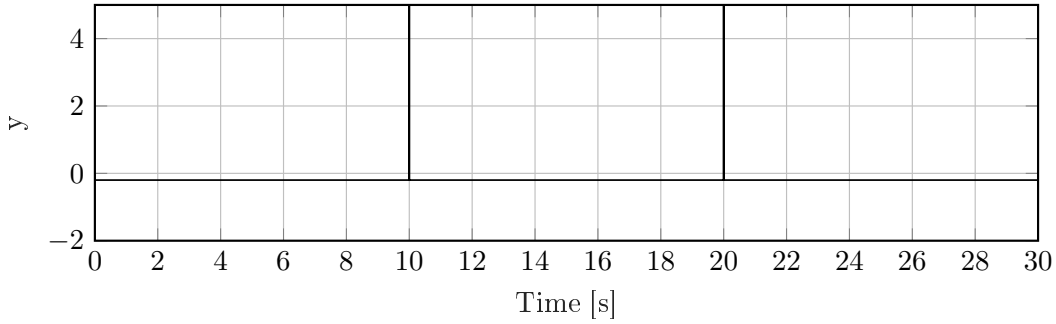

Figure B.2: Derivative

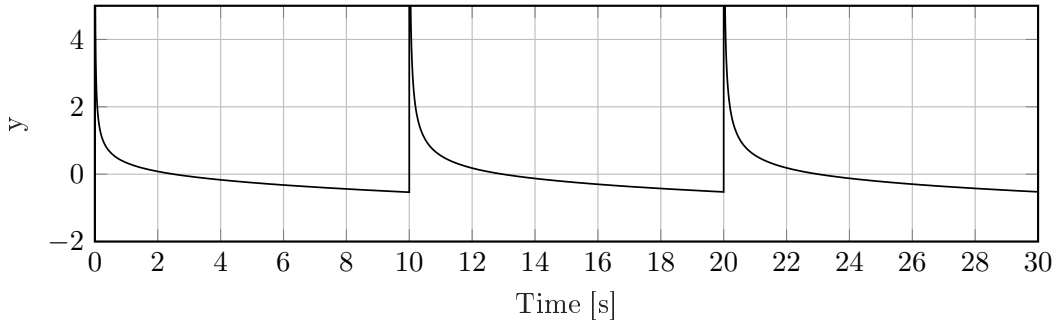

Figure B.3: Half-Derivative

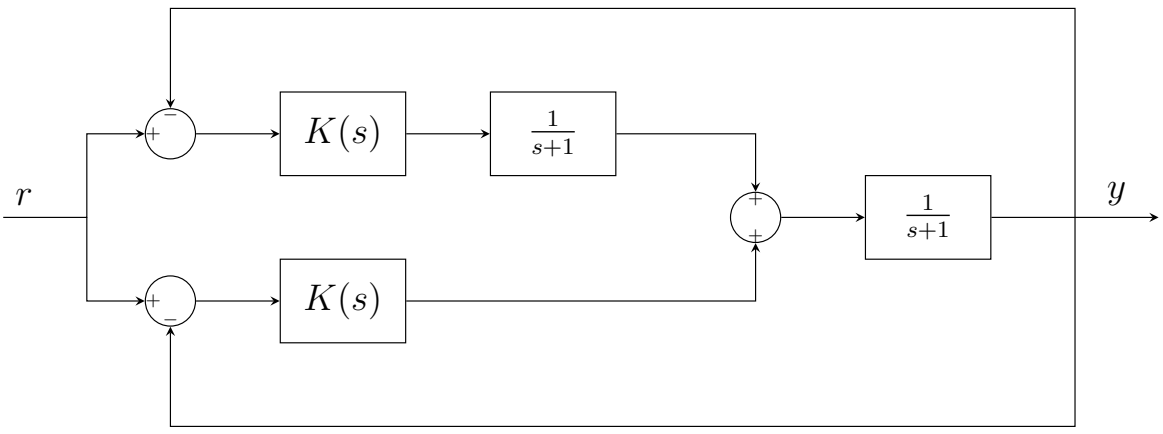

Figure B.4: FPID Comparison Block Diagram

$$K_{ID} = 2\frac{1}{s} + s, \tag{B.11}$$

$$K_{FID} = 2\frac{1}{s} + s^{\frac{1}{2}}. \tag{B.12}$$

The reference function is a simple unity step at $t = 5\,\mathrm{s}$. The responses of the different controllers to this reference step are shown in figure B.5. The I-controller shows the worst performance: it has the slowest startup of the three controllers, the largest overshoot, and shows strong oscillations between controllers. The ID-controller shows better startup and dampens the overshoot (the increasing control error generates a response in the derivative), but later oscillations are not substantially improved in amplitude or duration. The FID controller shows startup performance between the I- and the ID-controller, greatly dampens the overshoot, and removes the oscillations. It quite clearly performs the best in this example.

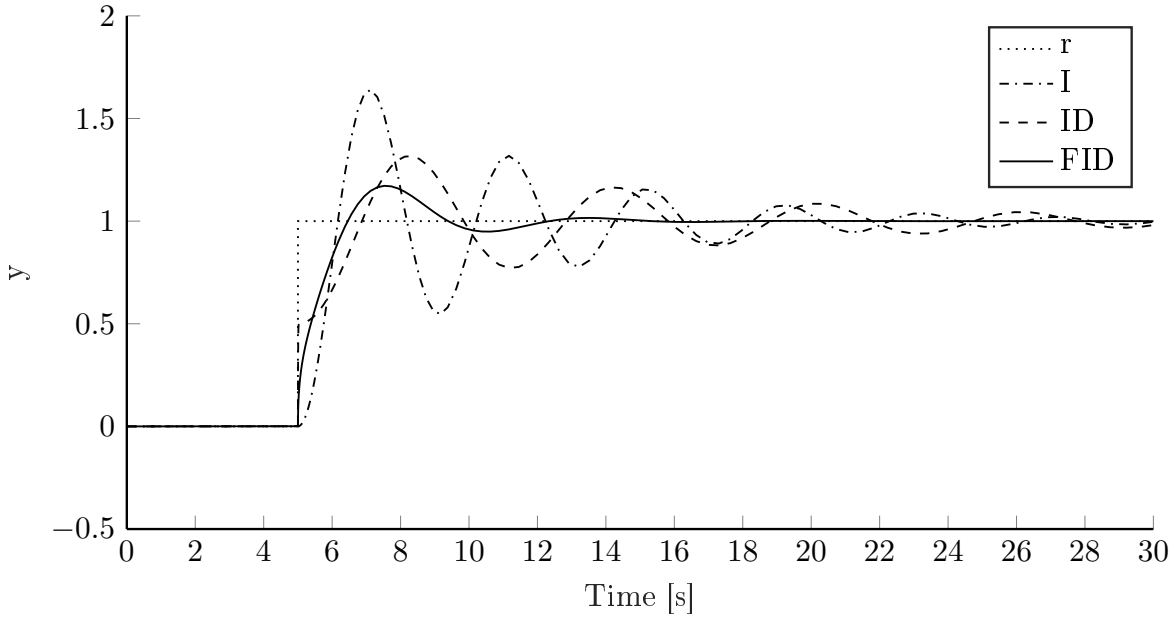

Figure B.5: Controller Comparison

Fractional PID controllers provide a generalization of ordinary PID controllers in the sense that the FPID controller

$$\begin{aligned} K(s) =& K_P + K_I s^{-\alpha} + K_D s^{\beta}, \\ & \alpha, \beta, \in \mathbb{R}_{>0}, \\ & K_P, K_I, K_D \in \mathbb{R} \end{aligned} \tag{B.13}$$

contains all possible ordinary PID controllers by allowing $\alpha = \beta = 1$. This means that, in theory, an algorithm that yields FPID controllers is strictly better than one which yields PID controllers because it increases the degrees of freedom of the controller design and therefore the potential of a desirable control response. In practice, this is often not the case because few plants are compatible with analytic algorithms for FPID synthesis.

The most widely used algorithms for FPID synthesis are instead metaheuristics, which means they are elaborate, computationally expensive, and do not guarantee any kind of optimality or generality. FPID controllers are also much more demanding to implement in a microcontroller due to the necessity of maintaining as long a function memory as possible to properly compute numerical fractional derivatives. This contrasts with a PID controller which only needs to maintain two controller values in memory, one for the integrator state and one for the last control error (to compute a numerical derivative). These drawbacks together mean that FPID adoption has been very timid and familiarity with them even among control system engineers is rather low.

Aggregation of Energetic Flexibility and Minkowski Sums

The representation of energetic flexibility is a vector space since the operating point of a technical installation in time can almost always be described as some vector $\vec{y}$ filled with values that represent the operation. Different operating points are represented by different entries in the vectors, and the set of all these possible operating points is a vector space B. For example, as far as power generation or consumption is concerned, a controllable generator can supply to a maximum of some sort of maximum apparent power $S_{\max}$, but it cannot absorb any real power whatsoever. This is a filled semicircle in the complex (PQ) plane, depicted here:

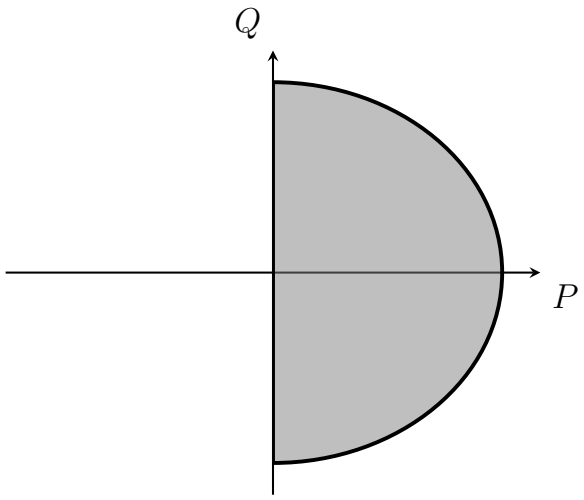

All the vectors inside this region up to and including the hull (the border) are valid operating points. Other installations might have different flexibility regions represented by different vector spaces. The combination, i.e. aggregation, of two vector spaces B_1 and B_2 into F is called the Minkowski sum:

$$F = B_1 \oplus B_2. \tag{C.1}$$

Minkowski sums can be visualized as overlaid hulls. Consider a sum of a rectangle and a semicircle:

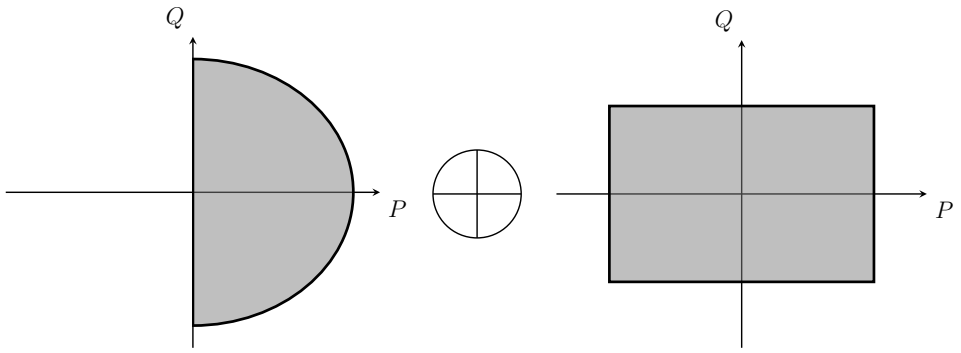

Strictly speaking, the Minkowski sum is a linear combination of all vectors in B_1 with all vectors in B_2. Due to the continuous nature of the vector space, this is obviously impossible to do on paper in most cases. Some mathematical description of the hull (the border) of F must be found that can be used to define the member vectors in terms of inequality constraints. Generally the method chosen here is to discretize the hull by generating a sampled polytope. When we overlay the hull of B_1 at the extremities of B_2, we see:

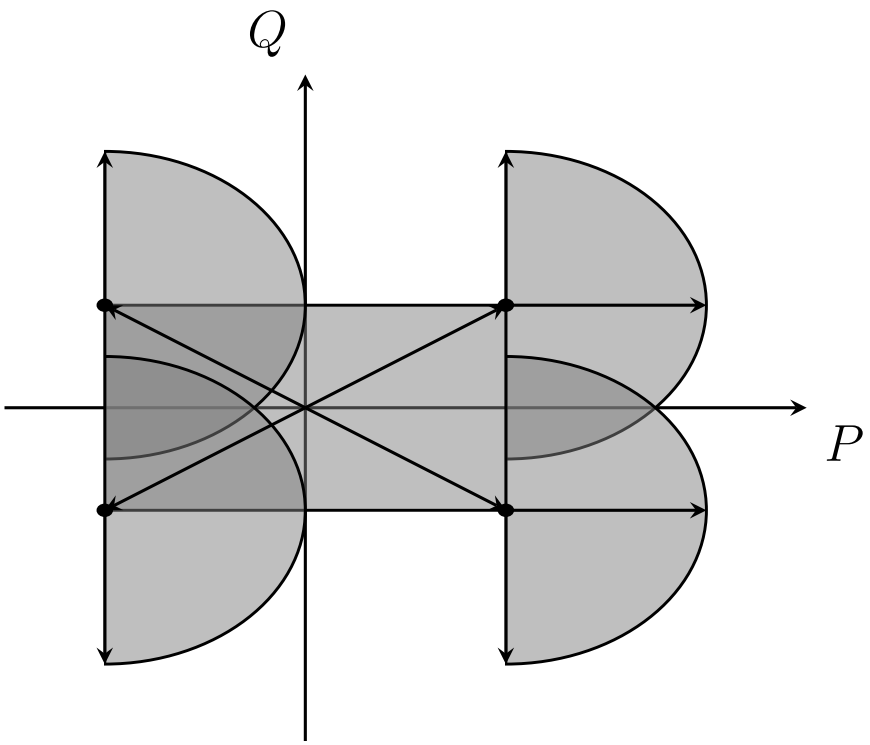

If we push the semicircle along the edge of the rectangle, the sum of all possible vectors taken from the sets of hull vectors constructs a new hull corresponding to F:

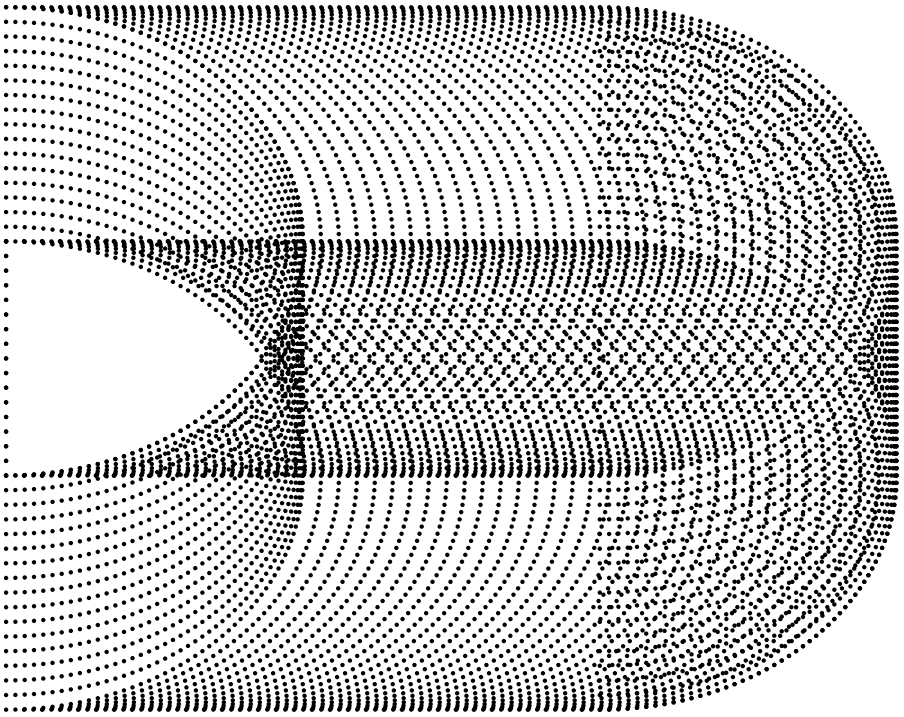

If the shape is convex, which is almost always the case in power systems, the hull of F is then computed relatively easily out of all these maxima using a divide-and-conquer algorithm testing for inequality membership in the set. All the points that do not define the hull of F can then be discarded since they are inessential to the definition of the vector space:

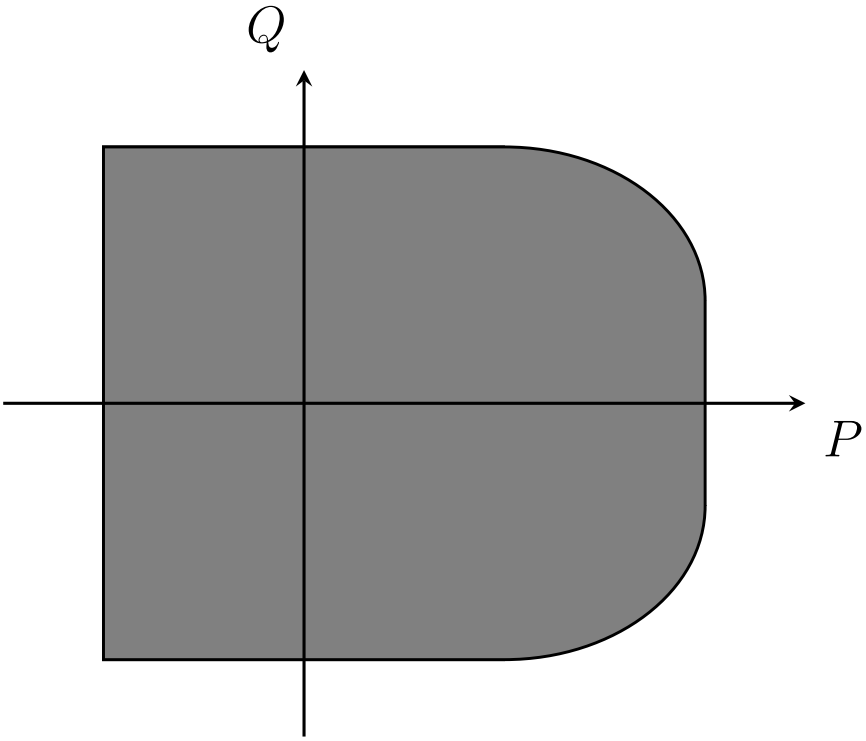

In the case of purely convex shapes, various simplifications can be made to speed up computation, but since Minkowski sums are not expensive to compute, these will not be elaborated here.

Parameters

D.1. Distributed Devices

Table D.1: Device Flexibility

Generator	Battery	VAR Comp.
4 MVA	±4 MW	±2 Mvar
≥ 0 MW[1]		

[1]This corresponds to a semicircle in the positive real side of the complex plane with a radius of 4 MVA.

Table D.2: Reference Signals

Time	[MW]	[MVA]
Initialization	-3	2
0 s	-2	-5
1 s	7	-4

Table D.3: Calculation Time By Algorithm

Algorithm	Calculation Time
SQP	0.02 s
Interior-Point	0.07 s

Table D.4: Dynamic Time Constants

T_{gen}	T_{bat}	T_{var}
0.2 s	0.01 s	0.01 s

$T_{\Sigma,P}$	$T_{\Sigma,P}$	$T_{\Sigma,Q}$	$T_{\Sigma,Q}$
0.210 s	0.049 s	0.169 s	0.217 s
$0\,\text{s} \leq t < 1\,\text{s}$	$1\,\text{s} \leq t < 2\,\text{s}$	$0\,\text{s} \leq t < 1\,\text{s}$	$1\,\text{s} \leq t < 2\,\text{s}$

D.2. Internal Control of Smart Power Cells

Table D.5: General Controller Parameters

$K_{\max}$	U_{dead}	U_{crit}
10	0.03 pu	0.06 pu

Table D.6: Controller Parameters (FID)

K_I	K_D	α	β
1	0.1	1	$\frac{1}{2}$

Table D.7: Controller Parameters (I)

K_I	K_D	α	β
1	0	1	1

Table D.8: Cable Parameters

r_+	r_0	l_+
$0.012\,73\,\Omega\,\text{km}^{-1}$	$0.3864\,\Omega\,\text{km}^{-1}$	$0.9337\,\text{mH}\,\text{km}^{-1}$
l_0	c_+	c_0
$4.1264\,\text{mH}\,\text{km}^{-1}$	$12.74\,\text{nF}\,\text{km}^{-1}$	$7.751\,\text{nF}\,\text{km}^{-1}$

Table D.9: Reference Steps

t	$P_{\text{ref},1}$	t	$P_{\text{ref},2}$	t	$Q_{\text{ref},1}$	t	$P_{\text{ref},2}$
0 s	25 MW	0 s	5 MW	0 s	0 Mvar	0 s	0 Mvar
10 s	0 MW	10 s	0 MW			10 s	3 Mvar
20 s	−4 MW					50 s	2 Mvar

Table D.10: Cable Lengths and Bus Indices

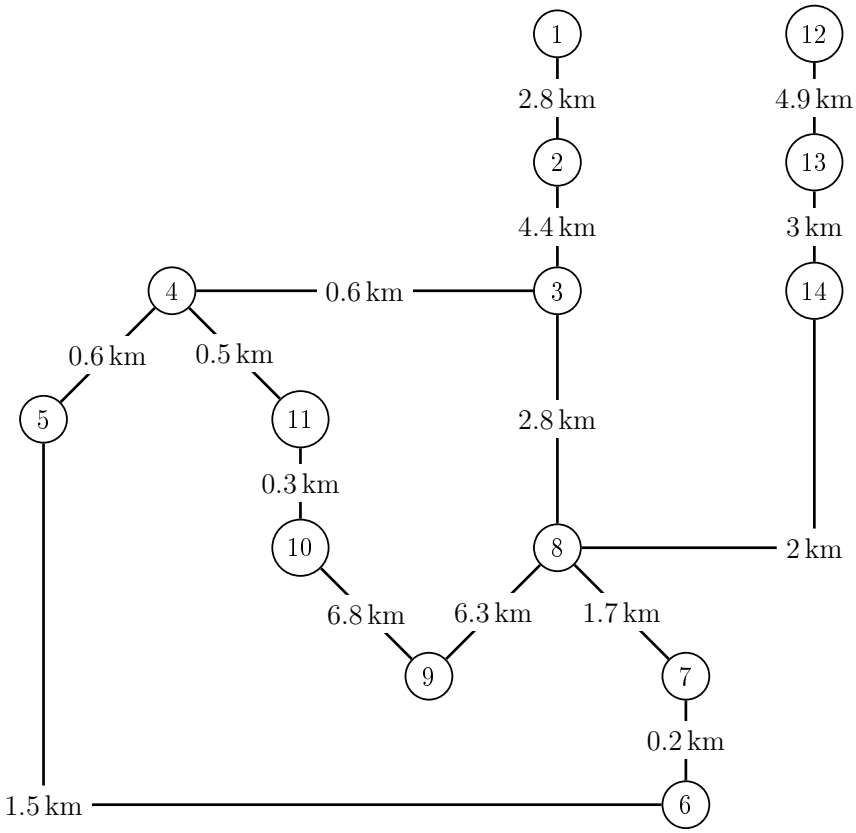

Table D.11: Load Parameters P_{load} (Active Power)

Bus 1	2	3	4	5	6	7
19.839 MW	10 kW	501 kW	431 kW	727 kW	548 kW	76.5 kW
Bus 8	9	10	11	12	13	14
586 kW	573 kW	543 kW	329 kW	500 kW	400 kW	200 kW

Table D.12: Load Parameters Q_{load} (Reactive Power)

Bus 1	2	3	4	5	6	7
4.367 Mvar	10 kvar	209 kvar	108 kvar	182 kvar	137 kvar	47 kvar
Bus 8	9	10	11	12	13	14
147 kvar	356 kvar	161 kvar	83 kvar	25 kvar	250 kW	50 kvar

D.3. Model Reduction of the SPC

Table D.13: Optimization Constants

γ_p	0.1	γ_g	0.4
ω	0.2	S	400.

Table D.14: Initialization Range

r'_+	$1 \cdot 10^{-3} \ldots 1 \cdot 10^{0} \Omega\,\mathrm{km}^{-1}$	P_1	$1 \cdot 10^{0} \ldots 1 \cdot 10^{9} \mathrm{W}$
r'_0	$1 \cdot 10^{-3} \ldots 1 \cdot 10^{0} \Omega\,\mathrm{km}^{-1}$	P_2	$1 \cdot 10^{0} \ldots 1 \cdot 10^{9} \mathrm{W}$
l'_+	$1 \cdot 10^{-6} \ldots 1 \cdot 10^{0} \mathrm{H}\,\mathrm{km}^{-1}$	Q_1	$1 \cdot 10^{0} \ldots 1 \cdot 10^{9} \mathrm{var}$
l'_0	$1 \cdot 10^{-6} \ldots 1 \cdot 10^{0} \mathrm{H}\,\mathrm{km}^{-1}$	Q_2	$1 \cdot 10^{0} \ldots 1 \cdot 10^{9} \mathrm{var}$
c'_+	$1 \cdot 10^{-9} \ldots 1 \cdot 10^{0} \mathrm{F}\,\mathrm{km}^{-1}$		
c'_0	$1 \cdot 10^{-9} \ldots 1 \cdot 10^{0} \mathrm{F}\,\mathrm{km}^{-1}$		
L	$1 \cdot 10^{0} \ldots 1 \cdot 10^{3} \mathrm{km}$		

Table D.15: Optimized Parameters

$r'_+ = 7.30 \cdot 10^{-3} \Omega\,\mathrm{km}^{-1}$	$P_1 = 1.98 \cdot 10^7 \mathrm{W}$
$r'_0 = 1.00 \cdot 10^{-3} \Omega\,\mathrm{km}^{-1}$	$P_2 = 6.91 \cdot 10^6 \mathrm{W}$
$l'_+ = 1.62 \cdot 10^{-2} \mathrm{H}\,\mathrm{km}^{-1}$	$Q_1 = 1.34 \cdot 10^7 \mathrm{var}$
$l'_0 = 1.51 \cdot 10^{-2} \mathrm{H}\,\mathrm{km}^{-1}$	$Q_2 = 1.74 \cdot 10^7 \mathrm{var}$
$c'_+ = 4.97 \cdot 10^{-5} \mathrm{F}\,\mathrm{km}^{-1}$	
$c'_0 = 9.02 \cdot 10^{-4} \mathrm{F}\,\mathrm{km}^{-1}$	
$L = 449 \cdot 10^0 \mathrm{km}$	

Table D.16: Generator Flexibility (Full Model)

DG 1	DG 2	DG 3	DG 4	DG 5	DG 6
3.650 MVA	3.075 MVA	3.325 MVA	2.600 MVA	2.700 MVA	2.575 MVA
DG 7	DG 8	DG 9	DG 10	DG 11	
2.550 MVA	3.600 MVA	2.750 MVA	2.975 MVA	2.975 MVA	

Table D.17: Generator Flexibility (Reduced Model)

DG 1	DG 2
16.3875 MVA	16.3875 MVA

D.4. Interconnected SPCs

Table D.18: Bus Flexibility

ADN #	Bus 1	Bus 2
1	20 MVA	16 MVA
2	17 MVA	19 MVA
3	19 MVA	18 MVA
4	8 MVA	23 MVA
5	22 MVA	21 MVA
6	18 MVA	17 MVA

Table D.19: HV Line Lengths

From Bus	To Bus	Length
1	2	10 km
2	5	30 km
5	4	30 km
4	3	10 km
1	6	30 km
6	4	30 km
1	3	60 km

Table D.20: HV Line Parameters

Positive-sequence	Zero-sequence
$65.34\,\mathrm{m\Omega\,km^{-1}}$	$213\,\mathrm{m\Omega\,km^{-1}}$
$7.96\,\mathrm{mH\,km^{-1}}$	$27.3\,\mathrm{mH\,km^{-1}}$
$57.01\,\mathrm{nF\,km^{-1}}$	$33.3\,\mathrm{nF\,km^{-1}}$